Molecular physiology of ankyrin-G in the heart:

Critical regulator of cardiac cellular excitability and architecture.

DISSERTATION

Presented in Partial Fulfillment of the Requirements for the Degree Doctor of Philosophy in the Graduate School of The Ohio State University

By

Michael Anthony Makara

Graduate Program in Integrated Biomedical Science

The Ohio State University

2016

Dissertation Committee:

Professor Peter J. Mohler, Ph. D, Advisor

Professor Noah L. Weisleder, Ph. D

Professor Thomas J. Hund, Ph. D

Professor Philip F. Binkley, M.D.

Abstract

Cardiovascular disease is the leading cause of death in the United States, claiming nearly 800,000 lives each year. Regardless of the underlying cardiovascular dysfunction, nearly 50% of these patients die of sudden cardiac arrest caused by arrhythmia. Development and sustainment of cardiac arrhythmia begins with dysfunction of excitability and structure at the cellular level. Therefore, in order to improve therapeutic options for these patients, a basic understanding of the molecular mechanisms regulating cardiac cellular excitability and structure is required. Decades of research have demonstrated that intracellular scaffolding polypeptides known as ankyrins are critical for the regulation of cellular excitability and structure in multiple cell types. Ankyrin-G (*ANK3*) is critical for regulation of action potentials in neurons and lateral membrane development in epithelial cells. Given its central importance for cellular physiology in excitable and non-excitable cell types, we hypothesized that functional ankyrin-G expression is critical for proper cardiac function. To test this hypothesis in vivo, we generated cardiac-specific ankyrin-G knockout (cKO) mice. In the absence of ankyrin-G, mice display significant reductions in membrane targeting of the voltage-gated sodium channel Nav1.5. This disruption in turn causes severely reduced whole cell sodium current, leading to significant conduction abnormalities, bradycardia, and ventricular arrhythmia and atrioventricular nodal block following infusion of Na_V channel

antagonists. In addition to regulating cardiac excitability, we also demonstrate a critical role for ankyrin-G in the regulation of the cardiomyocyte cytoarchitecture. Specifically, ankyrin-G cKO mice show disrupted cellular distribution of the desmosomal protein plakophilin-2 (PKP2) at baseline. In a setting of pressure overload-induced heart failure we observed severe disruptions to the cellular localization of PKP2. Further, as desmosomes mediate the integration of the intermediate filament protein desmin, we demonstrate the reduced expression of desmin at the intercalated disc (ID) in the setting of mislocalized PKP2. Mechanistically, we correlate these molecular changes with significant reductions in systolic function and increased propensity for bradyarrhythmia in ankyrin-G cKO mice following transverse aortic constriction (TAC). As ankyrin-G is significantly increased two weeks post TAC, we hypothesize that ankyrin-G expression is required for the early, compensatory phase of ventricular remodeling. Our hypothesis is further strengthened by the observation that functional ankyrin-G expression is severely reduced in multiple forms of human heart failure. We conclude that ankyrin-G is a critical regulator of both excitability and molecular architecture of the intercalated disc. We further hypothesize that remodeling of this ankyrin-G-dependent molecular environment is a critical step in the development of human arrhythmia and structural heart diseases.

Dedication:

To my parents, Ray and Trish, for their unending love, support, and wisdom throughout my life. Nothing I have accomplished would ever have been possible without you. From the bottom of my heart, I am so thankful that I have two such wonderful parents.

Love you so much,

Mike

Acknowledgments

After six months of late nights, extensive reading, and countless revisions, my dissertation is nearing completion. Throughout this whole process, my focus was locked on the daunting task of trying to condense an incredible expanse of information into a coherent story with specific hypotheses, results with significant scientific merit, and conclusions presented in the context of the current literature. And now, after adding the finishing touches and final references, I find myself sitting at my computer, reflecting on this whole process. The only thing that I can think at this point is how incredibly thankful I am to have such a wonderful group of family, friends, coworkers, and mentors in my life. Therefore, I would be remiss if I did not take this opportunity to sincerely thank all of you.

To my parents, Ray and Trish. Words cannot possibly begin to describe the love and support that you have given me throughout my life. Mom and Dad, I dedicated this work to you because I truly would not be the person I am today without having such incredible people to call parents. For 26 years, you have been a constant source of love and understanding for which I am eternally grateful. I count myself blessed to be your son and I hope that I have made you proud to call yourselves my parents. To my brother David. Thank you for the love, the laughs, and all the good times. Without fail, you are able to brighten even my darkest day with your larger-than-life personality. I am so proud and thankful to have such an extraordinary person for a brother.

To my (*at this point in time*) fiancé Ting-Ting. With every day that passes, I realize how lucky I am to have fallen in love with such an amazing person. You have brought such happiness to my life, more happiness than one could ever hope to wish for. Thank you for being an untiring source of love, friendship, and compassion in my life and for being so supportive throughout this process. Although I do not know what life has in store for us, I do know that the only place I want to be is right by your side all the days of my life. I love you so much, Ting-Ting.

To my family and friends. It is no exaggeration when I say that I have the best people I know looking out for me. I thank all of you for your unwavering love and friendship that has made my life so wonderful. I am forever grateful to have such an amazing group of people that I can call my friends and family.

To my thesis committee, Noah Weisleder, Tom Hund, and Philip Binkley. I sincerely appreciate all the guidance and mentorship that you have provided me over these past four years. Your input has been invaluable to the advancement of my project, my scientific understanding, and my professional career. Sincerely, I could not wish for a better group of scientists or a better group of people to chair my thesis committee.

Lastly, to my mentor Peter Mohler. Four years goes by pretty quick, doesn't it? From the bottom of my heart, thank you so much for everything you have done for me on both a professional and personal level. Thank you for constantly demanding my best in lab and for challenging me to always ask and answer the tough questions in my research. I have learned so much from you over these past four years and I am incredibly thankful to have you as a mentor.

Vita

May 2007 .....Canfield High School

May 2011 .....B.S. Biology, Youngstown State University

July 2011 to Present .....Graduate Research Associate, Department of Physiology and Cell Biology, The Ohio State University

Publications

1. Little SC, Curran J, Musa H, Kline CF, **Makara MA**, Higgins J, Hund TJ, Mohler PJ. Protein phosphatase 2A regulatory subunit B56α limits phosphatase activity in the heart. Sci Signal 2015; 386.
2. Curran J, Musa H, Kline CF, **Makara MA**, Little SC, Higgins JD, Hund TJ, Band H, Mohler PJ. Eps15 Homology Domain-containing Protein 3 Regulates Cardiac T-type $Ca2^{+}$ Channel Targeting and Function in the Atria. J Biol Chem 2015. Epub ahead of print.
3. Curran J, **Makara MA**, Mohler PJ. Endosome-based protein trafficking and $Ca(2^{+})$ homeostasis in the heart. Front Physiol. 2015; 6: 34.

4. Smith SA, Sturm, AC, Curran J, Kline CF, Little SC, Bonilla IM, Long VP, **Makara M**, Polina I, Hughes LD, Webb TR, Wei Z, Wright P, Voigt N, Bhakta D, Spoonamore KG, Zhang C, Weiss R, Binkley PF, Janssen PM, Kilic A, Higgins RS, Sun M, Ma J, Dobrev D, Zhang M, Carnes CA, Vatta M, Rasband MN, Hund TJ, Mohler PJ. Dysfunction in the βII spectrin-dependent Cytoskeleton Underlies Human Arrhythmia. Circulation 2015; 131: 695-708.

5. Radwański PB, Brunello L, Veeraraghavan R, Ho H, Lou Q, **Makara MA**, Belevych AE, Anghelescu M, Priori SG, Volpe P, Hund TJ, Janssen PM, Mohler PJ, Bridge JH, Poelzing S, Györke S. Neuronal Na^+ Channel Blockade Suppresses Arrhythmogenic Diastolic $Ca2^+$ Release. Cardiovasc Res. 2014; 262.

6. Chang KJ, Zollinger DR, Susuki K, Sherman DL, **Makara MA**, Brophy PJ, Cooper EC, Bennett V, Mohler PJ, Rasband MN. Glial ankyrins facilitate paranodal axoglial junction assembly. Nat. Neurosci. 2014; 17: 1673-168.

7. **Makara MA**, Curran J, Little SC, Musa H, Polina I, Smith SA, Wright PJ, Unudurthi SD, Snyder JS, Bennett V, Hund TJ, Mohler PJ. Ankyrin-G coordinates intercalated disc signaling platform to regulate cardiac excitability in vivo. Circulation Research. 2014; 115: 929-38.

8. Curran J, **Makara MA**, Little SC, Musa H, Liu B, Wu X, Polina I, Alecusan JS, Wright P, Li J, Billman GE, Boyden PA, Gyorke S, Band H, Hund TJ, Mohler PJ. Ehd3-dependent endosome pathway regulates cardiac membrane excitability and physiology. Circ Res. 2014; 115:68-78.

9. Hund TJ, Smith SA, **Makara MA**, Mohler PJ, Cellular and Molecular Pathobiology of the Cardiac Conduction System. Willis, Ch.7. Elsevier. 2013.

Fields of Study

Major Field: Integrated Biomedical Science Program

Table of Contents

List of Tables

List of Figures

List of Abbreviations

Adenosine diphosphate	ADP
Adenosine Triphosphate	ATP
Angiotensin converting enzyme	ACE
Ankyrin	ANK
Arrhythmogenic right ventricular cardiomyopathy	ARVC
Atrial fibrillation	AF
Atrioventricular	AV
Axon initial segment	AIS
Bicarbonate	HCO_3^-
Ca^{+2}/Calmodulin-dependent protein kinase II isoform δ	CaMKIIδ
Calcium	Ca^{+2}
Carbon dioxide	CO_2
Cardiac-specific knockout	cKO
Cardiovascular disease	CVD
Celsius	C
Change in Gibb's free energy	ΔG
Chlorine	Cl^-
Coulomb	C
C-terminal domain	CTD

Desmocollin-2	DSC-2
Desmoglein-2	DSG-2
Desmoplakin	DSP
Dilated cardiomyopathy	DCM
Dissociation constant	K_d
Electrical potential across the sarcolemma	E_M
Electrocardiogram	ECG
Excitation contraction	EC
Faraday constant	F
Flippase recognition target	FRT
Green fluorescent protein	GFP
Hypertrophic cardiomyopathy	HCM
Implantable cardiac defibrillators	ICD
Intercalated disc	ID
Inward rectifying K^+ channel	Kir
Kelvin	K
Kilodalton	kDa
Madin-Darby Canine Kidney	MDCK
Magnesium	Mg^{+2}
Membrane-binding domain	MBD
Micromolar	μM.
Millimolar	mM

Millivolts	mV
Mitochondrial uniporter	MCU
Modified Tyrode	MT
Molar	M
Mole	mol
Na^+ current density	I_{Na}.
Na^+/Ca^{+2} exchanger	NCX
Na^+/K^+ ATPase pump	NKA
Nanometer	nm
Nanomolar	nM
Nernst potential for K^+	E_K
Nernst potential for Na^+	E_{Na}
Neurofascin-186	NF-186
Neuronal cell adhesion molecule	NrCAM
Nitogen	N_2
Oxygen	O_2
Permeability of Cl^-	pCl
Permeability of K^+	pK
Permeability of Na^+	pNa
Phosphate-buffered saline	PBS
Plakoglobin	JUP
Plakophilin-2	PKP2

Potassium	K^+
Ryanodine receptor type 2	RyR2
Sarcoplasmic reticulum	SR
Sarcoplasmic reticulum ATPase pump	SERCA2a
Short hairpin RNA	shRNA
Sinoatrial	SA
Small interfering RNA	siRNA
Sodium	Na^+
Spectrin binding domain	SBD
Sudden cardiac arrest	SCA
Transverse aortic constriction	TAC
Valence	z
Voltage-gated sodium channel	Na_V
Wild Type	WT
Zonula occludens 1	ZO

Chapter 1: Introduction

The heart is tasked with pumping oxygen and nutrient rich blood to every tissue in the body through a myriad of arteries, arterioles, and capillaries. The singular purpose of the organ leads many lecturers to begin extensive lessons on cardiac physiology with the following phrase: "The heart is a pump." In essence, all pumps work the same way. One form of kinetic energy (electrical, thermal, magnetic, etc.) is translated into mechanical energy to forcibly move fluids. The heart itself is an electromechanical pump, translating an electrical signal (action potential) into mechanical energy (contraction). Using the analogy of the pump, there must be a mechanical component to the organ that can perform work necessary to pump blood throughout the body. The pumping function of the heart derives from the highly *synchronized* contraction of millions of cardiac muscle cells (cardiomyocytes) in response to a *coordinated* electrical activation of the heart. However, despite major advances in the understanding of cardiac physiology and disease from the single molecule to the organ system level, cardiovascular disease (CVD) remains the number one cause of death in the United States, claiming nearly 800,000 lives each year[1].

Several factors contribute to this alarmingly high rate of CVD-related deaths. First, an estimated 85.6 million American adults are currently living with one or more types of cardiovascular disease, including hypertension, angina pectoris, myocardial

ischemia or infarction, stroke, and heart failure[1]. Second, average life expectancy has increased significantly over the past century. According to the 2016 Heart Disease and Stroke Statistics published by the American Heart Association, of the aforementioned 85.6 million U.S. adults living with CVD, an estimated 43.7 million of these individuals are 60 years of age or older[2]. As CVD incidence increases with age, statistical probability dictates that more cases of CVD will be seen. Although CVD was generally believed to be an aging-related disease, the rates of obesity and diabetes in American adults and, sadly, adolescents have increased steadily year after year. Unfortunately, due to the increases in these comorbidities, CVD is rapidly becoming a concern at younger and younger ages[2].

Regardless of the underlying cause of cardiac dysfunction[3], more than 50% of patients with CVD die of suddenly of arrhythmia, or abnormal electrical regulation of the heart.[4, 5] During an arrhythmia, the pattern of electrical activation in the heart is disrupted, compromising cardiac pump function as a result. Unfortunately, in many patients with CVD, the arrhythmias developed are so severe as to produce complete cessation of cardiac pump function, rapidly leading to the death of the patient, a phenomenon known as sudden cardiac arrest (SCA). As approximately 210,000 individuals die each year of SCA in the United States[2], development of antiarrhythmic therapies has remained at the forefront of modern medical science. Unfortunately, even with an entire field focused on this problem, therapeutic treatment and prevention of arrhythmia remains lacking. For prevention of secondary sudden cardiac arrest (i.e. patient has already suffered an SCA), implantable cardioverter-defibrillator (ICD) therapy offers the greatest benefit in most

patient populations[4]. However, these devices interrupt arrhythmia by delivering a painful and debilitating electrical shock, severely decreasing quality of life for the patient. For primary prevention of SCA (i.e. patient has not suffered SCA, but is at risk[6]), medical therapy with anti-arrhythmic drugs (e.g. β-blockers, Class I/III anti-arrhythmic drugs, etc.) and/or anti-hypertensives (ACE inhibitors, aldosterone antagonists, etc.) is generally advised prior to implantation of an ICD[4]. Although some medical therapies show promise in reducing rates of SCA[7, 8], several clinical trials have demonstrated that anti-arrhythmic drug therapy can result in increased mortality compared to placebo in patients with CVD[9, 10]. More striking, 25% of patients suffering primary SCA have no symptoms before experiencing cardiac arrest[2]. These failed attempts to medically prevent primary and secondary SCA demonstrates the extremely complex nature of human arrhythmias. **In order to reduce the burden of SCA clinically and develop/refine therapeutic options, we must first gain new insight into basic cardiac physiology and pathophysiology at the molecular, cellular, organ, and animal level.**

Electrical Activation of the Heart: Stimulus for Contraction

The heart itself is composed of four chambers consisting of two atria and two ventricles. For the heart to function as a pump, the atria and ventricles must contract and eject blood, with the atria contracting ahead of the ventricles. When a chamber contracts (systole) it ejects blood uni-directionally into the adjacent chamber or artery. To effectively pump blood, however, the chambers must relax (diastole) to fill for the next heartbeat. Importantly, for a chamber to contract, the cardiomyocytes comprising the

chamber need to be excited by an action potential[11]. As a result, the heart has developed a highly coordinated pattern of electrical stimulation necessary to produce synchronized pump function. Clinically, we can monitor the electrical activation of the heart using the electrocardiogram (ECG). A representative waveform is shown illustrated in Figure 1[12]. The electrical impulse necessary to stimulate contraction originates in a specialized collection of cells in the right atrium known as the sinoatrial (SA) node[13]. Also termed the pacemaker of the heart, the SA node spontaneously generates action potentials and therefore sets the rate at which the myocardium (heart muscle) is excited[14], approximately 60 beats per minute in humans. Having a heart rate too low (<60 bpm) or too high (>100 bpm) results in arrhythmias termed bradycardia and tachycardia, respectively[15]. The SA nodal impulse propagates to and activates the right and left atrium, causing atrial systole. This corresponds to the P-wave on the ECG. Before the atria contract, however, the majority of blood entering the atria flows passively through the atrioventricular valves (tricuspid and mitral) and into the ventricle. This passive flow represents 80% of the ventricular end diastolic volume. After atrial systole, the remaining 20% of ventricular end diastolic volume is pumped from the atria to the ventricles. This event is often termed the "atrial kick."[16] As most of the blood entering the ventricles arrives via passive flow, atrial function is not strictly necessary for life. For example, the most common arrhythmia seen clinically is termed atrial fibrillation (AF), an erratic and uncoordinated activation of the atria. Although this condition can severely impair atrial function, this arrhythmia is not as life-threatening due to the extensive

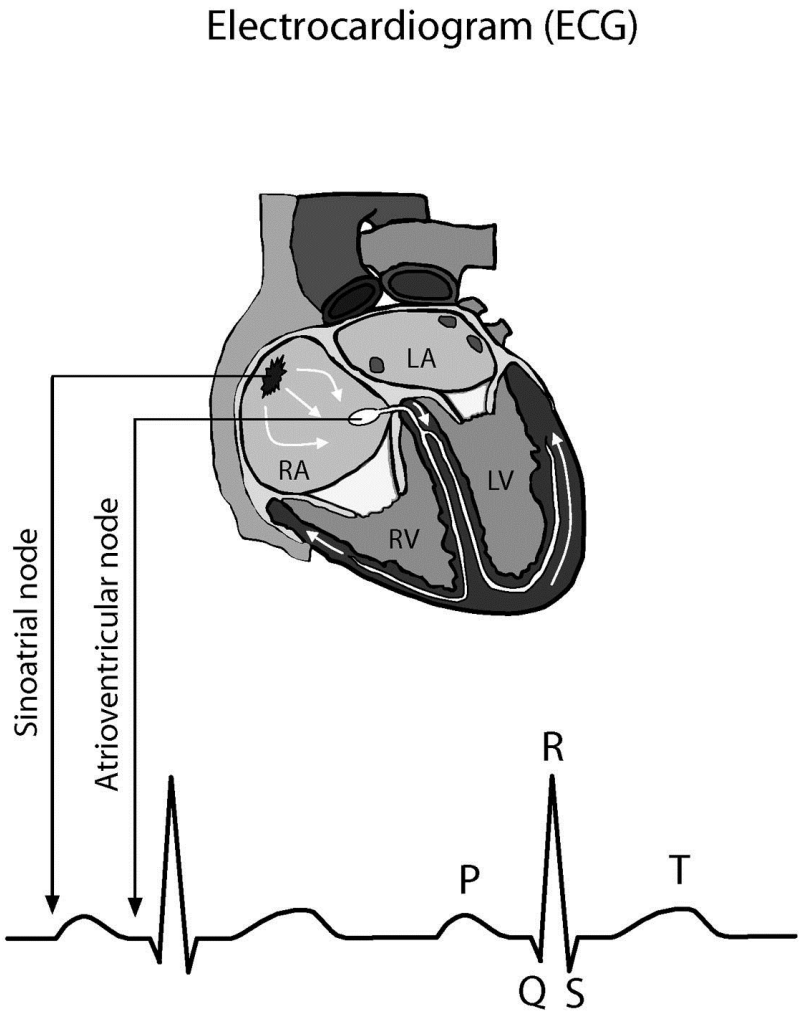

Figure 1. The cardiac conduction system and electrocardiogram (ECG).

White arrows trace the spread of electrical activation through the heart. A representative ECG waveform is also presented, correlating changes in the ECG with spread of electrical activation through the heart. RA= right atria, RV= right ventricle, LA=left atria, LV=left ventricle

amount of passive ventricular filling. However, as blood can pool and clot in the fibrillating atria, AF patients are routinely placed on anti-coagulation therapies[17].

Once the electrical impulse propagates through the atria, it then encounters a non-conducting fibrous annulus between the atria and ventricles. This blockage of electrical activation is necessary to ensure that the atria contract before the ventricles, providing time for the atrial kick during ventricular filling. However, the electrical signal must propagate to the ventricles to produce ventricular systole. This pathway is provided by another group of specialized cells known as the atrioventricular (AV) node. The primary role of the AV node is to slow the impulse to keep atrial systole out of phase with ventricular systole. At this time, there is no activation of the myocardium, corresponding to the PR interval on the ECG. The AV node then conducts the impulse to the AV bundle (or bundle of His) where it is transferred to the high-velocity conduction pathways known as the right and left bundle branches. Composed of cells known as Purkinje fibers, the right and left bundle branches rapidly conduct the impulse to the ventricular tissue, causing ventricular systole. This corresponds to the QRS complex on the ECG. In some patients, the transfer of the impulse from the atria to the ventricles can be blocked. The ECG of these patients displays a P wave without a subsequent QRS. This arrhythmia is AV block or Type II heart block[15].

After electrically activated, the ventricles contract. This contraction causes an increase in chamber pressure that closes the unidirectional AV valves, preventing backflow of blood into the atria. The ventricles first contract without a change in ventricular volume (isovolumic contraction). When the developed pressure in the

ventricle overcomes pressure present in the pulmonary artery in the case of the right ventricle and aorta in the case of the left, the semilunar valves open causing rapid ejection of blood into either the pulmonary or systemic circulation. As mentioned earlier, the chambers of the heart must also relax (i.e. diastole) and fill with more blood to be an effective pump. After systole, both chambers undergo a period of relaxation without a change in ventricular volume (isovolumic relaxation). Using the left ventricle as an example, when left ventricular pressure drops below left atrial pressure, the mitral valve opens allowing blood flow and increases left ventricular volume[16]. The relaxation (or repolarization) of the ventricles corresponds with the T-wave on the ECG. The interval from the onset of the QRS complex until the end of the T-wave is termed the QT interval[15]. Clinically, lengthening of the QT interval is associated with increased probability of ventricular tachyarrhythmias[15]. Importantly, many of the arrhythmias resulting in SCA occur within the ventricles, making these chambers of central importance to the study of arrhythmia[4].

As is often the case with large problems, the genesis of cardiac arrhythmia begins with a very small cause: dysregulation of excitability at the level of the individual cardiomyocyte. The presence of specific combinations of ion channels, transporters, and membrane ion pumps underlies the excitable nature of the individual cardiomyocyte. A common finding in multiple forms of CVD, however, is remodeling of these electrical constituents of the cardiomyocyte plasma membrane, producing dysfunctional excitability in the heart at the cellular level. Coupled with structural remodeling at the cardiac tissue level (e.g. fibrosis, pathological hypertrophy, infarct, etc.), aberrant

cardiomyocyte excitability is a breeding ground for the trigger and sustainment of cardiac arrhythmia[15]. **In order to effectively treat cardiac arrhythmia, we must first understand the cellular mechanisms producing normal cardiac cellular excitation as well as the molecular disruptions responsible for altered cardiomyocyte excitability**.

Cardiac Ankyrins and Congenital Human Arrhythmia

Adding another layer of complexity are the significant numbers of patients harboring genetic mutations causing fatal cardiac arrhythmia. Since the 1980's, multiple studies have linked single nucleotide polymorphisms with human arrhythmia diseases such as Long QT syndrome[18], Brugada syndrome[19], atrial fibrillation[20], and catecholaminergic polymorphic ventricular tachycardia[21]. Most of these genetic variants occur in genes encoding for the transmembrane, pore-forming subunits of various cardiac ion channels. However, ion channels themselves are not singular proteins. They are macromolecular complexes composed of the pore-forming subunit (α-subunit), modulatory β-subunits, and what are classically termed channel interacting proteins. Associated with the majority of ion channels, channel interacting proteins can influence ion channel forward trafficking, membrane retention and recycling, and local regulation.

Evidence for the importance of channel interacting proteins for cardiac excitability came in 2003 with the identification of a human variant in the gene *ANK2* in a French kindred with a family history of Long QT syndrome and sudden cardiac death[22]. *ANK2* encodes for the intracellular scaffolding protein ankyrin-B. The family of ankyrin polypeptides consists of three members: ankyrin-R, ankyrin-B, and ankyrin-G (encoded

by genes *ANK1*, *ANK2*, and *ANK3* respectively). Derived from the Greek word *ankyra* meaning anchor[23, 24], ankyrins bind directly to integral membrane proteins within the plasma membrane and anchor them to molecules known as spectrins in the underlying cytoskeletal architecture. With respect to cellular excitability, ankyrin polypeptides are responsible for the development of densities of voltage-gated sodium (Na_V) channels at the axon initial segment in neurons necessary for the generation of electrical impulses known as action potentials[25, 26]. Ankyrins also play structural roles in cells, targeting cell adhesion molecules known as cadherins in epithelial cells, necessary for the biogenesis of the lateral membrane[27, 28]. Further highlighting the importance of ankyrin-dependent membrane organization, human variants in each member of the ankyrin family have been associated with severe human diseases ranging from structural deformities in red blood cells to neuropsychiatric disorders and cardiac arrhythmia.[29-31]. These roles of ankyrins in human disease will be detailed in later sections. Using mice heterozygous for *Ank2* null allele, Mohler et al., 2003 demonstrated that ankyrin-B was necessary to target several molecular transporters, such as the Na^+/K^+ ATPase (NKA) pump and Na^+/Ca^{+2} exchanger (NCX), in the cardiomyocyte plasma membrane[22]. Further, haploinsufficiency of ankyrin-B in mice led to extreme heart rate variability, QT interval prolongation, and severe ventricular arrhythmia leading to animal mortality. Subsequently, work from the Mohler lab demonstrated that human variants in ankyrin-B also linked with atrial fibrillation[31], sinus nodal disease[32], and sudden cardiac death[33, 34].

Clearly the evidence indicates an indispensable role for ankyrin polypeptides in human cardiac physiology. However, most of the study on cardiac ankyrins has focused

specifically on ankyrin-B. This changed in 2004, when a 47-year old female with a history of heart palpitations was admitted to the emergency room after suffering a syncopal episode at rest[35]. Upon admittance, the patient demonstrated runs of self-terminating ventricular tachycardia and a 1 mm ST-elevation. Echocardiographic investigation demonstrated a structurally normal heart and programmed electrical stimulation could not evoke any clinically relevant arrhythmia. On the basis of the presentation, a diagnosis of Brugada syndrome was given. Brugada syndrome was confirmed by intravenous infusion of flecainide eliciting a 3 mm ST elevation with coved type morphology (Type I Brugada syndrome)[36]. At the time, Brugada syndrome was primarily associated with loss-of-function mutations in the *SCN5A* gene[37], encoding the cardiac isoform of the voltage-gated sodium channel Nav1.5. These *SCN5A* mutations led to decreases in cardiomyocyte sodium current, disrupting cardiac excitability as a result. Sequencing of the *SCN5A* gene in this patient revealed a single nucleotide variation G3157A, encoding for a glutamic acid (E) to lysine (K) transition mutation at position 1053 (E1053K). This mutation occurred in a highly conserved stretch of amino acids present in many Na_V channel isoforms. Two independent investigations in 2003 demonstrated that this stretch of nine amino acids (VPIAVA**E**SD) was sufficient to interact with the adapter protein ankyrin-G (encoded by human *ANK3*)[38, 39].

Knowing this, Mohler et al., 2004 demonstrated that Nav1.5 associated with 190 kDa ankyrin-G in cardiac tissue. Further, the researchers determined that the E1053K mutation inhibited the ankyrin-G/Nav1.5 interaction, leading to disrupted cellular localization of virally-transduced E1053K Nav1.5 channels in isolated rat

cardiomyocytes. Although mutant channels displayed alterations in the properties of activation, inactivation, and recovery from inactivation (explained in detail in the following sections), it was hypothesized that the arrhythmia witnessed in the patient were due to dysregulated cellular targeting of Nav1.5 leading to decreased cellular sodium current[35]. This investigation was followed by work conducted by John Lowe in 2008. Lowe, using shRNA-mediated knockdown of ankyrin-G expression in neonatal rat cardiomyocytes, demonstrated that the absence of ankyrin-G in cardiomyocytes caused decreases in functional sodium current explained by alterations in cellular targeting of Nav1.5[40]. Although these in vitro experiments demonstrated a functional requirement of ankyrin-G for proper cardiac excitability, the role of ankyrin-G in the heart in vivo is unknown and untested. **The primary objective of this study is to determine the molecular function of ankyrin-G with respect to cardiac physiology and pathophysiology.** Before we can understand how ankyrin-G regulates cardiac physiology, we must first investigate the discovery of ankyrin polypeptides and their role in the organization of the plasma membrane of the cell.

Evolution of the Cell Membrane Hypothesis

Although the existence of the cell membrane has been known since the late 17th century[41], the molecular composition remained unknown until relatively recently. The determination of the molecular identity of the cell membrane is classically credited to Charles Ernest Overton. Overton, using biological membranes isolated from various tissues, tested the permeabilities of those membranes to various dissolved solutes.

Overton found that polar hydrophilic substances such as sugars, amino acids, salt compounds, and glycerol rarely crossed the plasma membrane whereas hydrophobic molecules such as aldehydes, alcohols, and hydrocarbons rapidly diffused across the plasma membrane with rates comparable to that of water. Further, Overton found that dyes that readily dissolve in lipid crossed the plasma membrane at a faster rate than lipid-insoluble dyes. Overton concluded that, due to the high permeability of the plasma membrane for lipophilic substances, the plasma membrane must be primarily composed of lipids[42]. Clues as to the molecular arrangement of the lipids the plasma membrane began with a study published in 1925 by Dutch scientists Gorter and Grendel looking at acetone-solubilized red blood cell membranes[43]. Based on a finding by Langmuir that lipids will form a monolayer on the surface of water, Gorter and Grendel compared the surface area covered by the solubilized membrane lipids compared to the calculated surface area of intact cells. Gorter and Grendel arrived at a ratio of 2:1, implying that lipids are arranged as a bilayer in biological membranes[43].

Building on the findings of Gorter and Grendel, English biologists Davson and Danielli proposed that the plasma membrane indeed contained a lipid bilayer, but this arrangement was not enough to account for the surface tension of the plasma membrane. To account for this, Davson and Danielli proposed that the bilayer is encased in proteinaceous material that also formed pores in the plasma membrane. This hypothesis, also termed the paucimolecular membrane model[44], was the leading theory of the cell membrane until 1972 when S.J. Singer and Garth Nicolson proposed their theory of the fluid mosaic model[45]. In their theory, Singer and Nicolson classified cellular proteins into

two classes: 1) peripheral proteins that were hydrophilic and required little solublization and 2) integral or membrane-associated proteins that were amphipathic, with both hydrophilic and hydrophobic areas enabling them to span the plasma membrane. As hydrophilic amino acid residues in the protein would be able to associate with the aqueous environment and hydrophobic amino acid residues located in the lipid bilayer, the fluid mosaic model is thermodynamically favorable compared to the Davson-Danielli hypothesis.

Singer and Nicholson envisioned these integral membrane proteins as icebergs floating on an ocean as discrete structures. However, this hypothesis implies that the integral membrane proteins can "float" around freely in the plasma membrane. However, we now know that these integral membrane proteins are "anchored" to specific membrane microdomains. One of the ways the cell has evolved to achieve the molecular anchorage is through the family of ankyrin polypeptides. Classically, ankyrin polypeptides bind to integral membrane proteins in the plasma membrane and anchor them to proteins known as spectrins in the underlying cytoskeleton. Although this investigation primarily centers on the molecular biology of ankyrin polypeptides, to understand the historical context of this investigation, we must first review the discovery of spectrin polypeptides.

Seminal Discovery and Investigation of Ankyrin Polypeptides

The discovery of spectrin polypeptides predates the discovery of ankyrin by more than a decade. In 1967, Marchesi and Palade demonstrated that trypsinized red blood cell

membrane fragments, also known as membrane ghosts, were associated with a proteinaceous material that formed coiled filaments visible by electron microscopy[46]. Published in *Science* in 1968, Marchesi and Steers, working again with erythrocyte membrane ghosts, perfected a way to purify and enrich the material that was associated with the red blood cell membrane. In doing so, the treatment caused the membranes to break up into small pieces, leading the researchers to hypothesize that this protein played a structural role in the erythrocyte. Because this protein was extracted from red blood cell ghost membranes, the researchers termed this new protein "spectrin"[47]. Subsequent investigations also demonstrated that spectrins interacted with globular actin. Published in *Nature* in 1975, Pinder et al. further showed that spectrin causes rapid polymerization of actin filaments. Pinder and colleagues demonstrated that preparations of pure actin or pure spectrin showed very slowly developing polymers as seen by electron microscopy. However, incubation of globular actin with spectrin molecules promoted rapid actin polymerization, causing increased viscosity of the preparation and visualized again via electron microscopy[48].

However, some uncertainty existed as to the precise cellular localization of the spectrin proteins. A key finding came in 1971, when Nicolson, Marchesi, and Singer demonstrated that these red blood cell ghost membranes can "reseal" into biconcave membranes when placed into isotonic solution. After fixation of the resealed membrane, ferritin-conjugated antibodies against human spectrin showed immunoreactivity only on the intracellular aspect of the red blood cell membrane preparations[49]. This led the researchers to conclude that spectrin is a cytoplasmic protein. However, this study gave

no indication as to whether the association of spectrin with the plasma membrane was direct or indirect through another protein. Published in 1977, elegant work by Bennett and Branton, using inside-out membrane preparations depleted of spectrin and actin, demonstrated that radiolabeled (^{32}P) spectrin associates with the intracellular aspect of the plasma membrane with a relatively high affinity (dissociation constant (K_d) = 10^{-7} to 10^{-8} M). They further showed that this binding was saturable at a high spectrin concentration and inhibited at high pH or with increasing amounts of unlabeled spectrin. Importantly, proteolysis of inside-out membrane ghosts completely abolished spectrin membrane binding. This led the researchers to hypothesize that the spectrin-membrane interaction occurred through an indirect association with an intermediary protein[50].

Interestingly, light proteolysis with trypsin inhibited approximately 50% of spectrin membrane association. At the same time, this proteolysis was sufficient to reduce the high molecular weight erythrocyte membrane proteins Band 2.1 and Band 3 almost entirely. Early electrophoretic experiments of erythrocyte membranes revealed the presence of distinct and reproducible banding patterns, with Bands 1 and 2 correlating with the spectrin polypeptides. Interestingly, cross-linking studies demonstrated that Band 1 and 2 associate as a dimer, early evidence of the existence of alpha and beta spectrin isoforms (explained in detail below). The identity of the remaining bands continued to elude the investigators, but due to large amounts of proteolysis of Bands 2.1 and Band 3, the researchers hypothesized that neither Band 2.1 nor Band 3 could serve as direct membrane attachment sites for spectrin. Still, the investigation posited that another

intermediary protein may use these membrane proteins as an attachment site and scaffold the spectrin molecules to the erythrocyte plasma membrane[50].

However, this hypothesis turned out to only be half-correct. Although an indirect, intermediate scaffolding protein between spectrin and the plasma membrane had been hypothesized, no evidence existed as to the identity of this molecule. In a study published in the *Journal of Biological Chemistry* in 1978, Bennett again showed that alpha-chymotrypsin digestion of inside-out red blood cell membrane ghosts inhibited ^{32}P-spectrin association with the membrane. Similarly, Band 2.1 and Band 4.1 also demonstrated near complete loss of expression following digestion. Further, following digestion, a 72 kDa fragment was released into solution. This 72 kDa fragment also complexed with native spectrin molecules with a 1:1 stoichiometry and competitively inhibited ^{32}P-spectrin association with the actin-spectrin depleted inside-out membrane preparations. Although the identity of the full-length protein mediating the membrane association of spectrin was not determined in this study, an antibody was created against the isolated 72 kDa fragment[51].

The hidden identity of the 72 kDa fragment was revealed in 1979 in a study by Bennett and Stenbuck. Using the newly developed anti-72 kDa antisera, Bennett and Stenbuck demonstrated that this antibody, when incubated with red blood cell membranes, specifically immunoprecipitated Band 2.1, a protein previously believed to not be the membrane attachment site for spectrin. Further, incubation of spectrin-depleted red cell membranes with increasing amounts of purified Band 2.1 inhibited spectrin reassociation. In light of these findings, Bennett and Stenbruk concluded that they had

identified the membrane attachment site for spectrin, suggesting that this protein be named ankyrin due to its anchoring capabilities[23, 24]. Subsequent investigation demonstrated that ankyrin associated with the cytoplasmic surface of with the transmembrane protein Band 3 in the erythrocyte plasma membrane with 1:1 stoichiometry[52]. This would become the basic model of ankyrin function: 1 molecule of ankyrin would associate with 1 integral membrane protein at one time. This ankyrin molecule would in turn interact with 1 molecule of spectrin in the cytoskeleton (i.e. one of the spectrin molecules in the spectrin dimer). The importance of the Band 3 – ankyrin – spectrin complex for red cell morphology is classically demonstrated by human variants in Band 3, ankyrin, and spectrin producing severe structural changes to the red cell membrane[29, 53, 54].

Canonical Structure of Ankyrins and Spectrins

In order to understand exactly how this ankyrin-spectrin complex functionally forms, we must first discuss the canonical structure of ankyrins and spectrins. Canonical ankyrin polypeptides can be divided into 3 functional domains: The membrane-binding domain (MBD), the spectrin binding domain (SBD), and the C-terminal domain (CTD). Originally identified as a 100 kDa membrane-attached fragment[55], the MBD is the primary site for ankyrin interaction with integral membrane proteins. The MBD is composed of 24 ankyrin (ANK) repeats[56], highly conserved protein binding motifs consisting of 33-34 amino acids arranged in a helix-turn-helix morphology[57]. The connections between the individual ankyrin repeats are highly variable in amino acid

identity, forming β-hairpin loops between adjacent ANK repeats often the site of protein-protein interaction. These β-hairpin loops are perpendicular to the helix-loop-helix motif, producing an L-shape to each repeat[57]. The 24 ANK repeats are then arranged in a super-helix forming a spiral hook, with the β-hairpin loops oriented to the inside of the cavity, readily accessible for protein-protein interaction[58]. Interestingly, ANK repeats are one of the most common protein motifs found in nature[59]. Although highly conserved domains, ANK repeats show a high degree of specificity for their interaction partners in part mediated by these β-hairpin domains[57].

The spectrin binding domain was first identified as the 72 kDa fragment released after digestion of red blood cell ghost membranes[51]. The SBD contains 2 ZU5 domains and 1 UPA domain arranged as ZU5-ZU5-UPA[60, 61]. Using truncated constructs of ankyrin-B, Mohler et al. 2004 demonstrated that the spectrin binding capability of ankyrin requires a 160 amino acid stretch (ankyrin-B 220 residues 966-1125) containing the first ZU5 domain with a small C-terminal portion. Further, targeted mutagenesis of ankyrin-B at DAR976AAA and A1000P (analogous to DAR999AAA and A1024P in ankyrin-G[28]) were sufficient to disrupt the ankyrin-spectrin interaction in neonatal cardiomyocytes[62]. Compared to the MBD and SBD, the function of C-terminal domain of ankyrin is the least-well known. The CTD of ankyrin is the most divergent among the domains, with ~11% homology between the c-terminus of ankyrin-B and ankyrin-G[63]. Clues to the function of the CTD arose in 1987 with the identification of Protein 2.2 in red blood cells, a splice form of ankyrin-R lacking amino acids 1513-1674 of the C-terminus. This ankyrin splice form bound to spectrin with a 3-fold higher affinity

compared to ankyrin comprising Band 2.1[64]. Further this isoform showed increased affinity for binding tubulin. Further investigations demonstrated that the C-terminal domain of ankyrin is responsible for mediating its cellular localization and function in neonatal cardiomyocytes[65].

The spectrin family of polypeptides is composed of two α-subunits and five β-subunits, each with multiple splice variants. From very early on in their discovery, spectrin polypeptides demonstrated the remarkable ability to self-assemble into polymers[47]. The smallest unit of assembly is a dimer[66] composed of an α- and β-spectrin polypeptide arranged in an antiparallel, head-to-toe fashion[67]. Further, in 1981 Morrow and Marchesi demonstrated that these αβ-dimers could stably associate into tetramers[68], visualized as ~200 nm rods 2 years prior by Shotton[69]. In 1984, Speicher and Marchesi demonstrated the presence of 106-amino acid repeats assembled into triple helices, what we now call spectrin repeats[70]. In 1990, Tse et al. demonstrated the molecular basis of tetramerization of spectrin dimers. The tetramers themselves associate as dimers opposed head-to-head, with the C-terminus of β-spectrin on one dimer contributing 2 helices and the N-terminus of α –spectrin on the adjacent dimer contributing 1 helix to form another spectrin repeat as a connector[67]. Early electron microscopic investigation indicated that ankyrin associated with the spectrin tetramer toward the middle of the polymer[71]. We now know that ankyrin polypeptides associate with β-spectrins at the 15th spectrin repeat[72]. β-spectrins also contain an actin-binding domain in their N-terminus facilitating the interaction between filamentous actin and the spectrin tetramer[73].

Although many early publications describe the role of ankyrins in red blood cells, the most significant finding in the study of ankyrins occurred in 1979. In publication in *Nature* in 1979, Bennett isolated membrane preparations from rat liver, brain, testes, kidney, and fat[74]. Using the antisera developed against the 72 kDa fragment, Bennett discovered that all these membrane preparations showed positive immunoreactivity for ankyrin. Because of the presence of ankyrin isoforms in the brain, the literature at this point begins to refer to the separate isoforms as ankyrin-R (for red blood cell) and ankyrin-B (for brain). This nomenclature appeared long before the identification of the *ANK1* gene on chromosome 8 encoding for ankyrin-R[75] and the *ANK2* gene on chromosome 4 encoding for ankyrin-B[76]. In reality, ankyrin-R and ankyrin-B are expressed in multiple tissues and together within the same cell. Further, a third ankyrin gene was discovered in 1995 located on chromosome 10. Given the gene name *ANK3*, this ankyrin isoform was shown to be expressed in multiple tissue types and included isoforms with very high molecular weight (~480 kDa). Because of its "general expression" and "giant size," this isoform of ankyrin was named ankyrin-G[77, 78].

Experimental Silencing of Ankyrin-G in the Cardiomyocyte

Now that the discovery and basic properties of ankyrin polypeptides have been discussed, we return to the primary objective of this dissertation: What is the role of ankyrin-G in the heart in vivo? Although we have in vitro data describing a select role for ankyrin-G in mediating cardiac excitability through its interaction with voltage-gated sodium channels, no in vivo data exist regarding the exact molecular function of ankyrin-

G in cardiac tissue. To answer this question, we have developed a cardiac-restricted ankyrin-G knockout (cKO) mouse. Through homologous recombination of a targeting vector, loxP sites were inserted flanking exons 22 and 23 of the *Ank3* mouse gene[79]. These 34 base-pair loxP sites can be thought of as "cut sites" added to the murine genome[80]. In the presence of the enzyme Cre recombinase, this stretch of DNA is excised, creating a premature stop codon within the Ank3 gene to prevent transcription. However, the Cre recombinase transgene in this animal model is under the control of the *Myh6* (α-myosin heavy chain) promoter, restricting its expression specifically to cardiomyocytes (atrial, ventricular, nodal)[81]. In the mouse, the *Myh6* promoter begins to become activated around embryonic day 11 with expression peaking from postnatal day 0 to 60[82]. This means that in this system, ankyrin-G expression is maintained during embryonic development and is silenced at the birth of the animal. Further details and characterization of this model can be found in Chapters 2 and 3 of this dissertation. Importantly, this ankyrin-G cKO mouse gives us the means to address our primary objective. However, a very important question has remained unaddressed to this point: what are my hypotheses regarding the function of ankyrin-G in the cardiomyocyte in vivo? A daunting question, indeed, given the small amount of data reported even mentioning ankyrin-G with respect to the heart. Fortunately, due to its ubiquitous nature, we have a wealth of experimental investigations detailing the function of ankyrin-G in a multitude of cell types. Specifically, studies conducted in renal and bronchiolar epithelium and neurons will be the primary experimental precedence upon which my hypotheses are built.

Ankyrin-G Regulates Ion Transport and Cellular Structure in Epithelial Cells

Epithelial cells line the external surface of all organs and are responsible for the entrance of all nutrients and exit of all waste from the organism as a whole. Recall, however, that the plasma membrane is impermeable to the flow of amino acids, glucose, and other nutrients into the cell. As the body requires these molecules in large quantities to sustain organ function, the epithelial cell membrane has evolved multiple pathways to facilitate the transport of these entities from the external environment and into systemic circulation. Let us use glucose transport in gut epithelium as an example. Maintenance of organ metabolism requires large amounts of glucose present to be converted into ATP for cellular energy. As a result, the apical epithelial membrane of the gut lumen, exposed to the external environment, must be able to scavenge the high concentrations of ingested glucose at a very high rate. However, the plasma membrane is impermeable to glucose and requires the presence of a glucose transporter[83]. Further, cytosolic concentration of glucose is relatively high compared to the concentration in the gut. Therefore, if this glucose transporter were just a pore that allowed free diffusion of glucose across the membrane, glucose would efflux out of the epithelial cells, severely decreasing the amount of glucose available to the organs of the body. Instead, diffusion of glucose into the epithelial cell is coupled to the very large Na^+ concentration gradient through the sodium/glucose symporter located on the apical cell membrane. As the dietary Na^+ concentration in the gut lumen is relatively high (~20 mM) compared to the cytosolic environment (~5mM), this drives glucose into the cell, enabling the absorption of as much glucose as possible from the gut lumen. However, this causes a large accumulation

of both glucose and sodium inside the epithelial cell. Glucose transporters on the basolateral membrane allow diffusion of glucose down its concentration gradient, out of the epithelial cell, and into the circulation[83]. But what about the large amount of cytosolic Na^+? A protein known as the Na^+/K^+ ATPase (NKA), located on the basolateral epithelial membrane is responsible for resetting the Na^+ gradient within epithelial cells. NKA, using chemical energy in the form of ATP, extrudes 3 Na^+ ions into the circulation and bring $2K^+$ ions into the cell. This resets the primary ionic gradients in the cell, enabling facilitated diffusion of glucose to occur again[84]. Therefore, this lateral membrane specification is critically important to the proper function of epithelial cells. Further, the function of NKA will become very important during our investigation of the electrical principles of excitable cells.

Several reports in the late 1980s demonstrated that ankyrin coimmunoprecipitated and colocalized with NKA in the basolateral membrane of Madin-Darby Canine Kidney (MDCK) cells and isolated renal tubule epithelium[85, 86]. Further investigations would demonstrate that epithelial ankyrin associated with spectrin, termed fodrin in the early literature, in the basolateral membrane in epithelial cells[85]. Interestingly, upon cell-cell association, soluble ankyrin-spectrin complexes become increasingly associated with NKA as demonstrated by co-sedimentation experiments[87, 88]. Similar to erythrocytes, ankyrin was also shown to associate with the anion exchanger, originally termed Band 3, at the basolateral membrane in renal epithelium[86]. This finding implied that ankyrin could possibly associate with multiple membrane proteins. However, in 1990, Davis and Bennett demonstrated that Band 3 and NKA associated with distinct sites on the ankyrin

molecule. Unlike Band 3 that interacted with the MBD of ankyrin with high affinity, the NKA-ankyrin association required the presence of the spectrin binding domain[89]. This finding seems insignificant at first. However, from an evolutionary standpoint, this result implies that the ankyrin polypeptide structure had evolved first and that Band 3 and NKA evolved ankyrin binding ability over time through divergent pathways. This explains the lack of a consensus ankyrin-binding site in integral membrane proteins. Upon the discovery of the *ANK3* gene in 1995, Peters et al., demonstrated that ankyrin-G was the primary ankyrin isoform expressed in the kidney, with only trace amounts of ankyrin-R and ankyrin-B[78]. In 1998, Thevananther et al., demonstrated the presence of an ankyrin-G isoform was 190 kDa in size that was restricted to lung and kidney epithelium[90]. Interestingly, cardiac tissue also showed the presence of 190 kDa ankyrin-G, which would later be shown to be the primary isoform of ankyrin-G expressed in the heart[35]. Similar to the findings of Davis and Bennett in 1990, Thevananther et al., showed that NKA associated with 190 kDa ankyrin-G at 2 distinct sites in vivo, one site in the distal N-terminus and one site in the spectrin binding domain. This study further showed that 190 kDa ankyrin-G localized specifically to the lateral membrane of MDCK cells[90].

As discussed previously, epithelial cells act as a physical barrier between the cells of the organ and the external environment. As a result, the epithelial cells have evolved molecular complexes to prevent the leak of fluid into the tissue, termed tight junctions, an anastomosing network of claudins, occludins, and junctional adhesion molecules linked to the actin cytoskeleton through an interaction with the protein zonula occludens 1 (ZO-1)[91]. Further, to increase the mechanical strength of the epithelial border, the epithelial

cell contains adherens junctions and desmosomes that link cell-cell contacts with the actin and intermediate filament cytoskeleton respectively[92]. The cell adhesion molecule E-cadherin is the integral membrane component mediating cell-cell adhesion at the epithelial adherens junction. Classically, E-cadherin forms homophilic cell-cell contacts in a Ca^{+2} dependent manner. The cytoplasmic domain of E-cadherin is then linked to p120, β-catenin, and α-catenin that scaffolds the membrane E-cadherin to the actin cytoskeleton[92]. In 1990, Nelson et al., demonstrated that ankyrin also associated with E-cadherin in renal epithelial cells. Recall that ankyrin-spectrin localization to the basolateral membrane in renal epithelium was increased by cell-cell contact. Further, truncation of the cytoplasmic domain of E-cadherin inhibited NKA and ankyrin-spectrin localization to the lateral membrane, suggesting that E-cadherin recruits these molecular players[93].

Fifteen years later, evidence of the functional importance of this ankyrin-cadherin interaction to epithelial biology came in a 2004 study by Kizhatil and Bennett published in the *Journal of Biological Chemistry*[27]. In this study, the researchers used small interfering RNA (siRNA) to knockdown expression of the 190 kDa isoform of ankyrin-G in human bronchiolar epithelium. Interestingly, loss of the 190 kDa ankyrin-G resulted in the loss of the lateral membrane specification. Further, reintroduction of 190 kDa ankyrin-G restored lateral membrane height after siRNA-mediated ankyrin-G knockdown. Importantly, even in the absence of ankyrin-G, E-cadherin was still localized to sites of cell-cell contact, but with increased levels of cytoplasmic E-cadherin. The same cellular distribution of β-catenin, which binds to the E-cadherin cytoplasmic

domain, was also seen in ankyrin-G depleted cells. However, lateral membrane localization of βII-spectrin was disrupted in the absence of ankyrin-G[27]. Further work demonstrated that siRNA-mediated knockdown of βII-spectrin in human bronchiolar epithelium also reduced lateral membrane height[28]. This finding is in agreement with a model where E-cadherin recruits the ankyrin-G / βII-spectrin complex to drive lateral membrane assembly, a model later confirmed by a follow-up study by the same group[79]. Further, in addition to maintenance of previously developed lateral membranes, de novo biogenesis of the epithelial lateral membrane is also shown to be dependent on ankyrin-G and βII-spectrin[28].

In addition, Bennett and colleagues identified a conserved ankyrin-G binding sequence in the cytoplasmic tail of E-cadherin. Using targeted mutagenesis to abolish the ankyrin-G binding site, the investigators further showed that E-cadherin exit from the trans-Golgi network is dependent on the ankyrin-G / E-cadherin interaction. Treatment of human bronchiolar epithelial cells with siRNA against ankyrin-G and βII-spectrin caused E-cadherin to accumulate in the trans-Golgi network as demonstrated with overlap with the trans-Golgi network marker golgin-97. Further, treatment of bronchiolar epithelium with nocodazole, a microtubule stabilizing drug, also reduced the exit of E-cadherin from the trans-Golgi network[94].

In light of these in vitro findings, Bennett and colleagues designed an ankyrin-G knockout mouse using Cre-Lox technology to determine the role of ankyrin-G in lateral membrane regulation in vivo. LoxP sites were inserted flanking exons 22 and 23 of the *Ank3* gene through homologous recombination techniques[79]. These mice were then

crossed with mice expressing Cre recombinase under the control of the β-actin promoter, effectively knocking out ankyrin-G expression in every tissue. Due to the critical importance of ankyrin-G in the nervous system (discussed in detail in the coming sections), the ankyrin-G knockout mice demonstrated 100% mortality by postnatal day two. Upon investigation of renal epithelium, Bennett and colleagues found that lateral membrane height was decreased in the absence of ankyrin-G. Further analysis of the cadherin superfamily demonstrated a conserved ankyrin-G binding site in both classic cadherins (E-cadherin, N-cadherin, VE-cadherin) as well as desmosomal cadherins (desmoglein and desmocollin). Further, the investigators identified di-leucine motifs resident within these ankyrin-G binding sequences. Targeted mutagenesis of the di-leucine motifs to alanines (LL-AA) resulted no change in the amounts of E-cadherin localized to the plasma membrane. Conversely, mutagenesis of conserved glutamic acid and aspartic acid residues critical for ankyrin-G / E-cadherin interaction resulted in proper lateral membrane targeting of E-cadherin (we will term this construct "Poly-A"). However, upon silencing of clathrin heavy chain, Poly-A E-cadherin was completely mislocalized. Further, double mutants (i.e. LL-AA and Poly-A) were completely mislocalized at baseline and after clathrin heavy chain deletion. These results show that apically mis-sorted E-cadherin is relocalized to the lateral membrane through clathrin-dependent endocytosis[79].

In a subsequent publication, Bennett and colleagues demonstrated that silencing of the both ankyrin-G and βII-spectrin resulted in an increase in bulk endocytosis of the lateral membrane in MDCK cells concomitant with a decrease in lateral membrane

height[95]. Deletion of clathrin heavy chain in the presence of ankyrin-G siRNA normalized lateral membrane height. Further, inhibiting clathrin-mediated endocytosis using the drug dynasore also normalized lateral membrane height. Together, these results demonstrate that ankyrin-G and βII-spectrin complexing with E-cadherin inhibits endocytosis of the lipids of the lateral membrane[95]. In summary, ankyrin-G regulates the cellular localization of NKA for maintenance of ionic gradients. Further, ankyrin-G prevents the endocytosis of E-cadherin, necessary for biogenesis and maintenance of the epithelial lateral membrane[96]. Interestingly, a similar mechanism is proposed for giant ankyrin-G opposing the endocytosis of GABAergic receptors, stabilizing somatodendritic GABAergic synapses[97]. Clearly, ankyrin-G can regulate both ionic concentration gradients and cell-cell adhesion. However, the functional in vivo consequence of these ankyrin-dependent cellular processes has yet to be determined in epithelial tissues.

Neuronal Excitability and Structure is Regulated by Ankyrin-G

Neurons are a highly specialized cell type, receiving excitatory and inhibitory inputs from multiple upstream neurons or receptors. These inputs summate in a spatiotemporal fashion at the axon initial segment, an area enriched with voltage-gated sodium channels. If the inputs summate to threshold, an action potential is generated and propagates down the axon. In myelinated neurons, clusters of voltage-gated sodium channels at small unmyelinated axonal segments termed nodes of Ranvier speed the propagation of the action potential via a process termed salutatory conduction[98]. The primary mechanism by which voltage-gated sodium channels localize to these specific

membrane domains is through their interaction with ankyrin-G[26, 99-101]. Further, several reports using genetically modified mouse models have demonstrated the necessity of ankyrin-G expression for proper neuronal excitability. Most indicative, however, are the host of human ankyrin-G variants linked with neurologic diseases such as bipolar disorder, autism, post-traumatic stress disorder, and schizophrenia, suggesting that ankyrin-G serves extremely critical roles in excitable cell types such as neurons[30, 102-105].

The term "excitable cell" refers to any cell that has the ability to produce action potentials. In its simplest approximation, an action potential is an *electrical message* that *propagates* across the plasma membrane of excitable cell types such as neurons, skeletal and cardiac muscle, and specialized glandular cells[98]. In all excitable cells, the action potential is produced to transmit a message and elicit a response inside the cell. In the neuron, for example, action potentials speed down the axon to the axon terminus where they induce, through a cascade of cellular events, the release of neurotransmitters into the neuronal synapse. These neurotransmitters then bind to receptors on downstream neurons or target cells to further transmit this message and/or produce an end effector function. At the organismal level, these neuronal action potentials are the foundation of complex behaviors such as movement, sensation, and cognitive function[98]. In the cardiomyocyte, the cardiac action potential (described in detail in coming sections) is used to signal the cardiomyocyte to contract as well as transmit that message to downstream cardiomyocytes to produce the concerted contraction of the heart. But how exactly can any cell be excited?

Elementary Electrical Principles of Excitable Cells

To understand how action potentials are generated in excitable cells, we must first understand the basic electrical principles of the cell. As mentioned previously, all cells are bound by a semipermeable barrier known as the plasma membrane. Early investigations dating back to the early 1900s demonstrate that the plasma membrane is composed of a bilayer of amphipathic phospholipids, with charged, hydrophilic head groups and non-polar, hydrophobic lipid tails[43]. In an aqueous solution, the amphipathic phospholipids will orient themselves so that their hydrophobic tails are facing each other and the hydrophilic head groups facing the aqueous environment. Small molecules, such as O_2, CO_2, and N_2 can freely diffuse across the plasma membrane. However, the plasma membrane acts a barrier to the diffusion of large molecules, proteins, lipids, and, importantly, charged ions. For charged ions (e.g. Na^+, K^+, Ca^{+2}, Cl^-) to cross the plasma membrane, integral membrane proteins such as ion channels, transporters, and ATP-dependent pumps must facilitate the crossing. Therefore, the plasma membrane can be thought of as selectively permeable to ions. The selective permeability of the plasma membrane for charged ions is best demonstrated by large concentration differences of ion populations across the plasma membrane. These ionic concentrations witnessed in the intracellular compartment (adapted from Hille 2001[106], Bers 2001[107]) and the extracellular space are listed in Table 1.

Ion	Intracell. [Ion] (mM)	Extracell. [Ion] (mM)
Na^+	5 – 20	135 - 145
K^+	140	3.5 - 5
Ca^{+2}	100 nM	1.8 - 2.52
Mg^{+2}	10 – 20	1 - 5
Cl^-	1 – 50	115
HCO_3^-	1 – 3	20 - 30

Table 1. Ranges of physiologic intracellular and extracellular ion concentrations

The differences in ion concentration between the cellular internal and external environment create concentration gradients. In the absence of an impermeable membrane, these concentration gradients would dissipate spontaneously via diffusion, the movement of molecules from an area of high concentration to an area of low concentration. The spontaneity of diffusion is thermodynamically favorable to a system as it both 1) increases the entropy (disorder) of the system as well as 2) releases energy. This release of free energy was quantitated by Nernst in the equation:

$$\Delta G = -RT \ln \frac{[ion]o}{[ion]i}$$

where ΔG is Gibb's free energy released during diffusion, R is the universal gas constant (8.31 J mol^{-1} K^{-1}), T is the temperature in Kelvin (often taken at 25 °C or 298 °K), and [ion]o and [ion]i are the concentrations of the ion in question in the extracellular and intracellular space respectively. Recall, however, the plasma membrane itself is

impermeable to the flow of ions, inhibiting spontaneous diffusion. For diffusion of a charged ion to occur, an ion channel needs to be present and open. Let us consider an ion channel that is selectively permeable to potassium (i.e. potassium channel). When the potassium channel opens, K^+ ions will diffuse from the inside of the cell (High $[K^+]$) to the outside of the cell (Low $[K^+]$). However, this diffusion of positive charge out of the cell will render the intracellular environment relatively more negative. This build-up of intracellular negative charge then acts to attract the positively charged K^+ ions back into the cell. The electrical energy pulling on the K^+ ions can be quantified by the equation:

$$\Delta G = -EzF$$

where E is the electrical potential (in volts) across the plasma membrane, z is the valence of the ion in question ($^+1$ for K^+, but would be -1 for Cl^-), and F is the Faraday constant (9.65×10^4 C mol^{-1}). What we can appreciate at this point is that the electrical energy opposing K^+ efflux out of the cell is opposite in direction to the energy of K^+ diffusion out of the cell. Progressively, these forces will achieve equilibrium such that there is no net flux of K^+ ions across the membrane. This equilibrium can be described with the following equation:

$$EzF = RT \ln \frac{[ion]o}{[ion]i}$$

The equation can be further arranged to describe the electrical potential at which the system achieves equilibrium:

$$E = \frac{RT}{zF} \ln \frac{[ion]o}{[ion]i}$$

E is referred to as the equilibrium potential or, most commonly, as the Nernst potential. Likewise, this equation is classically referred to as the Nernst equation. Using the values in Table 1, we can calculate that the Nernst potential for K^+ (E_K) ([K^+]o = 5 mM / [K^+]i = 140 mM), is -85.5 mV. However, we also have multiple other ionic gradients present across the membrane. For example the Nernst potential for Na^+ (E_{Na}) ([Na^+]o = 140 mM / [Na^+]i = 10 mM) is 67.7 mV and for Cl- ([Cl-]o = 115 mM / [Cl-]i = 20 mM) is -44.9 mV. In a healthy ventricular cardiomyocyte, experimental investigation has shown that the electrical potential across the sarcolemma (E_M) at rest is approximately -80 mV. How does this occur? If we calculate the Nernst potential just for monovalent ions (i.e. z=1) using the following formula:

$$E = \frac{RT}{F} \ln \left(\frac{[K]o + [Na]o + [Cl]i}{[K]i + [Na]i + [Cl]o} \right)$$

we arrive at a value of -12.2 mV, drastically different from the experimental measurements. Note, due to the negative charge on the chlorine ion, the intracellular and extracellular [Cl^-] have been switched to make z=1. However, this equation falsely makes the assumption that, at rest, the permeability of K^+ (pK) = pNa = pCl. As the resting membrane potential is closer to the Nernst potential of K^+, the sarcolemmal permeability for K^+ must, by definition, be larger than Na^+ and Cl^- permeability. In fact, pK is

approximately 100 times greater than pNa in a resting cell. By factoring in relative ionic permeability, we arrive at the Goldman-Hodgkin-Katz formula[106]:

$$E = \frac{RT}{F} \ln \left(\frac{pK[K]o + pNa[Na]o + pCl[Cl]i}{pK[K]i + pNa[Na]i + pCl[Cl]o} \right)$$

where relative ion permeability for Na^+, Cl^-, and K^+ is 1 : 10 : 100. Factoring in the relative permeability of each ion, we arrive at a value of -74.3 mV, much closer to the experimentally-determined value.

Recall, however, that the plasma membrane is impermeable to charged ions; their crossing must be facilitated. To increase the permeability of any charged ion requires the activation or opening of ion channels in the plasma membrane. Simply stated, ion channels are low-resistance pores in the plasma membrane that selectively facilitate the diffusion of specific charged ions. Let us use Na^+ channels as an example. At rest, the plasma membrane can be said to have a high resistance to the flow of Na^+ ions due to the closed state of Na^+ channels. When the Na^+ channels open, membrane resistance for Na^+ decreases, causing an influx of Na^+ ions for two reasons. First, Na^+ will diffuse from an area of high [Na^+] to an area of low [Na^+]. Second, the negative membrane potential of the cell at rest will attract the positively charged Na^+ ions into the cell. This movement of charged ions creates an electrical current (I). From an electrical standpoint, this relationship can be modeled for the Na^+ gradient by using Ohm's law where:

$$Current\ (I) = \frac{Driving\ Force}{Membrane\ Resistance} = \frac{E_M - E_{Na}}{R_{M,Na}}$$

Let us consider the system at rest. Using the derived values mentioned previously for E_M and E_{Na}, (-74.3 mV and 67.7 mV respectively) we arrive at a value of -142 mV for the driving force on sodium. Contrast this with a driving force of 11.2 mV for K^+ ions. The negative sign on the sodium driving force means that any derived value for Na^+ current will be negative, implying that the sodium current will flow into the cell when sodium channels are activated. At rest, when the Na^+ channels are in the closed state, membrane resistance is very high, in effect producing an extremely small Na^+ current. However, this changes when membrane Na^+ channels are activated. When the Na^+ channels activate, membrane resistance for Na^+ becomes relatively small, facilitating rapid influx of Na^+ ions into the cell and producing an inward Na^+ current. As this Na^+ current brings E_M to more positive potentials, we say that this current acts to depolarize the cell. Conversely, if more K^+ channels were to open, membrane resistance to K^+ would decrease and cause an outward K^+ current. As this decrease in membrane K^+ resistance would act to bring E_M to more negative potentials, we say that this K^+ current act to repolarize the cell. Importantly, this rapid increase in Na^+ current acts to set in motion a series of stereotypic changes in the membrane potential of excitable cells known as the action potential.

Much of our current understanding of the ionic basis of the action potential derives from biophysical work conducted from the late 1930s to the early 1950s.

Working with giant squid axons, Curtis and Cole demonstrated a dramatic increase in membrane conductance during an action potential with little change in membrane capacitance[106]. This finding again demonstrates three very important points: 1) The plasma membrane itself is not leaking ions (in opposition to the "membrane breakdown" hypothesis of the action potential prominent at the time) and 2) the plasma membrane at rest has a very high resistance to the flow of ions 3) cellular excitation signals some constitutive membrane component to permit ionic flux across the membrane, responsible for this surge in membrane conductance[106]. Although several hypotheses were present at the time, we now know that these ions flow through integral membrane proteins such as ion channels and transporters during the action potential.

Ion Channel Structure and Function

Although we have talked generally about ion channels to this point, we must now investigate their specific structure and function in order to properly understand the development of action potentials. Ion channels are comprised of a combination of transmembrane proteins with an extracellular face and intracellular domains. Ion channels themselves are comprised of the pore-forming α-subunit and regulatory β-subunits. On the intracellular side, α-subunit interacts with regulatory elements, protein trafficking machinery, and cytoskeletal architecture. On the basis of structure, the α-subunits of ion channels can be separated into two groups. First are the protein families of Na^+, Ca^{+2}, and K^+ ion channels. These channels are each composed of 4 domains (DI-IV), with each domain comprised of 6 transmembrane segments (S1-6) with alpha-helical

secondary structure. In Na^+ and Ca^{+2} channels, all four domains are translated as one entire protein, whereas K^+ channels are translated as individual domains that assemble to produce a functional ion channel. Although their molecular makeup is slightly different, the anatomy of the channels is quite similar. First, each ion channel contains an aqueous central pore through which ions will pass. However, as can be inferred by Curtis and Cole, these pores are not constitutively open. These pores must be stimulated to open through a process called "channel gating[106]."

In response to binding of a specific-ligand, mechanical stretch, or membrane voltage, ion channels can be stimulated to open. With respect to the understanding of the action potential, the mechanisms of voltage-gating are the most characterized at this time. Each domain of the ion channel contains a voltage sensing mechanism on transmembrane segment 4 (S4). Recall that these transmembrane segments are alpha helical. At resting membrane potential, polar charged amino acid residues on the S4 domain face the central aqueous pore. When the membrane reaches a specific electrical potential, different for each species of ion channels, these charged residues rotate away from the central pore causing the S4 domain to twist outward in a helical motion. This translation of the S4 domain then acts to open the channel pore. This process is termed voltage-dependent activation. After voltage-dependent activation of an ion channel, selective ions begin to flow across the plasma membrane through the open pore depending on their respective electrochemical gradient. However, once an ion channel activates and passes current, ion channels begin to inactivate. Channel inactivation is not simply an "off" state for the channel. In the inactivated state, the ion channel will not open in response to a stimulus.

The ion channel must first recover from channel inactivation in order to be opened again. Once the ion channel has recovered, it can be considered in the "off" state, ready to be stimulated to open again by appropriate membrane voltage[106].

Neuronal Action Potential Initiation and Propagation

Knowing these basic properties of ion channels now enables us to investigate the mechanisms producing a neuronal action potential. Consider a neuron at rest with no incoming stimulation. Recall that the resting membrane potential of a cell ranges from -80 to -70 mV, driven by a high permeability of the plasma membrane for K^+. In terms of ion channels, K^+ channels in the neuronal plasma membrane causing E_M to be approximately equal to E_K. These K^+ channels are a specialized subset of ion channels termed inward rectifiers (Kir). Instead of six transmembrane segments live voltage-gated K^+ channel subunits, Kir channel subunits have two transmembrane segments. Further, these Kir channels have a unique property: at membrane potentials below E_K (~ -70 mV), these channels demonstrate a negative, inward current. This switches to a positive, outward current from -70 mV to – 30 mV, responsible for governing the increased membrane permeability of K^+ at rest that sets the resting membrane potential[108].

During stimulation, an upstream neuron releases a neurotransmitter (Glutamate, GABA, 5-HT, Dopamine, etc) that binds to a neurotransmitter receptor in the dendrites of the neuron. These neurotransmitter receptors are ligand-gated ion channels. In other words, these channels are stimulated to open in response to binding of a specific chemical. Once again, these channels are selective for specific species of charged ions.

Let us consider the glutamate receptors that are selectively permeable to Na^+ ions. Upon opening of the glutamate receptors, Na^+ conductance of the plasma membrane increases, causing the development of local depolarization of the plasma membrane also known as an excitatory postsynaptic potential. This potential then propagates to the surrounding membrane as a graded potential that decays very quickly with increasing distance from the initial site of depolarization. However, if the neuron is sufficiently stimulated by glutamate and enough excitatory post synaptic potentials are produced, these waves of depolarization can summate at an area of the neuron known as the axon initial segment (AIS)[98].

At the AIS is a very large density of voltage-gated sodium channels. The family of voltage-gated sodium channels (encoded by 10 individual genes[109]) begin to activate at approximately -50 mV. If the excitatory postsynaptic potentials integrated at the AIS summate beyond -50 mV, this causes the individual sodium channels to activate very rapidly, further depolarizing the plasma membrane. This further depolarization causes a positive feedback mechanism that opens a large amount of sodium channels, causing a rapid increase in Na^+ conductance at the plasma membrane. Further, this depolarization also acts to close the Kir channels that govern the resting membrane potential, driving the AIS membrane E_M closer to E_{Na}. This event is commonly referred to as the upstroke of the action potential. A very important property of voltage-gated sodium channels is rapid inactivation. Within 1-2 msec after activation, voltage-gated sodium channels rapidly inactivate. These Na_V channels will remain in the inactivated state until the membrane voltage returns to more negative potentials. The biophysical basis of Na_V channel

inactivation is provided by the DIII-DIV linker also known as the inactivation gate. In this model, after fast activation this DIII-DIV linker region swings up to associate and block the channel pore. Early studies of sodium channels demonstrated that intracellular perfusion of proteases to digest the domain linker regions inhibited Na_V channel inactivation. Further, antibodies directed specifically to the DIII-DIV linker also inhibited fast inactivation. Through targeted mutagenesis studies, 3 specific residues (Isoleucine-Phenylalanine-Methionine) have been shown to act as the "latch" between the DIII-DIV linker. To transition from the inactivated state to the closed state, the Na_V channel must next recover from inactivation. This process again is also voltage dependent, requiring the return of the membrane voltage to more negative membrane potentials. The processes of rapid inactivation and recovery from inactivation are extremely critical to unidirectional propagation of the action potential in the neuron, preventing backflow of the stimulated action potential into the cell soma[109].

As discussed already, the opening of the Na_V channels triggers the upstroke of the action potential, causing cellular depolarization. However, the increase in membrane potential also stimulates the opening of voltage-gated K^+ channels, which have a higher threshold for activation (~ -20 mV). As the Na_V channels rapidly inactivate (i.e. decreased membrane Na^+ conductance), membrane permeability for K^+ increases due to the opening of the K^+ channels, resulting in a peak in the action potential amplitude and then a rapid repolarization of the membrane potential as E_M returns to values close to E_K[109]. At this point, the ionic gradients of Na^+ and K^+ have diminished and must be reset in order for subsequent action potentials to fire. This is accomplished by the Na^+/K^+ ATPase pump

(NKA). By hydrolyzing one molecule of ATP, NKA pumps 3 Na^+ ions out of the cell and brings 2 K^+ ions into the cell and resets the ionic gradients at the AIS[106]. Once the action potential develops at the AIS, it must propagate down the axon to the axon terminus. However, over a certain distance the action potential begins to decay. To prevent this, many neurons are coated in an insulating layer of cell membrane, termed myelin. This layer helps to preserve the amplitude of the action potential by preventing leakage of current out of the axon. Even with this insulation, the action potential will eventually decay a needs to be re-established. This is accomplished by further densities of Na_V channels located in gaps between the myelination known as nodes of Ranvier. Once the decaying action potential enters into the node of Ranvier, the resident Na_V channels open and create a new, full-amplitude action potential. This mode of action potential propagation is known as salutatory conduction, speeding the transmission of the impulse to the axon terminus to produce end effector function[98]. As we can clearly see, for proper initiation and propagation of the neuronal action potential, Na_V channels need to be localized at very discrete microdomains. Over 25 years of investigation have demonstrated that ankyrin-G is critical to the development and maintenance of these excitable microdomains in the neuron.

In 1979, Bennett and colleagues demonstrated the presence of ankyrin in nervous tissue using antisera developed against the spectrin binding domain of erythrocyte ankyrin[74]. Further, work conducted by the same group in 1987 demonstrated that ankyrin was uniformly distributed throughout the neuronal cell soma and the axon, with no immunoreactivity witnessed in dendrites[110]. However, this ubiquitous arrangement of

ankyrin is in stark contrast with the discrete localization noticed for voltage-gated sodium channels in the neuron. Regardless, elegant work by the Angelides group[25] demonstrated that purified voltage-gated sodium channels co-purify with ankyrin and spectrin peptides. By reconstituting purified rat neuronal voltage-gated sodium channels into synthesized vesicles, Srinivasan et al., demonstrated that ^{125}I-labelled ankyrin associated with the "extracellular" surface of these vesicles with a Kd of 20 nM and a molar ratio of 0.53 pmol ankyrin / pmol sodium channel. However, as these sodium channels are artificially reconstituted into these vesicles, probability dictates that ~50% of these channels would be oriented with the extracellular face of the channel facing the extracellular environment, preventing an interaction with ankyrin. Therefore, the researchers concluded that ankyrin and Na_V channels interact with a 1:1 stoichiometry[25]. In 1992, the same group would go on to demonstrate that ankyrin binds to the neuronal Na_V channels through a site in the first 11 ANK repeats, a site different than that for Band 3 or the NKA isoforms[111].

As mentioned previously, Na_V channels have a highly localized localization whereas immunostaining with anti-ankyrin antibodies revealed a diffuse distribution of ankyrin within the neuron. If ankyrin was the molecular mechanism localizing Na_V channels, how would there be any targeting specificity? An answer to this question came in 1995 with the identification of giant, neuronal specific isoforms of a novel ankyrin isoform, termed ankyrin-G[112]. Bennett and colleagues identified novel cDNAs encoding for large (480 / 270 kDa) ankyrin-G isoforms. Using ankyrin-G-specific antisera, the investigators showed specific localization of ankyrin-G at the nodes of Ranvier and axon

initial segments. This study was also the first to demonstrate the presence of 190 kDa ankyrin-G in the heart. These "giant" isoforms of ankyrin-G contain a serine-rich domain and an extended tail domain between the SBD and CTD. A follow up study in 1998 demonstrated that these serine-rich and tail domains in the giant ankyrin-G isoforms limited the diffusion of ankyrin-G from the axon initial segment[113]. Importantly, a 1998 study from the Bennett laboratory demonstrated the functional consequence of this neuronal population of ankyrin-G in vivo. Using mice with cerebellum-specific deletion of ankyrin-G, Zhou et al. demonstrated that ankyrin-G was required for the clustering of Na_V channels at the axon initial segment[26]. Further, neurons from these animals displayed increased threshold of activation due to decreased AIS density of Na_V channels leading to severe ataxia in these animals. Providing a molecular basis for the Na_V channel-ankyrin-G interaction, two independent studies in 2003 demonstrated the presence of an ankyrin-G binding sequence within the DII-DIII linker, conserved across all isoforms of Na_V channels[39]. This motif is also functionally conserved in the KCNQ2/3 channels that cluster at the AIS and nodes of Ranvier in an ankyrin-G-dependent manner[114]. In 2000, Berghs et al. demonstrated that ankyrin-G scaffolds these channels to a new spectrin isoform at the AIS and nodes of Ranvier termed βIV-spectrin[115].

In 1996, ankyrin-G was also shown to associate with several structural elements within the neuron including neurofascin and neuronal cell adhesion molecule (NrCAM) at the node of Ranvier[116] and subsequently the AIS in 1998[117]. Also known as L1-CAMs, these cell adhesion molecules are members of the immunoglobulin superfamily of cell adhesion molecules and associate with ankyrin-G through a FIGQY motif in their

intracellular domain[117]. Functionally, these L1-CAMs mediate cell-cell adhesion with myelinating glial membranes of Schwann cells (peripheral nervous system) and oligodendrocytes (central nervous system), necessary for proper axonal myelination that speeds action potential transmission[118]. In 2001, work from the Bennett laboratory demonstrated that knockout of ankyrin-G in cerebellar neurons resulted in the disruption of Nav1.6, βIV-spectrin, and neurofascin at the AIS. Further, time-course experiments revealed that ankyrin-G / βIV-spectrin targeting to the AIS precedes the arrival of densities of Nav1.6 and neurofascin by as much as seven days in vivo[101]. Unlike the AIS that can form in the absence of myelinating glia, nodes of Ranvier require glial contact to form properly[119]. A study conducted by the Salzer laboratory in 2007 provided the molecular mechanism behind this finding[120]. Cytoplasmic sequences of exogenously expressed Neurofascin-186 (NF-186) were found to be necessary for localization at the AIS, whereas extracellular domains of NF186 were required for targeting of NF-186 to the node of Ranvier. Further, neurons subjected to exogenous expression of NF-186 lacking its intracellular FIGQY domain demonstrated preserved localization at the node of Ranvier with reduced expression of ankyrin-G. This demonstrates that nodes of Ranvier assemble in a different sequence than the AIS. However, it was demonstrated that NF-186 required ankyrin-G for its stabilization at the node of Ranvier and that ankyrin-G knockdown almost entirely prevented the development of functional nodes of Ranvier. Interestingly, ankyrin-G in oligodendrocytes is necessary for proper targeting of NF-155 isoform to the paranodal region of nodes of Ranvier. Further, oligodendrocyte-specific ankyrin-G knockout severely delayed the development of proper paranodal

regions, resulting in slowed conduction velocity of neuronal action potentials in P7 neurons[121].

As stated earlier, ankyrin-G interacts with βIV-spectrin in neurons, colocalizing at the AIS and nodes of Ranvier. As we have seen previously, knockout of ankyrin-G in cerebellar neurons results in the mislocalization of βIV-spectrin[101]. However, Komada et al. 2002 demonstrates that silencing of βIV-spectrin resulted in reduced clustering of both ankyrin-G and neuronal Na_V channels at the AIS. Further, these researchers also confirmed that silencing of ankyrin-G also resulted in disruption of βIV-spectrin and neuronal Na_V channels localization at the AIS[122]. This finding, confirmed by several subsequent reports, demonstrates that ankyrin-G and βIV-spectrin stabilization at the AIS is codependent on the presence of both molecules[123, 124]. Recall from earlier that ankyrins associate with spectrins through their respective spectrin binding domains. However, recent work investigating the giant 480 kDa ankyrin-G isoform specific to neurons is challenging this dogma. 480 kDa ankyrin is translated from a transcript containing the giant exon 37. Therefore, Jenkins et al. 2015 created exon 37-specific ankyrin-G knockout mice to specifically investigate the function of this 480 kDa ankyrin-G isoform. Interestingly, removal of just the 480 kDa ankyrin-G isoform was sufficient to eliminate the targeting of Na_V channels, KCNQ2, βIV-spectrin, and neurofascin at the AIS and drastically reduced the number of nodes of Ranvier present in the axon[125]. Functionally, this resulted in a slower rate rise to achieve threshold of activation and slowed action potential firing rate. As discussed previously, giant ankyrin-G isoforms have a serine-rich

domain. Surprisingly, this isoform recruited βIV-spectrin through a site in this serine-rich domain (Serine 2417), instead of the canonical SBD domain[125].

Molecular Physiology of Ankyrin-G in Cardiac Tissue

As evidenced by the investigation of ankyrin-G in non-cardiac cell types, ankyrin-G can regulate both cellular excitability as well as cellular structure. However, as we can see from investigations in epithelium and neurons, ankyrin-G is not homogenously expressed throughout the entire cell. Instead, ankyrin-G shows a highly localized distribution in these cell types. The cardiomyocyte is no exception. Work from multiple laboratories has indicated that ankyrin-G is preferentially localized to the intercalated disc (ID) membrane domain in the cardiomyocyte, with minor amounts of ankyrin-G located in the transverse tubules[35, 126, 127]. Located at the terminal edges of the cardiomyocyte, the ID contains three distinct functional domains: 1) the fascia adherens domain, 2) desmosomes, and 3) gap junctions[128]. Unlike epithelial lateral membrane domains, cardiac fascia adherens domains are primarily composed of N-cadherin[129]. Like E-cadherin, the cytoplasmic domain of N-cadherin associates with β-catenin and α-catenin to scaffold N-cadherin to filamentous actin[129, 130]. Demonstrating its functional importance, knockout of N-cadherin in mice results in embryonic lethality and abnormal cardiac development[131]. Further, induced deletion of N-cadherin in adult mice results in disruption of fascia adherens structure as well as dilated cardiomyopathy and ventricular arrhythmia[132]. Again similar to the epithelial lateral membrane, the intercalated disc also contains desmosomes, analogous to spot welds between adjacent cells[133]. Cardiac

desmosomes are composed of the desmosomal cadherins desmocollin-2 (DSC-2) and desmoglein-2 (DSG-2), mediating homo- or heterophilic interaction with desmosomal cadherins on adjacent cardiomyocytes. The cytoplasmic tails of DSC2/DSG2 in turn interact with the cytoplasmic scaffolding proteins plakoglobin (JUP) and plakophilin-2 (PKP2). JUP and PKP2 then bind to the cytoplasmic molecule desmoplakin (DSP) which in turn binds to the intermediate filament cytoskeleton, composed of desmin in the cardiomyocyte[134]. Importantly, loss-of-function mutations in each member of the cardiac desmosome have been implicated in arrhythmogenic right ventricular cardiomyopathy, a cardiac disorder characterized by severe ventricular arrhythmia and fibrofatty replacement of cardiac tissue[135].

Analogous to pores between cells, gap junctions act to physically unite the cytoplasm of adjacent cardiomyocytes. To accomplish this, gap junction hemichannels located on opposing membranes unite to form the gap junction[136]. In ventricular myocytes, these hemichannels are composed of hexamers of connexin-43 molecules[137]. Functionally, gap junctions act as a low resistance pathway for the flow of current[138]. This property enables rapid conduction of the cardiac action potential between adjacent cardiomyocytes, synchronizing cardiac contraction[139]. In the setting of heart failure, one common finding is the lateralization of gap junctional plaques, greatly slowing the propagation of the excitatory impulse between cells[140]. This slowing, or in some cases block, of the transmission of the action potential results in the production of reentrant cardiac arrhythmia[138]. Also present at the intercalated disc are large densities of the Na_V channel Nav1.5[141]. Consider a chain of cardiomyocytes linked in series. An action

potential in the first cell, initiated by the rapid opening of Nav1.5, propagates to the next cell through the gap junctional plaques. This injection of current from the upstream cell depolarizes the cardiomyocyte cell membrane, activating the density of Nav1.5 located at the intercalated disc to produce the cardiac action potential[142]. Although theoretical modeling of this system has indicated that this polarized distribution of Na_V channels is not necessary for action potential propagation at baseline, preferential localization Nav1.5 to the intercalated disc is of critical importance to transmit this electrical impulse during settings of decreased cell-cell coupling via gap junctions[143].

Molecular Basis of the Cardiac Action Potential

The ventricular cardiac action potential can be divided into five phases. The resting membrane potential is commonly referred to as Phase 4 of the action potential. In the cardiomyocyte, the resting membrane potential is set by the inward rectifying K^+ channel Kir2.1, producing the current I_{K1}[144]. As we have seen in neurons, the upstroke of the cardiac action potential is known as phase 0, governed by the rapid activation of the Na_V channel isoform Nav1.5 (encoded by the *SCN5A* gene) producing a large, inward depolarizing Na^+ current known as I_{Na}. This action potential propagates across the plasma membrane and down the transverse tubules, tubular invaginations of the plasma membrane to activate voltage-gated Ca^{+2} channels located in these membranes[12]. After the peak of the cardiac action potential, the membrane potential begins to repolarize, creating a notch in the action potential termed phase 1. This is due to the activation of the voltage-gated K^+ channels Kv4.2 and Kv4.3, producing an outward, repolarizing current

known as I_{TO} (transient outward)[145]. Phase 2, also known as the plateau phase, is characterized by activation of L-type voltage-gated Ca^{+2} channels termed Cav1.2 specifically localized in the transverse tubules[146]. Activation of Cav1.2 in the ventricular cardiomyocyte is responsible for the initiation of Ca^{+2}-induced Ca^{+2} release from the sarcoplasmic reticulum to activate the sliding filament mechanism producing cellular contraction (described in detail below). Phase 3 is composed of multiple repolarizing K^+ currents such as I_{Kr}, I_{Ks}, I_{Kur}, and the reactivation of I_{K1}, further repolarizing the cardiomyocyte plasma membrane back to resting membrane potential[145]. Like in other excitable cell types after an action potential, the ionic gradients are re-established by the NKA pump[147], also highly localized to the transverse tubule domain[22].

Ca^{+2}-induced Ca^{+2} release and the Sliding Filament Mechanism

As stated earlier, the influx of Ca^{+2} into the cardiomyocyte during phase 2 of the action potential acts to initiate the process of Ca^{+2}-induced Ca^{+2} release from the sarcoplasmic reticulum. Upon activation of Cav1.2 in the transverse tubules, small amounts of Ca^{+2} enter the cardiomyocyte. The transverse tubule membrane is in close proximity to the junctional area of sarcoplasmic reticulum (SR), a structure termed the dyad (1 transverse tubule and 1 junctional SR)[107, 148]. These entering Ca^{+2} ions bind to the ryanodine receptor type 2 (RyR2) in the sarcoplasmic reticulum[11]. Ca^{+2} binding to the RyR2 then triggers it to open. As the concentration of Ca^{+2} is relatively higher in the SR (~100 μM[149]) and very low in the cytosol (100 nM[150]), this opening of RyR2 causes an influx of Ca^{+2}, known as the Ca^{+2} transient, into the cytosol, raising cytosolic calcium

concentration. This increase in cytosolic Ca^{+2} then activates the sliding filament mechanism to produce cellular contraction. Instead of relying on diffusion of Ca^{+2} from the plasma membrane to the cell interior to activate all RyR2, propagation of the cardiac action potential down the transverse tubule system ensures that the Ca^{+2} release from all RyR2 is synchronized to produce a uniform contraction[151].

Once the Ca^{+2} is released from RyR2, it activates the sliding filament mechanism to produce contraction. In the cardiomyocyte, electron microscopic studies demonstrate a highly ordered array of actin and myosin filaments in a ratio of 4 actin filaments to 1 myosin filament arranged in a hexagonal array[152]. Electron microscopy shows a highly ordered banding pattern in the cardiomyocyte, with each individual unit termed a sarcomere linked together in series across the entire length of the cardiomyocyte. Z-lines (or Z-disks) act as the site of actin filament integration. The M-lines are anchor points for the myosin filaments. The A-band represents the entire length of the myosin filament and the I-band represents the non-overlapping region between the actin filament and the myosin filament terminus. When stimulated to contract, the myosin and actin filaments slide in an antiparallel direction with respect to each other. This shortens each sarcomere (i.e. pulls the Z-lines closer together) causing cellular contraction. This understanding of muscle contraction is termed the sliding filament mechanism[152].

The sliding filament mechanism, and therefore cellular contraction, occurs by a process known as cross-bridge cycling. The myosin filament is created by the polymerization of multiple monomers of myosin. The individual myosin molecule is a molecular motor composed of a tail domain, a neck region of variable length, and an

actin-binding head domain with ATPase activity[153]. The tail domains of the myosin molecules integrate into a myosin filament with the head domains radiating outward. When the myosin molecule encounters a molecule of ATP, the myosin ATPase site rapidly hydrolyzes the ATP causing a conformational change to the myosin neck region[153]. The transfer of energy extends the myosin head domain and is stored as potential energy to produce pulling force, analogous to a loaded gun ready to be fired. The actin filament is composed of multiple partners. Actin monomers polymerize into filamentous actin and contain binding sites for the myosin head region. To prevent the actin-myosin interaction until necessary to produce a contraction, a molecule known as tropomyosin covers the myosin binding sites on the actin filament[154].

With potential energy stored in the myosin motors and the actin-myosin interaction inhibited by tropomyosin, how then is a contraction produced? To regulate contraction, the troponin complex (composed of Troponin-T, Troponin-C, and Troponin-I) mediates the myosin binding site availability on the actin filament in a calcium (Ca^{+2}) dependent manner[154]. In response to elevated levels of intracellular Ca^{+2} ions sensed by troponin-C, the troponin complex acts to move the tropomyosin molecules, exposing the myosin-binding sites on the actin filament. This event facilitates the actin-myosin interaction[153]. When the primed myosin head domains interact with the actin filaments, this causes the myosin neck to flex back to its original position, pulling on the actin filaments and pulling the Z-disks closer together. ADP and inorganic phosphate then diffuse from the myosin molecule, with ADP diffusion being the rate limiting step in the entire reaction of cross-bridge cycling. Another molecule of ATP is required to bind to

the myosin ATPase site to facilitate the release of the actin filament by the myosin motor. The absence of available ATP would preserve the myosin-actin interaction, producing a tetanic response[153].

As elevation of intracellular Ca^{+2} concentration produces cellular contraction, removal of Ca^{+2} from the cytosol will deactivate cross-bridge cycling[153], allowing the individual cardiomyocytes to relax, allowing the chamber as a whole to fill with blood during diastole. Removal of Ca^{+2} from the cytoplasm occurs through two main ways. First, the Na^{+}/Ca^{+2} exchanger (NCX) in the transverse tubule plasma membrane will export 1 Ca^{+2} ion in exchange for the influx of 3 Na^{+} ions[155]. As there is an imbalance of charge transported, activation of NCX is electrogenic, causing an inward, depolarizing I_{NCX} current necessary for the maintenance of the action potential plateau[156]. The amount of Ca^{+2} removed from the cytoplasm under normal conditions is equal to the amount of Ca^{+2} influx from Cav1.2 during cellular activation[107] (~37% of total systolic Ca^{+2} in humans[157]). Second, Ca^{+2} can be extruded from the cytosol through the sarcoplasmic reticulum ATPase pump (SERCA2a in the heart). Located on the longitudinal SR[158], SERCA2a is inhibited by the small protein phospholamban[159], but this inhibition is removed via phosphorylation of phospholamban[160] by protein kinase A (serine 16) and CaMKII (threonine 17)[161]. In humans, the proportion of Ca^{+2} taken back up into the SR via SERCA2a is approximately 63% of total systolic Ca^{+2} in humans[157]. Further pathways of Ca^{+2} extrusion also include the plasma membrane Ca^{+2} ATPase pump as well as into mitochondria via the mitochondrial uniporter MCU accounting for less than 2% of Ca^{+2} extrusion. Regardless of the pathway, the extrusion of Ca^{+2} from the cytosol

results in the decay of the Ca^{+2} transient and myocyte relengthening[107]. This process of excitation – Ca^{+2} release – myocyte shortening – Ca^{+} reuptake is known collectively as excitation contraction (EC) coupling[107]. Interestingly, ankyrin polypeptides have been shown to be critical regulators of multiple members of the EC-coupling machinery.

Cardiac Ankyrins Regulate Excitation-Contraction Coupling

In 2003, Mohler et al. demonstrated that a human variant in *ANK2* (ankyrin-B E1425G) causes lengthening of the QT interval, termed Long QT Type 4, causing a lethal polymorphic ventricular tachyarrhythmia[22]. Over the next decade, human mutations in *ANK2* have been linked to sinus nodal disease, atrial fibrillation, ventricular arrhythmia, and sudden cardiac death[31, 32, 162]. Mechanistically, these arrhythmias manifest due to alterations in select members of the EC-coupling machinery. Recall from the earlier discussion that multiple members of the EC-coupling machinery are heavily localized to the transverse tubule membrane domain in the cardiomyocyte. In 1993, work from the Philipson laboratory demonstrated the molecular basis of the localization of one of these proteins, NCX, in the cardiomyocyte[163]. Using antibodies raised against erythrocyte ankyrin, this investigation demonstrated the presence of a 220 kDa isoform of ankyrin in cardiomyocyte membrane preparations that localized specifically to the transverse tubule membrane domain. Further, this investigation demonstrated a direct association between purified NCX and ^{125}I-labelled ankyrin[163]. These results were further confirmed in 1997 by electron microscopic investigation of using immunogold staining for ankyrin in rabbit cardiomyocytes[164].

Upon identification of the E1425G ankyrin-B mutation, Mohler et al., 2003 demonstrated that ankyrin-B $^{+/-}$ cardiomyocytes demonstrated reduced expression and improper cellular localization of NCX1. Further, these myocytes also demonstrated disrupted localization and expression of α1 / α2 NKA isoforms as well as the IP3 receptor[22]. These disruptions in transverse-tubule localization of these components of EC coupling lead to lethal arrhythmias in ankyrin-B$^{+/-}$ mice and abnormal Ca^{+2} transients in neonatal cardiac myocytes[22]. Importantly, no changes were seen in expression of RyR2, SERCA2a, or Nav1.5, in contrast to findings conducted in neonatal ankyrin-B null myocytes[165, 166]. Interestingly, expression of GFP-tagged E1425G ankyrin-B in ankyrin-B$^{+/-}$ cardiomyocytes demonstrated normal cellular distribution, but could not rescue the disrupted targeting of NCX / NKA[22]. Further investigation would demonstrate that IP3-receptor interacted with ankyrin-B at membrane repeats 22-24[167] and NCX1 at membrane repeats 16-18[168]. However, the E1425G ankyrin-B mutation, similar to most identified human ANK2 mutations, occurs within the regulatory C-terminal domain of the ankyrin[162], suggesting a role for this domain in regulating protein-protein interaction or protein targeting. As predicted by Mohler in 2003, removal of ankyrin-B from the cardiomyocyte should mimic the effects of cardiac glycosides, compounds that inhibit NKA[107]. By limiting Na^{+} extrusion from the cytosol, the Na^{+} gradient driving NCX to extrude Ca^{+2} from the cytosol would diminish (even worse with less NCX, as seen in ankyrin-B $^{+/-}$ cells)[169]. This would cause an increase in cytosolic Ca^{+2} and therefore higher Ca^{+2} concentration in the SR. Although this would lead to larger Ca^{+2} transients and stronger cardiac contraction[11], this increase in SR Ca^{+2} load would act to make RyR2

hypersensitive and cause an increase in spontaneous RyR2 opening[170]. This would result in increased probability of pro-arrhythmic Ca^{+2} waves and sparks in ankyrin-$B^{+/-}$ mice, a finding confirmed by Despa et al. in 2012[171].

With respect to ankyrin-G, a handful of reports have demonstrated a critical role for ankyrin-G in mediating targeting of the Na_V channel Nav1.5 (*SCN5A*) in vitro. As discussed previously, the initiation of the ventricular (and atrial) action potential, and EC-coupling as a result, is dependent on the opening of the Na_V channel Nav1.5 in the cardiomyocyte. Nav1.5 accounts for 80-95% of total I_{Na} in human cardiomyocytes, with the remainder supplied by the tetrodotoxin-sensitive neuronal isoforms (Nav1.1, Nav1.2, Nav1.3, and Nav1.6)[172-174]. Several lines of evidence support the critical importance of Nav1.5. Human loss-of-function mutations in *SCN5A* result in decreased I_{Na}, producing a constellation of arrhythmias known as Brugada syndrome. Conversely, gain-of-function *SCN5A* mutations can also cause Long QT type 3, lengthening the cardiac action potential due to inability of channels to inactivate properly[21, 175]. Further, *SCN5A* variants have also been implicated in sick sinus syndrome[176]. Although Nav1.5 is not expressed in the sinus node itself, the atrial cells surrounding the SA node demonstrate high expression of Nav1.5, necessary to transmit the SA nodal impulse into the atrial tissue[176]. Interestingly, although not entirely explained, *SCN5A* mutations localizing to the voltage-sensor domain (S4) have also been associated with dilated cardiomyopathy[177]. Experimentally, *Scn5a* $^{+/-}$ mice display severe electrocardiographic abnormalities such as prolonged PR and QRS intervals, slowed ventricular activation, inducible and spontaneous atrial and ventricular arrhythmia, and fibrotic replacement of ventricular

tissue[178, 179]. Due to its critical importance for cardiac excitability, the cardiomyocyte has evolved multiple mechanisms to traffic, localize, and regulate Nav1.5 at the plasma membrane.

Targeting Nav1.5 in the Cardiomyocyte: An Evolving Understanding

Recall that all ion channels are made of an α-subunit, regulatory β-subunits, and channel interacting proteins. Several channel interacting proteins have been demonstrated to associate with Nav1.5. At the C-terminus of the Nav1.5 molecule is a highly conserved PDZ-binding domain (residues SIV). This PDZ binding domain can theoretically interact with cytoskeletal proteins containing PDZ domain. With respect to the SIV domain in Nav1.5, the cytoskeletal molecules syntrophin and SAP97 have been shown to associate. In 1998, Gee et al. demonstrated that sodium channels from cardiomyocyte plasma membranes co-immunoprecipitated with α- and β-syntrophins, critical members of the dystrophin glycoprotein complex[180]. A 2006 study from the Abriel laboratory further demonstrated that these syntrophins scaffold Nav1.5 to dystrophin itself[181]. Using mice deficient in dystrophin, the Abriel laboratory demonstrated reductions in total Nav1.5 membrane expression coupled with decreased I_{Na} current density. In 2011, work from the same group demonstrated that the dystrophin glycoprotein complex specifically targets Nav1.5 to the lateral membrane of the cardiomyocyte[182]. Recall, however, that Nav1.5 localizes heavily to the intercalated disc as demonstrated by immunostaining and electrophysiologic recordings. In the same investigation, the Abriel laboratory demonstrated that Nav1.5 associated with the PDZ domain of the protein SAP97 at the

intercalated disc. By silencing SAP97 with shRNA or truncating the SIV motif of Nav1.5, the investigators showed decreased membrane targeting of Nav1.5 Further, as shRNA-mediated silencing of SAP97 reduced sodium current density, the researchers concluded that SAP97 may be responsible for localization of a subset of Nav1.5 at the intercalated disc[182]. However, more recent work with mouse models of Nav1.5 SIV truncation have demonstrated disrupted localization of Nav1.5 only at the lateral membrane and not at the intercalated disc[183]. Further, cardiac-specific SAP97 knockout mice do not demonstrate disrupted localization or functional expression of Nav1.5 at the intercalated disc, suggesting that PDZ-dependent targeting of Nav1.5 is provided mainly through interaction with syntrophin[184]. Interestingly, a report from the Jalife lab added further complexity to this story. In a study published in 2012, Milstein et al. demonstrated that Nav1.5 was complexed with Kir2.1 (mediating I_{K1}) via SAP97 and that SAP97 silencing caused reductions in the both respective current densities. Further overexpression or genetic silencing of Kir2.1 caused respective increases or decreases to Nav1.5 expression and I_{Na} current density[185].

Ziane et al. 2010 demonstrated a functional interaction between Nav1.5 and the cytoskeletal protein α-actinin-2. Transfection of Nav1.5 into tsA201 cells produced significantly greater sodium current density when coexpressed with α-actinin-2. Further, the researchers demonstrated colocalization at the Z-lines in human cardiac sections as well as the interaction of the spectrin repeat domains of α-actinin-2 with the DIII-DIV linker region of Nav1.5[186]. A similar finding was found by Wu et al. 2008 for the cytoplasmic protein MOG1. Coexpression of MOG1 and Nav1.5 in HEK293 cells and

neonatal cardiomyocytes resulted in increased sodium current density due to increased amounts of Nav1.5 membrane expression. Further, MOG1 was shown to associate with Nav1.5 in the DII-DIII linker region and colocalize with Nav1.5 at the intercalated disc[187].

Clearly multiple mechanisms are present to stabilize functional Nav1.5 expression at the cardiomyocyte plasma membrane. However, a clear mechanism for the development of the densities of Nav1.5 at the intercalated disc has not yet been determined. The best evidence for the molecular mechanism targeting Nav1.5 to the intercalated disc is provided by study conducted on ankyrin-G. As discussed previously, Nav1.5 contains a highly conserved ankyrin-G binding sequence in the DII-DIII linker. In 2004, a human *SCN5A* mutation causing Brugada syndrome was identified producing an amino acid change in the ankyrin-G binding sequence (E1053K)[35]. In this study, Mohler and Rivolta demonstrated that ankyrin-G and Nav1.5 functionally interact via this DII-DIII linker and colocalize at the intercalated disc of the cardiomyocytes. Expressing mutated HA-tagged E1053K Nav1.5 into rat cardiomyocytes demonstrated that this sequence was necessary for localization of Nav1.5 at the intercalated disc and the transverse tubule membrane domain. Expression of these channels in HEK cells further showed decreased sodium current density (due to lack of membrane targeting) as well as delayed recovery from inactivation[35].

To more specifically address the role of ankyrin-G in targeting Nav1.5 to the plasma membrane, Lowe et al. 2008 treated isolated rat cardiomyocytes with shRNA for ankyrin-G. Interestingly, shRNA-mediated silencing of ankyrin-G resulted in decreased

expression of Nav1.5 as well as ~50% reduction in peak sodium current density without reductions in whole cell calcium current density. Immunostaining of adult rat cardiomyocytes further showed that localization of Nav1.5 at the intercalated disc is greatly reduced in the absence of ankyrin-G. Interestingly, the researchers further demonstrated that ankyrin-G associated with Nav1.5 through ANK repeats 14 and 15, in contrast to the site of interaction with neuronal Na_V channel isoforms[40].

Ankyrin-G Associates with βIV-spectrin in the Cardiomyocyte

Recall that ankyrins classically associate with isoforms of β-spectrin in the cytoskeleton. In the heart, ankyrin-B has been demonstrated to associate with βII-spectrin[62]. Further, recent investigation has demonstrated that βII-spectrin is required to target ankyrin-B in adult murine cardiomyocytes and human mutations in the ankyrin-B SBD domain produce arrhythmia[188]. Like in the neuron, ankyrin-G associates with βIV-spectrin in the cardiomyocyte at the intercalated disc. Further, βIV-spectrin is required to target the Ca^{+2}/calmodulin-dependent protein kinase II isoform δ (CaMKIIδ) into close proximity to Nav1.5 to regulate its function by phosphorylation at serine 571 in the DI-DII loop. Using a spontaneous βIV-spectrin truncation mouse model that removed the CaMKIIδ binding site (qv3J), Hund et al. 2010 demonstrated that CaMKIIδ targeting to the intercalated disc was abolished even in the presence of a fully formed βIV-spectrin / ankyrin-G / Nav1.5 complex[189].

CaMKIIδ is a multifunctional serine/threonine kinase that becomes activated due to elevated levels of Ca^{+2} or after adrenergic stimulation[190]. In a setting like heart failure,

characterized by massive adrenergic stimulation, CaMKIIδ becomes hyperactivated, producing RyR2 hypersensitivity, increases in Ca^{+2} current via channel facilitation, and phosphorylation of Nav1.5 at multiple sites in the DI-DII loop region[191]. Although multiple phosphorylation sites have been reported with debate focused on their relative importance, the act of Nav1.5 phosphorylation by CaMKIIδ causes 3 functional changes to whole cell Na^{+} current: 1) Decreased peak Na^{+} current density (only reported by Hund et al. 2010) 2) shift of channel availability to more negative potentials, and 3) an increase in the proportion of non-inactivating channels producing a phenomenon termed "late" Na^{+} current[189, 191-193]. This increase in cytosolic Na^{+} reduces the driving force for Na^{+} across the plasma membrane, reducing the amount of Ca^{+2} that can be extruded from the cytoplasm. This results in elevated cytosolic Ca^{+2} and an increase in the SR Ca^{+2} content as a result[194]. This elevation of cytosolic Ca^{+2} and Ca^{+2} load results in RyR2 hypersensitivity, producing spontaneous, proarrhythmic Ca^{+2} release from RyR2 (i.e. sparks/waves)[195, 196]. Late Na^{+} current also prolongs the action potential, another proarrhythmic substrate[193]. As a result, pharmacologic therapies aimed at this "late" component of I_{Na} have been the subject of multiple clinical trials[197, 198].

With respect to the debate over which phosphorylation site is most functionally relevant, recent work published in the journal Circulation by the Hund laboratory using mice with serine 571 ablation (S571A) demonstrated that this site is required for the development of late Na^{+} current at baseline and after transverse aortic constriction (TAC) to produce heart failure. Further, S571A mice displayed reduced amounts of arrhythmia and preserved cardiac function after TAC, compared to WT mice and phosphomimetic

S571 mice (S571E)[199]. These results strongly suggest that phosphorylation of Nav1.5 at S571 is chiefly responsible for arrhythmia associated with CaMKIIδ-dependent Nav1.5 phosphorylation. Although activated CaMKIIδ can directly associate with the DI-II linker of Nav1.5[191], Hund et al. 2010 would hypothesize that βIV-spectrin is necessary for this interaction to occur in vivo. Recall from work in neurons, ankyrin-G is required for the recruitment of βIV-spectrin to the AIS. Our ankyrin-G cKO animal model now enables us to address this question in the cardiomyocyte in vivo. Specifically, our model whether ankyrin-G is functionally required recruit the βIV-spectrin/ CaMKIIδ complex and scaffold to Nav1.5 for functional regulation.

Ankyrin-G: Possible Structural Regulation at the Intercalated Disc?

As we have seen in neurons, ankyrin-G can mediate both cellular excitability and cellular structure. Once again, the cardiomyocyte is no exception. However, unlike the very clear structural roles that ankyrin-G plays in the neuron through mediating L1CAM / neurofascin, the structural role for ankyrin-G in the cardiomyocyte is only beginning to be studied. Implications for a structural role for ankyrin-G in the cardiomyocyte came in a 2011 study conducted by the Delmar laboratory. In this study, Sato and colleagues demonstrated that ankyrin-G associated with the desmosomal protein plakophilin-2 (PKP2) as well as connexin-43, the primary component of gap junctions in ventricular cardiomyocytes. Further, knockdown of ankyrin-G in monolayers of neonatal rat ventricular cardiomyocytes resulted in the reorganization of PKP2 expression, leading to decreased cell-cell adhesion. Ankyrin-G silencing also resulted in the reorganization of

connexin-43 in monolayer preparations[200]. Although the three components of the intercalated disc are visualized as discrete structures by electron microscopy[140], this was not the first study to demonstrate functional cross-talk between the structures of the intercalated disc. As experimental evidence indicates that ankyrin-G may be regulating multiple integral intercalated disc components, we must examine previous work demonstrating this molecular cross-talk at the intercalated disc.

The first example of this comes from a study in 2005 by the Radice laboratory investigating the functional consequence of silencing N-cadherin in the mouse heart. Recall, that the fascia adherens junction, composed of N-cadherin in the heart, scaffolds to filamentous actin through its interaction with α- and β-catenin and is visualized as a unique and discrete structure compared to gap junctions and desmosomes. However, induced-deletion of N-cadherin caused the dissolution of gap junctional and desmosomal structures evidenced at the electron microscopy level. These results were confirmed via severe reduction in expression of desmosomal proteins desmoplakin and plakoglobin and the gap junctional protein connexin-43. These changes produced extensive fibrosis, systolic dysfunction, and lethal cardiac arrhythmia[201]. The molecular basis of this gap junctional remodeling was demonstrated in by Shaw et al. in 2007. In this study, researchers determined that connexin-43 traffics to areas of cell-cell contact via microtubule-dependent traffic. The microtubule plus end binding protein EB1 interacts with β-catenin and p150glued of the fascia adherens structure to target gap junctions to sites of cell-cell contact. Further, using an N-cadherin blocking peptide that prevented cell-cell adhesion further disrupted the traffic of connexin-43 to sites of cell contact[202].

As N-cadherin mediates the integration of actin filaments, this would be the expected site of ankyrin-G / βIV-spectrin complex association at the intercalated disc. As experimental evidence reveals that ankyrin-G is chiefly involved in targeting Nav1.5 in vitro, it is no surprise that recent investigations reveal that the overwhelming majority of Nav1.5 colocalizes with N-cadherin at the intercalated disc[203].

With respect to the cardiac desmosome, the Delmar laboratory demonstrated that PKP2 silencing also decreased localization of connexin-43 at sites of cell-cell contact, as demonstrated by decreased dye transfer between cell pairs after PKP2 knockdown[204]. Further, Delmar demonstrated either direct or indirect association between PKP2 and connexin-43[200]. Interestingly, work conducted again by the Delmar group also demonstrated that silencing of desmosomal PKP2 resulted in decreased peak Na^+ current in cultured adult cardiomyocytes[205]. Further, an association between PKP2 and Nav1.5 was demonstrated via co-immunoprecipitation experiments[200]. Functionally, mice with heterozygous knockout of PKP2 (PKP2-Hz) display ~25% reduction in whole cell Na^+ current and inducible ventricular arrhythmia after administration of the Na^+ channel blocker flecainide[206]. However, these mice did not display any reduction in Nav1.5 expression or apparent cellular mislocalization. In a subsequent study by the Delmar laboratory, missense mutations in PKP2 also result in decreased Na^+ current when expressed in PKP2-silenced HL-1 cells compared to WT PKP2. Further, this investigation would demonstrate that Na^+ current was selectively reduced at the intercalated disc in PKP2-Hz cells. However, in this study, PKP2-Hz animals now exhibited decreased expression of Nav1.5 colocalizing with N-cadherin at the intercalated

disc, in contrast to previous work[207]. Although these results are contradictory, a role for the desmosome in mediating Na^+ current was further defined by work with mice overexpressing a mutant DSG2 isoform (Dsg2-N271S) also resulting in minor reductions in Na^+ current and severe ventricular arrhythmia[208]. Silencing of desmoplakin in HL-1 cells also causes severe reductions in whole-cell Na^+ current[209]. Further, human desmosomal mutations causing ARVC cause severe reductions in the intercalated disc population of Nav1.5 regardless of which desmosomal protein is mutated[210]. These results indicate that the desmosome either directly or indirectly through ankyrin-G are also critical regulators of Nav1.5 function at the intercalated disc.

Recall, that ankyrin-G is implicated in regulating connexin-43 localization to the plasma membrane in cardiomyocytes[200]. SiRNA against ankyrin-G in monolayers of neonatal rat ventricular cardiomyocytes disrupts normal connexin-43 localization at sites of cell-cell contact and reduced junctional conductance in these preparations[200]. How is this occurring? The gap junction plaque is composed of two areas. The first area, in the center of the plaques is composed of united hemichannels, producing functional unison of adjacent cytoplasm to propagate the cardiac action potential. On the periphery of the gap junctional plaque is an area termed the "perinexus" composed of large populations of singular hemichannels associated with the scaffolding protein zonula occludens-1 (zo-1)[211]. Interestingly, zo-1 has been demonstrated to scaffold connexin-43 to αII-spectrin in the cardiomyocyte[212]. Recall from earlier studies, ankyrin polypeptides bind to the center of the spectrin tetrad to a molecule of β-spectrin. If the spectrin tetrad can only interact with zo-1 or ankyrin-G at any one time, reduction of ankyrin-G may then favor increased

accumulation of zo-1 at the intercalated disc. This would increase the size of the gap junctional plaque (i.e. more connexin-43 hemichannels) due to the increased abundance of uncoupled hemichannels. This hypothesis was confirmed by the Delmar group in 2013. Si-RNA mediated ankyrin-G silencing resulted in larger gap junctional plaques leading the researchers to speculate that ankyrin-G acts to restrict the size of connexin-43 plaques[213].

Several other lines of evidence suggest that ankyrin-G may be functionally interacting with connexin-43. Cardiac-specific deletion of connexin-43 did not result in changes to any member of the fascia adherens or desmosome complexes[214]. However, treatment of isolated rat cardiomyocytes with siRNA against connexin-43 resulted in ~40% decreased peak Na^+ current density. Further, mice heterozygous for connexin-43 demonstrated decreased localization of Nav1.5 at the intercalated disc[215]. Most perplexing is the studies conducted on mice lacking the last 5 c-terminal amino acids of connexin-43. Although the connexin molecules in these animals traffic to the plasma membrane normally and couple as a functional connexon, intercalated discs in these mice display greatly reduced localization of Nav1.5. Further, although the zo-1/connexin-43 interaction is maintained, these mice display lethal ventricular arrhythmia and sudden cardiac death[216]. This finding was expanded upon in 2014 by the Delmar laboratory. Using the same mouse model, the Delmar group demonstrated that microtubule capture at the intercalated disc was severely impaired, leading to reduced delivery of Nav1.5[203]. However, ankyrin-G localization / expression was not determined in this study.

Importantly, multiple studies have demonstrated remodeling of the Na_V channel complex associated with human desmosomal variants causing ARVC and Brugada syndrome[210, 217]. However, the VGSC complex has also been shown to be disrupted in acquired CVD. In 2005, Valdivia et al., demonstrated that cardiomyocytes isolated from failing human and canine myocardium demonstrate severely reduced levels of Na^+ current[218]. This decrease in Na^+ current density is also witnessed in murine heart failure models and diabetic rabbit ventricular cardiomyocytes[219, 220]. Further, work from the Delmar laboratory demonstrated loss of ankyrin-G immunoreactivity at the intercalated disc in a sheep pulmonary hypertension model. This was correlated with the cellular redistribution of Nav1.5, connexin-43, and desmosomal components in right ventricular cardiomyocytes[126]. These findings suggest an extensive ankyrin-G interactome at the intercalated disc. Further, as changes to Na^+ current density seem to be an underlying finding in multiple forms of heart failure, investigation of ankyrin-G in disease states may shed light on both the electrical and structural remodeling seen in heart failure.

Ankyrins in Acquired Human Disease

Although multiple studies have demonstrated that variants in *ANK1*, *ANK2*, and *ANK3* lead to severe human disease, ankyrins themselves are dysregulated in acquired disease states. In 1993, Bennett and colleagues demonstrated that ischemic conditions decrease levels of ankyrin polypeptides in kidney and brain[221]. Further work by Yoshida in 1997 demonstrated that ankyrin in the heart is degraded by the Ca^{+2} activated protease calpain after myocardial ischemia[222]. These results were mirrored by the work of Kashef

et al. 2012 demonstrating that activated calpain and reactive oxygen species also caused decreases in ankyrin-B[223]. With respect to ankyrin-G, work by the Rasband laboratory has demonstrated that ankyrin-G and βIV-spectrin are also degraded by calpain activation after traumatic brain injury[224]. In the heart, work from the Boyden lab represent the only data regarding the fate of ankyrin-G in cardiovascular disease states. In a canine myocardial infarct model, cells isolated from the border zone of the infarct actually demonstrate an increase in ankyrin-G expression as early as 48 hours post infarction[127]. Clearly more work will be required to determine the role of ankyrin-G in acquired CVD states.

Overview of Proposed Hypotheses

Given the wealth of published experimental data regarding the molecular physiology of ankyrin-G, several hypotheses can be made regarding the functional outcome of silencing ankyrin-G in the cardiomyocyte in vivo. First, given the role of ankyrin-G in targeting Nav channels in neurons, we hypothesize that silencing ankyrin-G expression in the cardiomyocyte will affect functional Nav1.5 expression. Further, as ankyrin-G localizes predominantly to the intercalated disc, we hypothesize that ankyrin-G may be a molecular mechanism responsible for the preferential localization of Nav1.5 at the intercalated disc membrane domain. Further, as data from epithelial cells demonstrate a structural role for ankyrin-G, we hypothesize that silencing of ankyrin-G will also produce severe structural phenotypes. Specifically, as in vitro data suggest that ankyrin-G regulates the desmosomal protein PKP-2, we hypothesize that functional PKP-

2 expression will be disrupted in the absence of ankyrin-G, possibly producing severe structural deficiencies in ankyrin-G cKO cardiomyocytes.

In this dissertation, I will provide data demonstrating that ankyrin-G cKO mice display significantly reduced expression of Nav1.5 at the intercalated disc. Further, we demonstrate that ankyrin-G is required for the development of a signaling complex around Nav1.5 (composed of CaMKIIδ and βIV-spectrin). In response to decreased targeting of Nav1.5, ankyrin-G cKO mice display bradycardia, conduction defects, and arrhythmia due to decreases in functional Na+ current. We will also demonstrate that the localization of the desmosomal protein PKP-2 is disrupted in the ankyrin-G cKO cardiomyocyte. Interestingly, we will also demonstrate that ankyrin-G cKO mice develop severe cardiomyopathic remodeling with age and after transaortic constriction (TAC). Interestingly, ankyrin-G cKO mice display severe systolic deficiency, pathologic ventricular remodeling, and bradyarrhythmic death. We hypothesize that ankyrin-G expression is required for proper cardiac compensatory response. Further, we provide evidence that functional expression of ankyrin-G is reduced in the setting of human heart failure. Therefore, we hypothesize that dysregulation of ankyrin-G may be a common event in the development and/or progression of human heart failure.

Chapter 2: Materials and Methods

Animals

Cardiac-restricted Ankyrin-G knockout (cKO) mice were generated as follows. LoxP sites were introduced via homologous recombination of targeting construct containing: 1) homologous DNA to exons 22 and 23 of the Ank3 gene, 2) Neomycin-resistance gene flanked by flippase recognition target (FRT) sites, 3) LoxP sites at terminal ends of construct. By homologous recombination, this construct is inserts by random chance into the mouse genome of embryonic mouse stem cells. Stem cells stably expressing the targeting vector are selected for based on neomycin resistance. Surviving stem cells are then treated with Flp recombinase to excise the neomycin resistance gene. These embryonic stem cells are injected into female mice, creating chimeric founder (F1) animals. The chimeric founders are then back-crossed with c57/bl6 wild type (WT) mice for germline transmission of the integrated loxP sites (i.e. F2 generation). These mice are then back-crossed with c57bl6 WT mice multiple generations to generate mice carrying the loxP sites on a clean c57bl6 background. To achieve cardiac-specific knockout of ankyrin-G, mice from F2 generation are crossed with mice expressing Cre recombinase under the control of the *Myh6* promoter (αMHC). For all experiments, WT and cKO male mice were used (aged 8 weeks at start of experiment, c57/bl6 background). To test the role of β_{IV}-Spectrin (*Sptbn4 gene in mice*) with respect to localization of ankyrin-G, Qv^{4J}

mice (on a c57/bl6 background) were also utilized. "Quivering" (qv) mice are a group of mice with spontaneous mutations in the Sptbn4 gene causing truncations in the β_{IV} spectrin protein[225]. As β_{IV}-Spectrin is critical for proper neuronal function, these mice spontaneously develop severe neurologic and neuromuscular phenotypes[225]. The truncation in qv^{4J} mice occurs in spectrin repeat 10, abolishing the ankyrin-G / βIV-spectrin interaction (ankyrin-G associates with βIV-spectrin at spectrin repeat 15). For aging studies , WT and cKO animals were aged to 15 months. All animal studies and surgeries were performed in accordance with the American Physiological Society Guiding Principles for Research Involving Animals and Human Beings, and approved by The Ohio State University Institutional Animal Care and Use Committee. The investigation conforms to the Guide for the Care and Use of Laboratory Animals published by the US National Institutes of Health (NIH Publication No. 85-23, revised 1996.)

Human Heart Tissue

Non-failing and failing (ischemic/non-ischemic) left ventricular tissue was obtained from explanted hearts undergoing heart transplantation through The Cooperative Human Tissue Network: Midwestern Division at The Ohio State University. The Institutional Review Board of The Ohio State University provided approval for the use of human subjects. Age and sex were the only identifying information acquired. This investigation conforms with the principles outlined in the Declaration of Helsinki. Ventricular samples were prepped for immunoblot as described below. Cryosections of human heart samples prepared and treated as described below.

Telemetry

At 8 weeks of age, WT and cKO mice were implanted with ETA-F10 radiotelemeters. Briefly, mice were anesthetized with 2.5% isoflurane and transferred to a heated, sterile surface. Anesthesia maintained at 1.5% for duration of procedure. Hair is removed from the ventral side of the animal and skin is sterilized with betadine. A midline incision is then made along the sternum of the animal. Using blunt dissection, a subcutaneous pocket is made on the right side of the animal at the abdominal level. A sterilized ETA-F10 telemeter is implanted in the pocket. The negative lead is placed subcutaneously in the right axilla and the positive lead is placed subcutaneously on the animals left side at the abdominal level. Following surgery, mice receive analgesia in the form of buprenorphine and are let to recover for seven days prior to electrocardiogram (ECG) recordings. Average resting heart rate, PR interval, QRS interval, QT interval were obtained from continuous 2 hr ECG recordings. Stress conditions were stimulated via the injection of epinephrine (2 mg/kg, i.p.). Mice were monitored for 2 hours to determine burden of arrhythmia. For TAC/sham experiments, animals were permitted to recover for 1 week following TAC/sham surgery. Mice were then implanted with telemeters as previously outlined and let to recover 1 week. Mice were analyzed at 2 weeks post TAC/sham operation. All telemetered ECG traces and waveforms were analyzed using P3 Plus software (Ponemah).

Subsurface Electrocardiography

For anesthetized surface ECG recordings, mice were anesthetized with 2% isoflurane and oxygen at rate of 1.0 L/min. Mice were placed in the prone position on a heated pad to maintain body temperature. Anesthesia maintained at 1% isoflurane at 1.0 L/min. Subcutaneous electrodes were placed in the lead II configuration and ECGs were recorded on a Powerlab 4/30 (AD Instruments). Baseline ECG was recorded for 3 minutes after anesthesia. Flecainide (20 mg/kg, i.p.)[226] was administered at 3 min after anesthesia and ECGs were recorded by the protocol detailed by Knollmann and colleagues.[227] ECG traces were analyzed using LabChart 7 Pro (AD Instruments) for average heart rate, PR interval, QRS interval, and QT interval.

Transverse Aortic Constriction (TAC) Experiments

To produce pressure-overload conditions, transverse aortic constriction (TAC) was performed on 8 week-old WT and cKO mice. Briefly, mice were anesthetized with isofluorane (2.5%) and intubated. Intubated mice were placed on respirator (120 breaths/min, 0.1 mL tidal volume) and anesthesia was maintained throughout procedure. The thoracic cavity was opened using a partial midline sternotomy and the transverse aorta was exposed via blunt dissection. Once the aorta was identified, a 6.0 Prolene suture was placed around the transverse aorta between the brachiocephalic and left common carotid artery. The suture was tightened around a 27-gauge needle placed next to the aorta to standardize degree of constriction. The needle was then removed, the thoracic cavity and overlying skin was closed, and appropriate analgesia was

administered (buprenorphine, 0.1 mg/kg, i.p.). For sham controls (age/sex matched), the identical protocol was utilized without the aortic constriction. At termination of experiments (6 weeks post TAC/sham surgery), mice were anesthetized (2% Avertin, 20 μL/g body weight, i.p.) and sacrificed via thoracotomy. Following euthanasia of animals, hearts, lungs, and tibias were removed for analysis.

Echocardiography

To assess cardiac function in vivo, 2D-echocardiography (Vevo 2100, Visualsonics) was performed at baseline, at 12 months of age, and at regular time intervals post TAC/sham intervention. Mice were anesthetized in induction chamber at 2% isoflurane in oxygen at flow rate of 1.0L/min. Mice were then placed in supine position on a heated stage and hair was removed from the chest using depilatory lotion. Anesthesia maintained at 1.5% isoflurane for duration of experiment. Heart rate was monitored throughout protocol to ensure proper anesthetic dosage. Using a MS-400 transducer, proper anatomical orientation was determined via imaging of the long axis of the heart. Once proper orientation was achieved, the transducer was turned 90 degrees to visualize short axis of the left ventricle. M-mode images recorded at the level of the papillary muscles. Images were analyzed to assess ejection fraction, chamber diameters, and ventricular wall thicknesses.

Immunofluorescence

Cardiomyocytes (left ventricle) and cardiac cryosections (5 μm thickness) were isolated/prepared from WT and cKO (baseline/TAC) hearts as follows. Hearts were

excised from animal and placed into cold Modified Tyrode (MT) solution (ref). For isolated cells, the hearts were then cannulated via the aorta and perfused with Hank's solution (Life Technologies) to clear the coronary circulation. The heart was then placed on a modified Langendorff apparatus and perfused with Solution A (0.065 mM EGTA in MT) to chelate free calcium and inhibit cardiac contraction. Hearts were then perfused with Solution B (0.01 mM $CaCl_2$ in MT) containing Type 2 collagenase (Worthington, 0.6 mg/ml) and Type XIV Protease from *Streptomyces griseus* (Sigma, 0.12 mg/ml) for digestion. Digested hearts were triturated in Solution C (0.1733 mM $CaCl_2$ in MT) to dissociate cells. Cells were strained and pelleted to enrich for live cardiomyocytes. For cardiac cryosections, hearts were excised from the animal and washed in cold phosphate-buffered saline (PBS) to remove blood from the heart. Washed hearts were then placed into molds filed with OCT medium (Tissue-Tek) and frozen in liquid nitrogen. Isolated cells and tissue slices were fixed and permeabilized in 100% ethanol at -20 ^{O}C. Cells/sections were blocked in 3% fish skin gelatin and 0.1% Triton X-100 in PBS. Cells/sections were stained with primary antibody overnight at 4 ^{O}C in blocking solution. Cells/sections were stained with secondary antibodies in blocking solution for >1 hr at room temperature. Secondary antibodies included Alexa-conjugated donkey anti-mouse 488, 568 and donkey anti-rabbit 488, 568. Cells were imaged on a LSM 780 confocal microscope (Carl Zeiss). Cells/sections were imaged using identical confocal settings between genotypes.

Immunoblotting and Antibodies

Human ventricular and murine whole heart lysates, following quantitation by BCA assay (Pierce), were loaded into 4-15% precast gels (BioRad) and transferred to nitrocellulose membranes. Membranes were blocked for >1hr at room temperature in 5% milk or 3% bovine serum albumin and incubated in primary antibody overnight at 4°C. Primary antibodies included ankyrin-G (1:10,000 homemade), ankyrin-G (1:1,000 Santa Cruz), CaMKIIδ(1:500, Badrilla), β_{IV} spectrin (1:1000, gift from M. Komada, Tokyo Institute of Technology, Yokohama, Japan), $Na_v1.5$ S571 (1:500) [189], $Na_v1.5$ (1:500) [189] N-Cadherin (1:2000, Invitrogen), connexin-43 (1:1000 Invitrogen), plakophilin-2 (1:500 Abcam), desmoplakin (1:1000, Santa Cruz), desmocollin-2 (1:1000, BD biosciences), Desmin (1:1000, Invitrogen), α-Tubulin (1:1000, Invitrogen) β-catenin (1:2000, BD Biosciences), ZO-1(1:1000, Invitrogen), ankyrin-B[65] (1:2000), Na/Ca exchanger (1:500, Swant), $Ca_v1.2$ (1:1000, Invitrogen), actin (1:2000, Santa Cruz), GAPDH (1:5000, Fitzgerald). plakophilin-2 (1:500 Abcam), GAPDH (1:5000, Fitzgerald). Secondary antibodies used were donkey anti-mouse-HRP and donkey-anti-rabbit-HRP (1:5000, Jackson Laboratories). Densitometric analysis was performed using Image Lab software and all protein expression data were normalized to GAPDH expression.

Biochemistry

Immobilized GST-fusion proteins were incubated with 100 µg left ventricular heart lysate overnight in pull-down buffer at 4 °C.[228] The samples were washed three times in pull-down buffer, eluted, and proteins were separated by SDS/PAGE. The gels were

transferred to nitrocellulose and immunoblotted. Nitrocellulose blots were developed using standard ECL protocols.

Histology

Hearts were excised and fixed in 10% formalin, processed and embedded into paraffin for sectioning. Hearts are sectioned along the long axis (4 chamber view) at a thickness of 10 microns. Sections are stained with hematoxylin and eosin (H&E) to examine general structure and histology and Masson's trichrome to visualize collagen deposition (fibrosis).

Electrophysiology

I_{Na} currents were recorded utilizing a patch-clamp configuration using an Axopatch 200B amplifier and Digidata 1440A digitizer on left ventricular myocytes. Data acquisition and analysis was performed using pCLAMP software (ver.10.3; Molecular Devices, Sunnyvale, CA). Sodium currents (I_{Na}) were recorded at room temperature (20-22 °C) with pipette resistances <2.8 MΩ when filled with pipette filling solution containing (in mM): NaCl (5), CsF (135), EGTA (10), MgATP (5), Hepes (5), pH 7.2. The extracellular bathing solution contained (in mM): NaCl (5), $MgCl_2$ (1), $CaCl_2$ (1.8), $CdCl_2$ (0.1), glucose (11), CsCl (132.5) and Hepes (20); pH was maintained at 7.4 with CsOH at room temperature. Appropriate whole-cell capacitance and series resistance compensation (≥60%) was applied along with leak subtraction. To assess the I_{Na} density, cells were held at -160 mV and stepped to various test potentials from -100 to 30mV in 5 mV increments, with 200 ms duration pulses and 2800 ms interpulse intervals. Voltage-

dependence of inactivation was assessed by holding the cells at -160 mV followed by a 300 ms test pulse from -140 to -40 mV in 5 mV increments; interpulse interval was 2700 ms. Recovery from inactivation was studied by holding cells at -160 mV and applying two 20 ms test pulses (S1, S2) to -45 mv, separated by increasing increments of 1 ms to a maximum S1-S2 interval of 50 ms. The S1-S1 interval was kept constant at 2000 ms. I_{Na} late was determined by quantifying the persistent current during an active voltage pulse at time range of 100-200msec after the activation of I_{Na} and was expressed as a percentage of I_{Na} peak amplitudes. Prior to quantification, baseline was set to zero. Action potentials were measured as described.[189, 192]

Calcium Measurements.

Myocyte calcium measurements were performed as described.[229]

Statistics

Data were analyzed using SigmaPlot 12.0. P values were determined with the unpaired Student T-test (2 tailed) in the case of single comparisons and with 1-way ANOVA in the case of multiple comparisons. The Newman-Keuls multiple comparison test was used for post hoc testing. If the data distribution failed normality tests with the Shapiro-Wilk test, rank-based ANOVA and the Dunn multiple-comparisons test were performed. Incidence of death following bradyarrhythmia, incidence of ventricular arrhythmia and AV block after flecainide, and incidence of death following epinephrine administration was analyzed by Chi Square Test. Kaplan-Meier survival analysis was used to determine risk

of mortality following TAC procedure. In all cases, a p-value <0.05 was considered statistically significant.

Chapter 3: Ankyrin-G Coordinates Intercalated Disc Signaling Platform to Regulate Cardiac Excitability In Vivo.

Introduction

$Na_v1.5$ (encoded by *SCN5A*) is the principal Na_V channel in the cardiomyocyte. In ventricular and atrial cardiomyocytes, $Na_v1.5$ regulates the rapid upstroke of the cardiac action potential (phase 0), initiating the process of excitation-contraction coupling. Proper Nav1.5 expression is critical for proper excitation and function of the sinoatrial (SA) and atrioventricular (AV) nodes, and atrial and ventricular myocytes [178, 230, 231]. Owing to its critical importance for proper cardiac physiology, human *SCN5A* mutations are linked with multiple forms of human CVD including sinus node dysfunction, atrial fibrillation, conduction defects, and ventricular arrhythmias.[231-233] Further, in the setting of acquired CVD, expression and select electrophysiological properties of $Na_v1.5$ become dysregulated, increasing the proarrhythmic potential in cardiovascular disease states. As a result, medical therapies targeted to select properties of $Na_v1.5$ have remained at the forefront of cardiovascular medicine.[234] Unfortunately, the molecular pathways underlying $Na_v1.5$ regulation remain largely undefined partially due to lack of essential *in vivo* data.

Over the past few decades, immunological and electrophysiological evidence has demonstrated that $Na_v1.5$ preferentially localizes to this intercalated disc microdomain,

although minor populations can be found throughout the entire cell. At the intercalated disc are structures known as gap junctions, molecular connections that serve as low resistance pathways for current flow between adjacent cardiomyocytes. This electrical unison of adjacent cardiomyocytes allows action potentials to propagate from one cell to the other, synchronizing the excitation of cardiac tissue to produce a coordinated contraction. As depolarizing current from an upstream cardiomyocyte passes through the gap junctions, these densities of $Na_v1.5$ channels are optimally placed to sense this depolarization and subsequently initiate another action potential. As gap junctions can uncouple in disease states, this intercalated disc localization of $Na_v1.5$ becomes even more critical to maintain proper electrical activation of adjacent cardiomyocytes in disease states. Although the field as a whole nearly unanimously agrees that $Na_v1.5$ is preferentially targeted to the intercalated disc, the molecular mechanism(s) producing this biased localization in vivo are unknown and untested.

Ankyrin polypeptides play critical roles in ion channel and transporter targeting in excitable and non-excitable cells, as described previously. Ankyrin-R (*ANK1*) links membrane transporters (Band 3) to the cytoskeleton in erythrocytes and human *ANK1* mutations cause hereditary spherocytosis.[53] Ankyrin-B (*ANK2*) is critical for ion channel and transporter targeting in heart, brain, and pancreas, and ankyrin-B dysfunction has been linked with sinus node disease, atrial fibrillation, ventricular arrhythmia, and diabetes.[22, 31, 32, 235, 236] Ankyrin-G (*ANK3*) has been shown to be necessary for the targeting and retention of voltage gated sodium channels (Nav1.2 and Nav1.6) to the axon initial segment and nodes of Ranvier in neurons.[26, 101] While *in vitro* work supports

an association between ankyrin-G and $Na_v1.5$ in heart[40, 237], little is known regarding the role of this interaction *in vivo*.

$Na_v1.5$ is principally regulated by membrane voltage. However, more recent data demonstrate that $Na_v1.5$ is secondarily modulated by the calcium/calmodulin-dependent kinase II (CaMKIIδ) for acute action potential modulation and propagation. [238, 239] Importantly, elevated CaMKIIδ activity in heart disease is associated with increased pro-arrhythmic $Na_v1.5$-dependent late sodium current ($I_{Na,L}$). [238, 239] The mechanisms underlying CaMKIIδ-dependent regulation of $Na_v1.5$ were unknown until recent work from Hund and colleagues revealed phosphorylation of the $Na_v1.5$ at Serine571 at baseline dependent on CaMKIIδ activity. Further, $Na_v1.5$ was hyper-phosphorylated at this site in disease states.[189] This work also demonstrated that CaMKIIδ was targeted to the intercalated disc through association with βIV-spectrin, a molecule originally identified in brain and linked with neurological disease.[225]. Importantly, this work suggested that CaMKIIδ coupling to $Na_v1.5$ may be dependent on an ankyrin-G / βIV-spectrin interaction.

Here we report the molecular basis of a novel signaling platform in heart that couples CaMKIIδ to $Na_v1.5$. Our *in vivo* data demonstrate that ankyrin-G serves as an ID receptor for both $Na_v1.5$ and βIV-spectrin. Mice harboring a conditional null allele for ankyrin-G in heart (cKO) are surprisingly viable, but display decreased $Na_v1.5$ expression and deficient localization at the intercalated disc. Functionally, these changes associated with decreased Na+ current (I_{Na}), producing bradycardia, conduction abnormalities, QRS prolongation, and ventricular arrhythmias in response to Na_v channel

antagonists. Further, ankyrin-G cKO mice show loss of βIV-spectrin recruitment to the intercalated disc membrane. The βIV-spectrin C-terminal domain associates with CaMKIIδ, and ankyrin-G cKO mice, as well as βIV-spectrin mutant mice lacking the C-terminal domain (qv^{4J}) show defects in CaMKIIδ targeting and CaMKIIδ-dependent regulation of $I_{Na,L}$. Finally, we report that the ankyrin-G-dependent protein platform links Na_v channels with broader intercalated disc signaling/structural nodes, as *in vivo* ankyrin-G loss results in remodeling of plakophilin-2, a resident desmosomal protein critical for intercalated disc integration with the intermediate filament-based cytoskeleton. Together, our findings identify a novel molecular platform critical for the membrane recruitment and regulation of $Na_v1.5$ in heart. These findings further provide new insight into the pathways underlying cardiac excitability in health and disease.

Results

Generation of mice with cardiac-specific deletion of ankyrin-G

Based on its role in assembly of excitable domains in the nervous system[240], and *in vitro* links with $Na_v1.5$ in myocytes[35], we hypothesized that ankyrin-G serves as a molecular platform for cardiac $Na_v1.5$ signaling. To address this hypothesis *in vivo*, we generated a conditional null mutant allele where exons 22 and 23 of the mouse ankyrin-G gene (*Ank3*) are flanked by LoxP sites ($Ank3^{f/f}$) and therefore are deleted in the presence of Cre recombinase (Figure 2A-C). We selectively eliminated ankyrin-G in post-natal cardiomyocytes by utilizing αMHC-Cre knock-in mice[81]; homozygous conditional knockout mice are referred to as αMHC-Cre; $Ank3^{f/f}$ or cKO. $Ank3^{WT/WT}$ age- and sex-

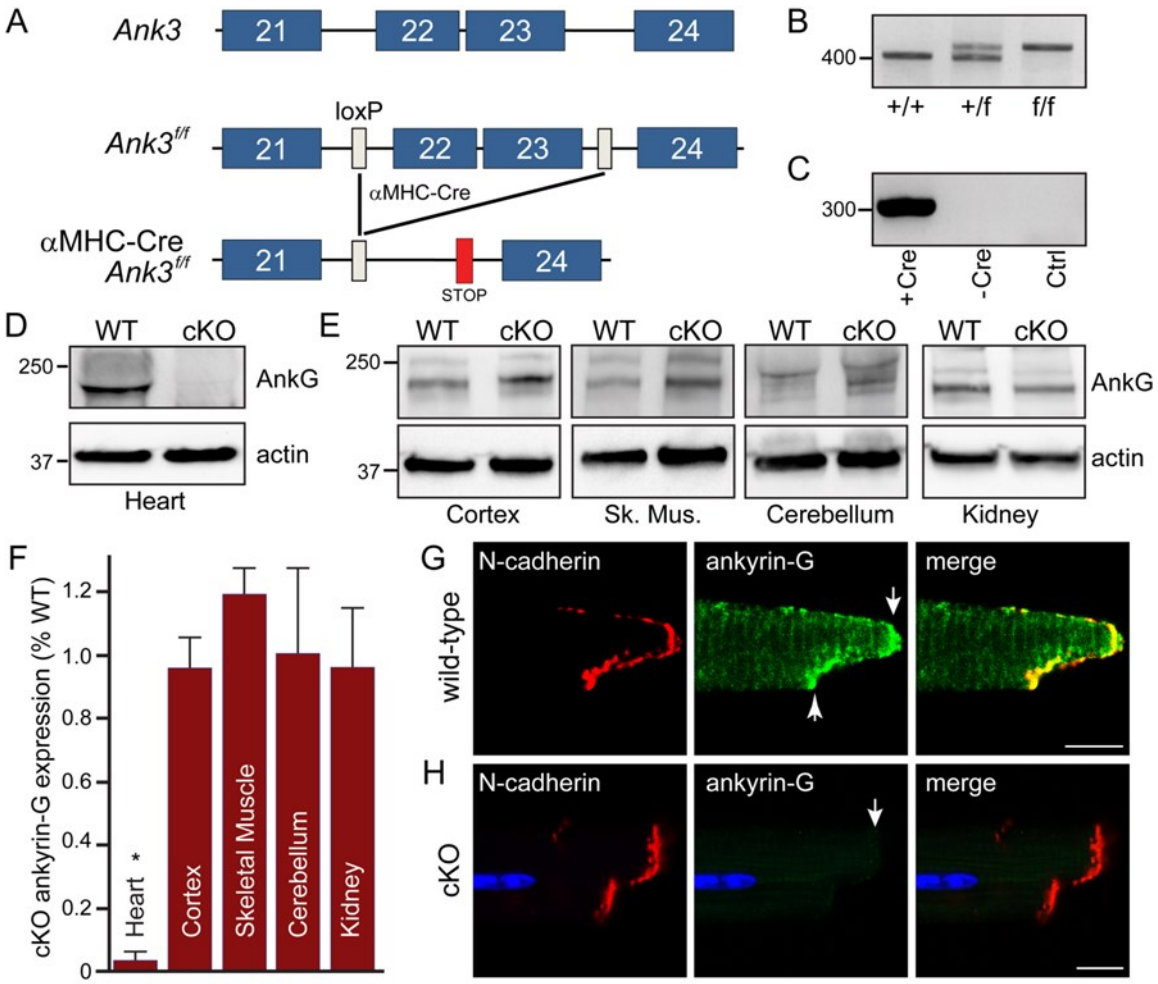

Figure 2. Generation of cardiac-specific ankyrin-G null mouse.

Scheme for generation of cardiac conditional ankyrin-G null mouse (cKO). LoxP sites were inserted to flank exons 22-23 in ankyrin-G gene (*Ank3*). Mice homozygous for

(Continued on Page 84)

(Figure 2 continued from Page 83)

loxP insertion (f/f) were crossed with mice expressing Cre recombinase under control of the αMHC promoter. Cre-mediated excision of exons 22-23 resulted in the production of a premature stop codon after exon 21. (**B**) Flox (*f*) allele (434 bp) and WT (+) allele (366 bp) identified by PCR. (**C**) Cre expression (+ Cre) evidenced by band at 300 bp not observed in WT animals (- Cre) and in no template control (Ctrl). (**D-E**) Ankyrin-G expression in WT and cKO mouse tissue lysates. Note that unlike heart, other tissues examined express multiple molecular weight forms of ankyrin-G. (**F**) Data from experiments in D-E were quantified and expressed relative to WT tissue (corrected for actin expression; n=4/genotype, $p<0.05$). (**G-H**) Expression of ankyrin-G (green) and N-cadherin (red) in WT and cKO myocytes (Bar=10 microns; arrow notes intercalated disc). DAPI (blue) was included to stain nuclei.

matched littermates were utilized as control mice. Surprisingly, cKO mice were viable, displayed no gross differences in size, weight, feeding, grooming, and showed no apparent deficits in motor function, unlike mice harboring selective deletion of cerebellar ankyrin-G.[240] Immunoblots from whole heart lysates showed elimination of ankyrin-G in cKO heart (Figure 2D). Selective loss of ankyrin-G in the heart was confirmed by immunoblot from cerebral cortex, cerebellum, skeletal muscle, and kidney of control and cKO mice where we observed no difference in ankyrin-G expression (Figure 2E-F). At the level of the single ventricular myocyte, ankyrin-G is enriched at the intercalated disc, as demonstrated by colocalization with N-cadherin (Figure 2G). Ankyrin-G expression at the intercalated disc (and minor population at transverse-tubule) was eliminated from cKO ventricular myocytes (Figure 2H).

Ankyrin-G cKO mice display abnormal $Na_v1.5$ targeting and function

Ankyrin-G is linked with VGSC function in cerebellar neurons.[240] We therefore examined $Na_v1.5$ expression, localization, and function in ankyrin-G cKO hearts. Consistent with an *in vivo* role of ankyrin-G for $Na_v1.5$ membrane targeting, we observed a significant decrease in $Na_v1.5$ expression in cKO hearts by immunoblot (Figure 3A-B, $p<0.05$). While primarily localized to the intercalated disc, $Na_v1.5$ is also found in secondary populations at the peripheral sarcolemma[183, 241] In line with immunoblot data, $Na_v1.5$ expression was significantly reduced in cKO compared with WT myocytes (Figure 3C-D). Moreover, consistent with the localization of ankyrin-G, we observed selective loss of $Na_v1.5$ from the intercalated disc in cKO myocytes (Figure 3C-F).

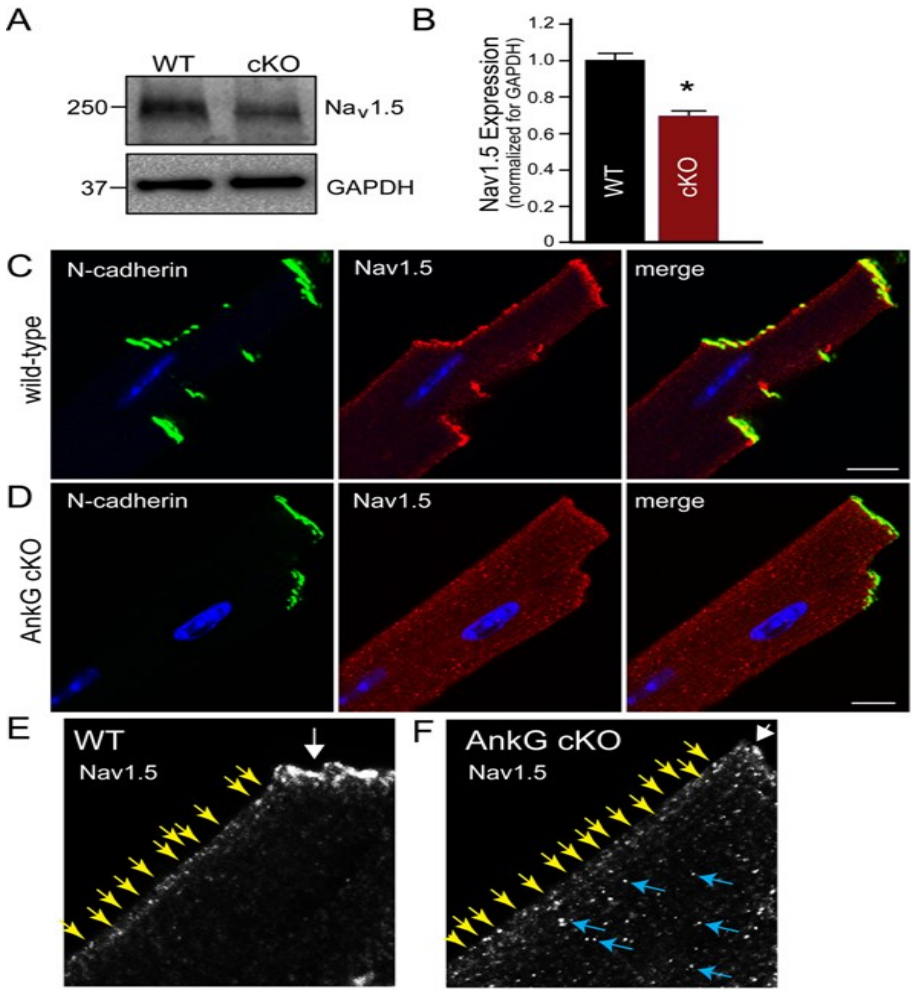

Figure 3. Ankyrin-G is required for myocyte Na$_v$1.5 expression and targeting

(**A-B**) Expression of Na$_v$1.5 in WT and cKO heart. In **B**, levels are normalized to GAPDH loading control (n=4/genotype; $p<0.05$). (**C-D**) Expression of Na$_v$1.5 (red) is

(Continued on Page 87)

(Figure 3 continued from Page 86)

significantly reduced at the intercalated disc of cKO myocytes (Bar=10 microns). Myocytes were co-labeled for N-cadherin (green) and nuclei (blue DAPI). (**E-F**) Magnified images of Nav1.5 immunostaining of peripheral sarcolemma and intercalated disc of WT and cKO myocytes. Note in E that Nav1.5 is present at both intercalated disc (white arrow) and peripheral sarcolemma membrane (yellow arrows). While disc staining is reduced in cKO myocytes, the sarcolemmal staining is unaltered (F). In cKO myocytes, we also observed intracellular Nav1.5-positive puncta (blue arrows).

However, $Na_v1.5$ immunostaining at the peripheral sarcolemma in cKO myocytes was unaffected (Figure 3C-F). This loss was specific for $Na_v1.5$ as expression levels of $Ca_v1.2$, Na/Ca exchanger 1 (NCX), and ankyrin-B were unchanged between WT and cKO hearts (Figure 4 A-C). Consistent with these data, we observed ~50% reduction in peak I_{Na} in cKO myocytes compared with myocytes from WT littermates (Figure 5A-D). Previous reports have indicated that ankyrin-G association with neuronal VGSC affects channel inactivation in heterologous cells. While I_{Na} was reduced in cKO myocytes, we observed no difference in $Na_v1.5$ steady-state voltage-dependent inactivation or recovery from inactivation (Figure 5 E-F). This selective reduction in I_{Na} is further consistent with in vitro data of shRNA-mediated ankyrin-G silencing in adult rat cardiomyocytes. Finally, consistent with prior findings in *Scn5a*$^{+/-}$ mice [242], loss of I_{Na} in cKO myocytes resulted in a significant decrease in action potential (AP) amplitude and maximum upstroke velocity (V_{max}; Figure 6 A-B). Together, these findings demonstrate an *in vivo* requirement of ankyrin-G for cardiac $Na_v1.5$ membrane expression and function.

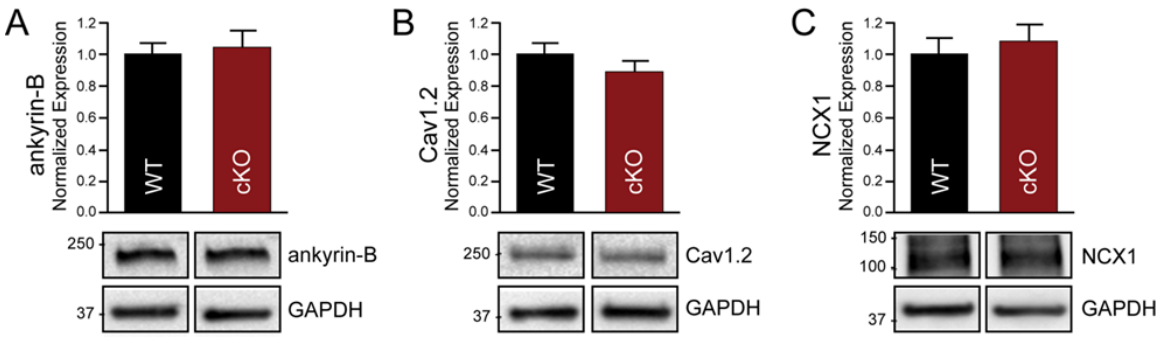

Figure 4. Ankyrin-B, Cav1.2, and NCX expression levels are not altered in cKO heart.

(**A-C**) Immunoblots and normalized expression levels of myocyte proteins in WT versus cKO heart (n=4/genotype; p=N.S.).

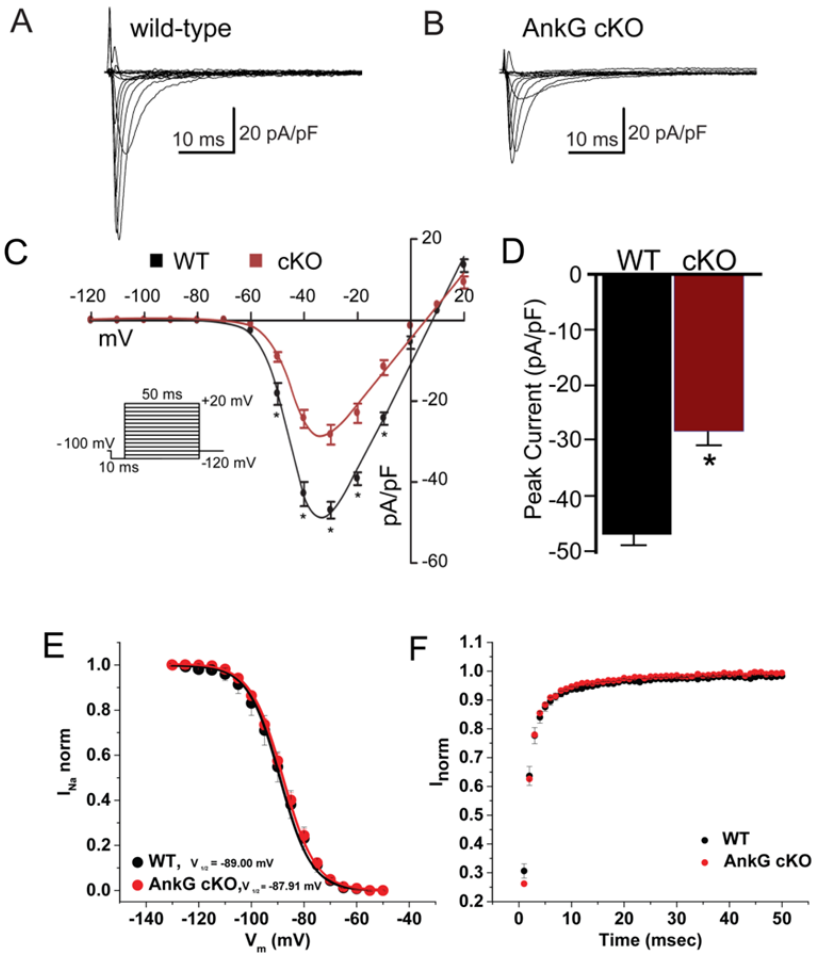

Figure 5. Ankyrin-G cKO ventricular myocytes display decreased whole cell I_{Na}.

(**A-B**) Representative I_{Na} traces from WT and cKO mouse myocytes. (**C-D**) Reduced I_{Na}

(Continued on Page 91)

(Figure 5 continued from Page 90)

current in cKO versus WT myocytes (WT: n=10; cKO: n=9; $p<0.05$). (**E**) Voltage-dependent inactivation and (**F**) time-dependent recovery of INa in WT (n=10)and cKO (n=10) myocytes. We observed no significant difference in either property between genotypes (N.S.).

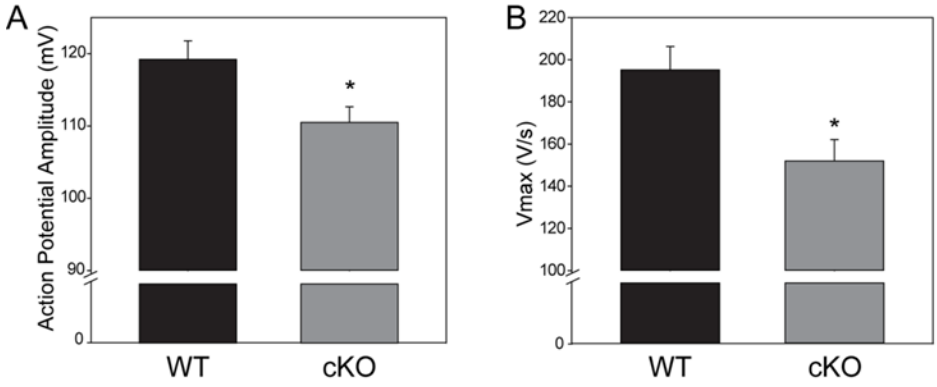

Figure 6. Ankyrin-G required for regulation of action potential phase 0.

Ankyrin-G cKO myocytes display defects in (**A**) action potential amplitude and (**B**) Vmax compared with WT myocytes, consistent with reduced INa (n>8/genotype; $p<0.05$.).

Ankyrin-G recruits βIV-spectrin to the cardiomyocyte intercalated disc.

Ankyrins partner with spectrin polypeptides to bridge membrane and cytoskeletal structures.[243] In the nervous system, while ankyrin-G and βIV-spectrin are both required for proper assembly of the axon initial segment, ankyrin-G appears to serve as the primary organizing protein. To investigate the functional relationship between ankyrin-G and βIV-spectrin in the heart, we tested the localization of βIV-spectrin in ankyrin-G cKO mice. In WT myocytes and cardiac tissue preparations, βIV-spectrin was concentrated at the intercalated disc membrane (Figure 7,8).[189] However, βIV-spectrin was nearly absent from the intercalated disc membrane of isolated cKO myocytes (Figure 7B), and in cKO cardiac tissue preparations (Fig 8B). Instead, we observed populations of βIV-spectrin -positive puncta near the peri-nuclear region in cKO myocytes (Figure 7B), indicative of impaired cellular targeting. Thus, we conclude that ankyrin-G is required for normal expression and intercalated disc recruitment of βIV-spectrin in cardiomyocytes.

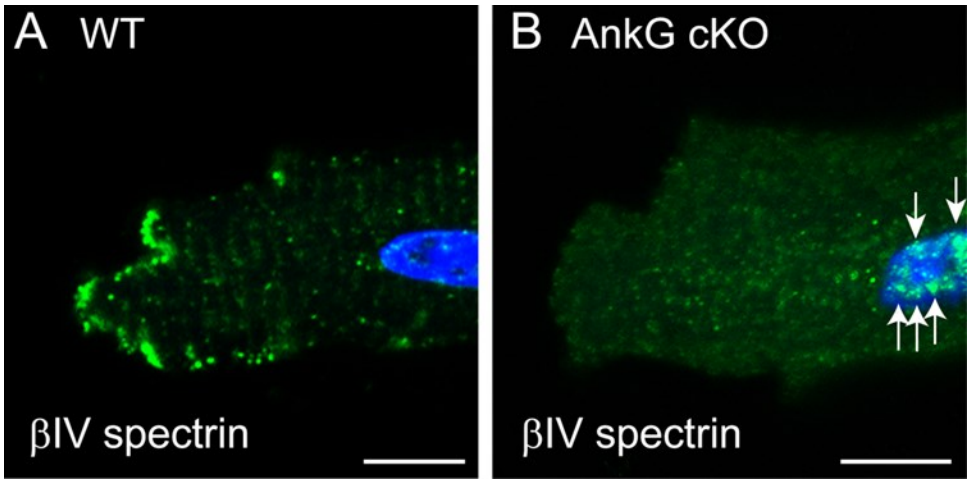

Figure 7. Ankyrin-G targets β_{IV} spectrin to the intercalated disc.

(**A-B**) β_{IV} spectrin intercalated disc targeting is altered in cKO myocytes. β_{IV} spectrin expression is clustered in the peri-nuclear region of cKO myocytes.

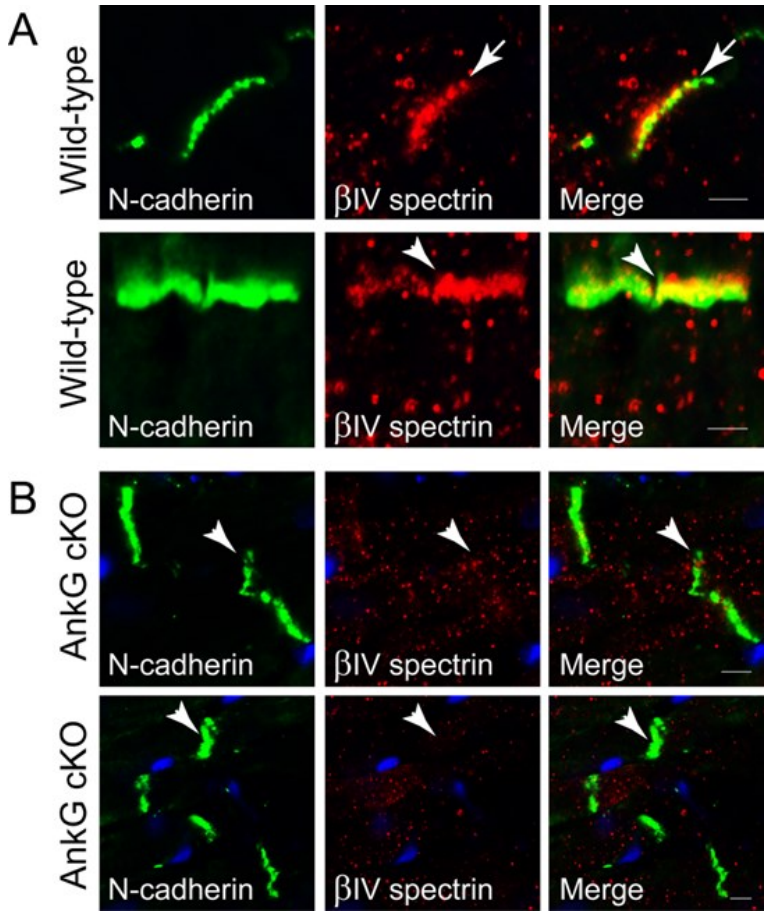

Figure 8. Ankyrin-G required for intercalated disc targeting of β_{IV} spectrin in cardiac tissue.

Heart sections from ankyrin-G cKO mouse (**B**) display reduced βIV spectrin intercalated disc staining (arrows) compared with WT heart (**A**). bar = two microns.

βIV-spectrin is not required for ankyrin-G or $Na_v1.5$ targeting in myocytes

We tested the converse requirement of βIV-spectrin for ankyrin-G and $Na_v1.5$ targeting in heart. For these experiments, we utilized a βIV-spectrin mutant mouse model (qv^{4J} mice) harboring a premature stop codon in the 10th spectrin repeat resulting in a truncated polypeptide lacking ankyrin-G-binding activity (located in 15th spectrin repeat; see Figure 9A[225, 228]). As expected, a GST- βIV-spectrin fusion protein harboring the qv^{4J} mutation lacked binding activity for ankyrin-G and $Na_v1.5$ (Figure 9B). In contrast to findings in neurons[244], qv^{4J} myocytes displayed no significant difference in ankyrin-G or $Na_v1.5$ expression compared to control hearts by immunoblot (Figure 9C-D). Further, we observed no difference in intercalated disc proteins N-cadherin or β-catenin in qv^{4J} hearts (Figure 9C-D). In line with immunoblot data, we observed no difference in ankyrin-G or $Na_v1.5$ localization at the intercalated disc between control and qv^{4J} myocytes (Figure 9E-H). However, consistent with the role of the βIV-spectrin C-terminus in CaMKIIδ targeting[189], qv^{4J} myocytes displayed a significant decrease in CaMKIIδ expression (Figure 9C-D, $p<0.05$). In summary, our findings define a requirement of ankyrin-G for βIV-spectrin targeting to the intercalated disc, whereas ankyrin-G is targeted to the disc independent of βIV-spectrin -binding.

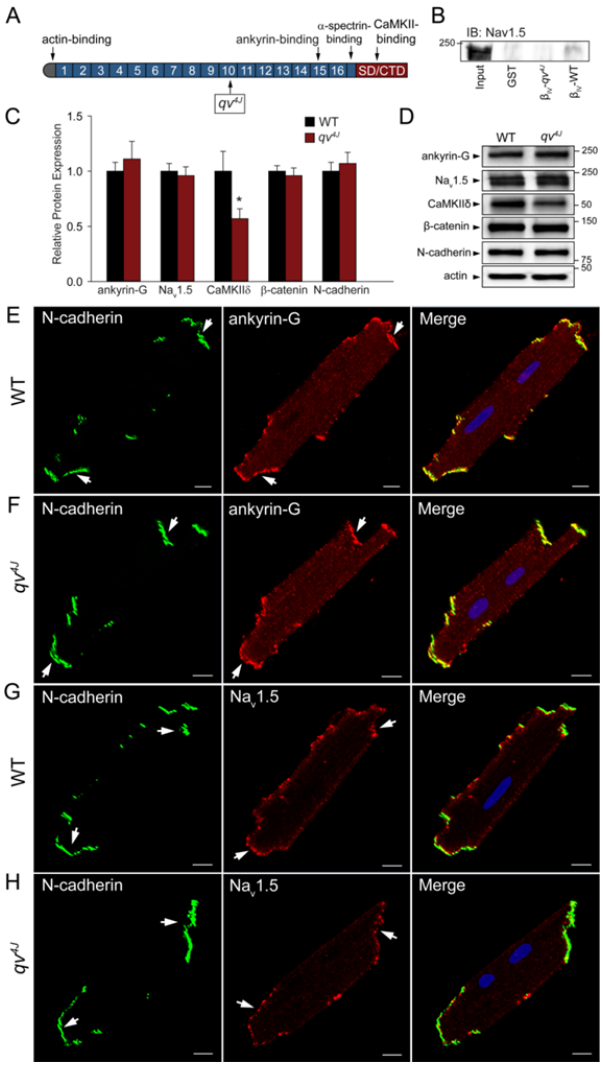

Figure 9. Ankyrin-G targets $Na_v1.5$ to the intercalated disc independent of β_{IV} spectrin.

(Continued on Page 98)

(Figure 9 continued from Page 97)

(**A**) Diagram of β_{IV} spectrin domains and location of qv^{4J} truncation upstream of ankyrin-G-binding site. (**B**) GST- β_{IV} spectrin associates with $Na_v1.5$ (via ankyrin-G). b_{IV} spectrin representing the qv^{4J} mouse truncation lacks binding activity for ankyrin-G and thus $Na_v1.5$. (**C-D**) WT and qv^{4J} hearts display no difference in expression of ankyrin-G or $Na_v1.5$ by immunoblot. CaMKIIδ levels are reduced in cKO hearts consistent with qv^{4J} allele lacking the CaMKIIδ-binding site (see **A**). Levels in C are normalized for actin expression (n=4/genotype; $p<0.05$). (**E-H**) WT and qv^{4J} myocytes display no difference in ankyrin-G or $Na_v1.5$ localization. Bar=10 microns.

Ankyrin-G recruits CaMKIIδ to the cardiomyocyte intercalated disc.

βIV-spectrin, via a short C-terminal motif, associates with CaMKIIδ [189] βIV-spectrin mutant mice lacking this C-terminal motif display aberrant CaMKIIδ intercalated disc targeting.[189] Based on the loss of βIV-spectrin in ankyrin-G cKO hearts (Figures 7,8), we hypothesized that ankyrin-G cKO hearts would display decreased CaMKIIδ expression and abnormal intercalated disc targeting. We observed reduced CaMKIIδ expression by immunoblot in cKO versus WT hearts (Figure 10A-B). With respect to localization, we observed selective loss of CaMKIIδ at the intercalated disc (i.e. location of βIV-spectrin) versus other myocyte membrane populations (i.e. transverse-tubules) in cKO cardiomyocytes (Figure 10C-D) and cKO cardiac tissue preparations (Figure 11 A-B). Thus, ankyrin-G, via βIV-spectrin, controls the intracellular targeting of CaMKIIδ to the intercalated disc.

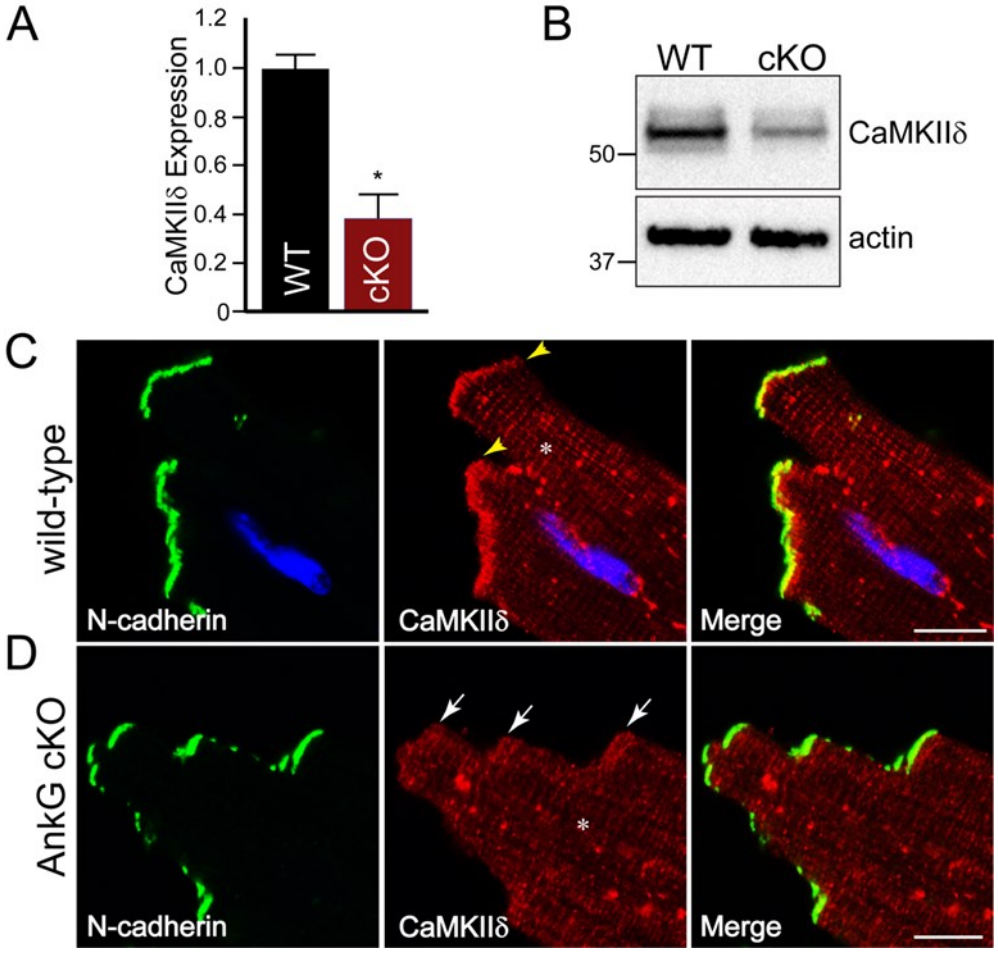

Figure 10. Ankyrin-G targets CaMKIIδ to the intercalated disc via β_{IV} spectrin

(**A-B**) *CaMKIIδ* expression and localization is altered in cKO myocytes. Levels in **A** are

(Continued on Page 101)

(Figure 10 continued from Page 100)

normalized for actin expression (n=4/genotype; $p<0.05$). (**C-D**) *CaMKIIδ* expression is selectively reduced at the intercalated disc of cKO myocytes (yellow arrows in C versus white arrows in D. Asterisk notes no change in CaMKIIδ localization at T-tubules between genotypes. Bar=10 microns.

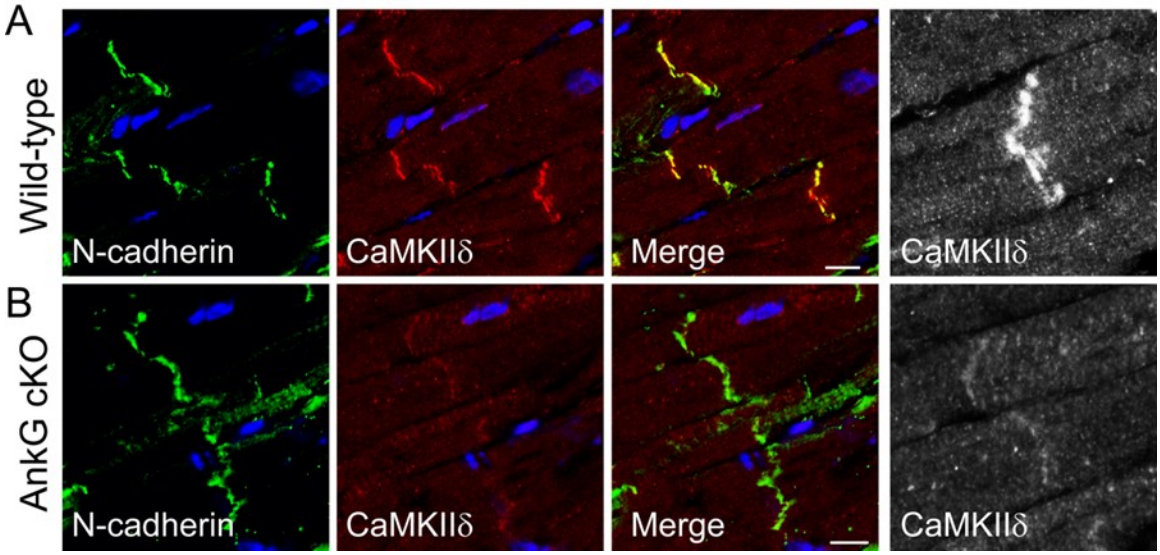

Figure 11. β_{IV} spectrin-dependent targeting of CaMKIIδ disrupted in ankyrin-G cKO cardiac tissue.

Heart sections from ankyrin-G cKO mouse (B) display reduced CaMKIIδ intercalated disc staining compared with WT heart sections (A) (bar equals ten microns). Black and white image on right is magnified view of CaMKIIδ localization.

Ankyrin-G recruits CaMKIIδ to regulate $Na_v1.5$ Phosphorylation

In response to sympathetic stimulation, CaMKIIδ phosphorylates $Na_v1.5$, via serine 571 (S571) to regulate $Na_v1.5$-dependent late current ($I_{Na,L}$).[189, 192] As evidenced by our data, ankyrin-G recruits both $Na_v1.5$ and CaMKIIδ to the intercalated disc (Figures 3, 10). In line with these data, we observed reduced $Na_v1.5$ S571 phosphorylation by both immunoblot and immunostaining in cKO myocytes compared with control cells (Figure 12 A-D). When corrected for peak I_{Na}, we did not observe differences in $I_{Na,L}$ between WT and cKO myocytes at baseline (Figure 13 A-D). However, consistent with the loss of CaMKII-dependent regulation of $I_{Na,L}$ in the absence of ankyrin-G, we observed a significant difference in Iso-induced $I_{Na,L}$ between WT and cKO myocytes (Online Figure VII). Specifically, while WT myocytes displayed nearly a two-fold increase in $I_{Na,L}$ in response to Iso, we observed no statistical change in $I_{Na,L}$ in cKO myocytes ±Iso regardless of the voltage of the test potential (Figure 13 C-D; $p<0.05$). Our combined data support an *in vivo* ankyrin-G-based platform with dual roles for $Na_v1.5$ recruitment and CaMKIIδ-dependent regulation.

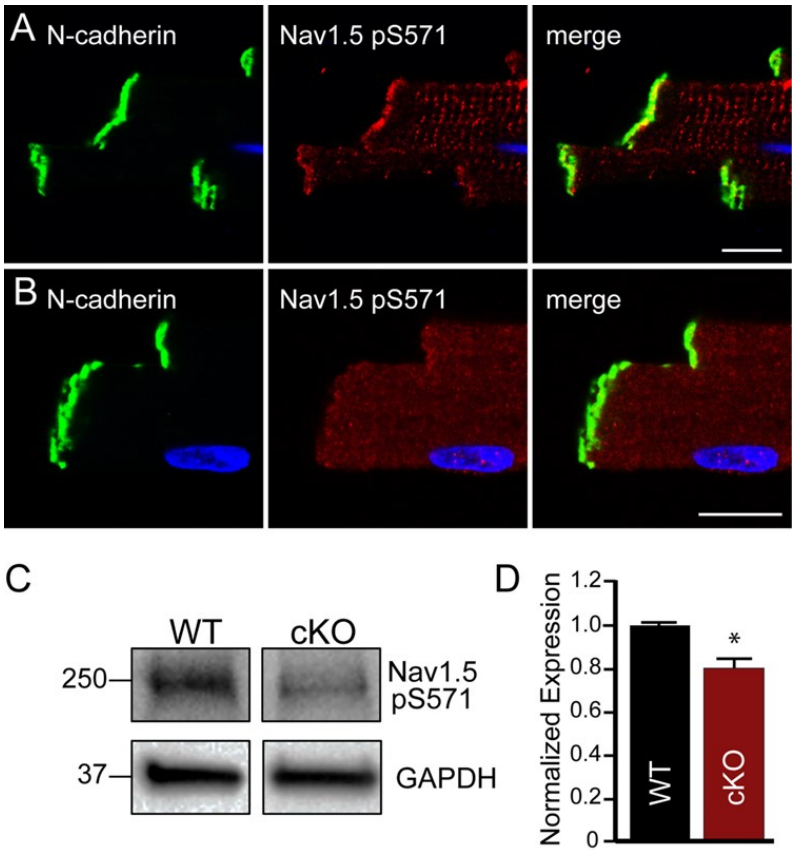

Figure 12. Ankyrin-G cKO myocytes display reduced phosphorylation of $Na_v1.5$ pS571

(A-B) Immunostaining of $Na_v1.5$ pS571 in WT and cKO myocytes. Bar=10 microns.

(**C-D**) $Na_v1.5$ pS571 levels are significantly reduced in cKO hearts compared with hearts of WT mice. Levels are normalized for GAPDH (n=4/genotype; $p<0.05$).

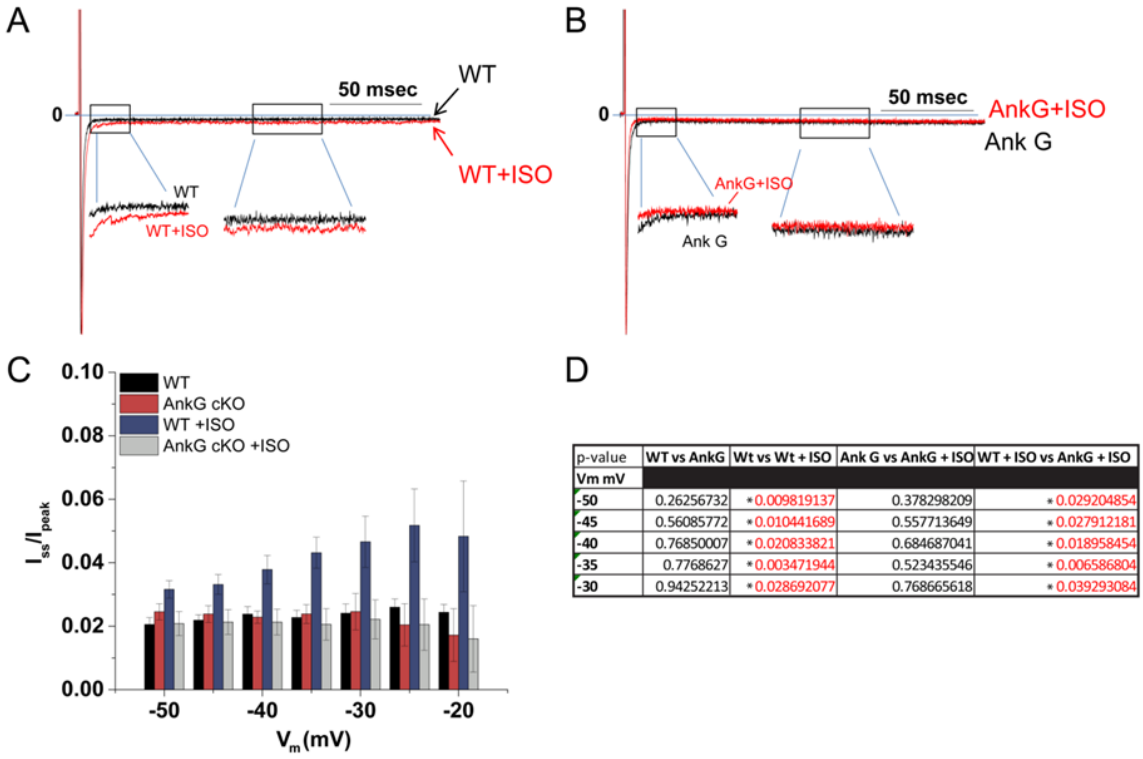

p-value	WT vs AnkG	Wt vs Wt + ISO	Ank G vs AnkG + ISO	WT + ISO vs AnkG + ISO
Vm mV				
-50	0.26256732	*0.009819137	0.378298209	*0.029204854
-45	0.56085772	*0.010441689	0.557713649	*0.027912181
-40	0.76850007	*0.020833821	0.684687041	*0.018958454
-35	0.7768627	*0.003471944	0.523435546	*0.006586804
-30	0.94252213	*0.028692077	0.768665618	*0.039293084

Figure 13. Iso-induced enhancement of $I_{Na,L}$ in WT but not ankyrin-G cKO myocytes

Transient and late INa currents evoked in response to 200 ms duration voltage clamp steps to -25 mV in the absence (black trace) and presence (red trace) of Iso in WT (A) and AnkG KO (B) myocytes. C) Bar graph of $I_{Na,L}$ at multiple experimental voltages

(Continued on Page 106)

(Figure 13 continued from Page 105)

±Iso. WT: -ISO (black), +Iso (blue). AnkG cKO: –Iso (red), +Iso (gray). D) $I_{Na,L}$ was significantly increased in the presence of ISO in WT cells at several of the tested voltages while currents from AnkG cKO myocytes were insensitive to ISO treatment. $n \geq 6$ for all conditions

Ankyrin-G cKO mice display bradycardia, conduction defects, and arrhythmia

Impaired $Na_v1.5$ function is associated with phenotypes of sinus node dysfunction, conduction defects, and ventricular arrhythmia.[231-233] We therefore tested the role of the ankyrin-G-dependent disc platform for cardiac electrical regulation. The electrocardiogram (ECG) of conscious ankyrin-G cKO mice was monitored by remote telemetry. Compared to WT controls, cKO animals exhibited significant reduction in resting heart rate. (Figure 14A-C). Impaired atrioventricular (AV) conduction in cKO mice was also readily apparent in cKO mice as evidenced by an increase in PR interval compared with control mice (Figure 14D-F). Moreover, cKO mice displayed a significant increase in the QRS interval, consistent with delayed intraventricular conduction (Figure 14D-E, G). In summary, *in vivo* findings strongly support a role of the ankyrin-G-based protein complex in regulation of $Na_v1.5$ function and cardiac excitability.

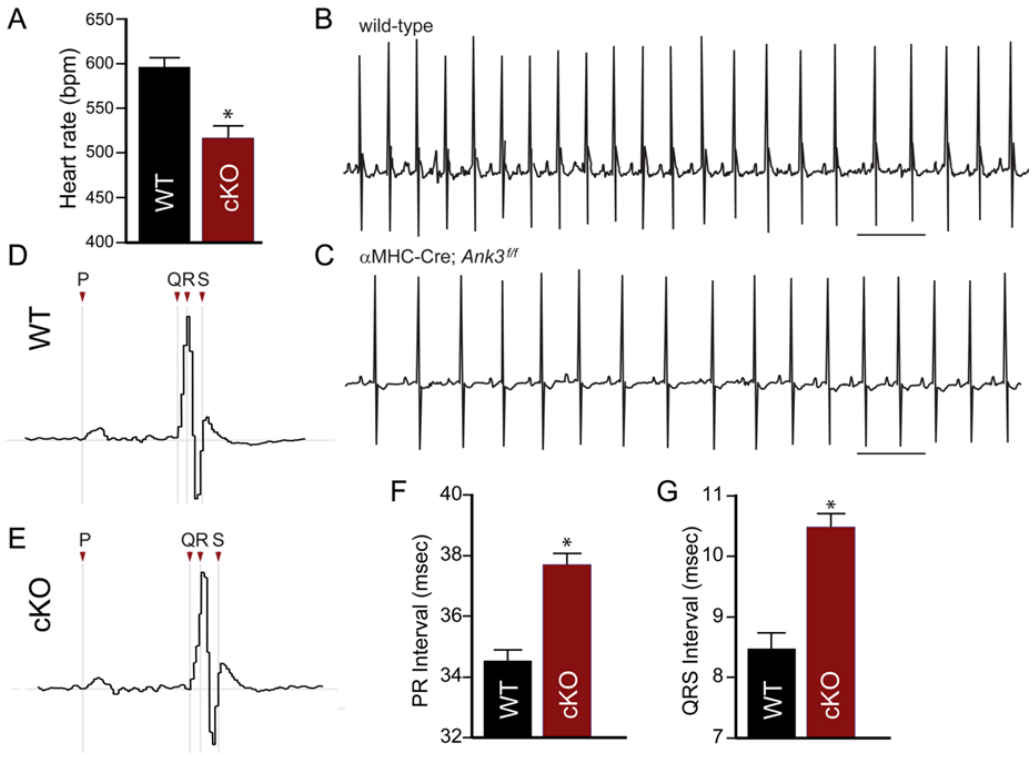

Figure 14. Cardiac-specific ankyrin-G null mice exhibit bradycardia and conduction abnormalities

(**A-C**) Ankyrin-G cKO mice display bradycardia compared with WT littermates (WT: n=5; cKO: n=7; $p<0.05$). Bar in B,C = 200 ms. Representative ECG traces for (**D**) WT

(Continued on Page 109)

(Figure 14 continued from Page 108)

and (**E**) cKO mice. cKO mice show increased PR (**F**) and QRS (**G**) intervals compared with WT mice (WT: n=6; cKO: n=7; $p<0.05$).

Flecainide induces bradycardia, QRS prolongation, and arrhythmia in cKO mice

Class 1C anti-arrhythmics ($Na_v1.5$ antagonists) may be utilized in clinical practice to identify individuals with $Na_v1.5$ abnormalities.[245] Moreover, these compounds (e.g. lecainide) have been used to uncover $Na_v1.5$-based arrhythmia mechanisms in animal models.[246, 247] To test the functional relevance of $Na_v1.5$ dysfunction in the ankyrin-G cKO mouse, we analyzed ECGs of anesthetized control and cKO mice following flecainide administration.[227, 248] At baseline, cKO mice displayed bradycardia compared to control mice (Figure 15A-B, E). Flecainide reduced heart rate in both control and cKO mice (Figure 15A-E). However, the effect of flecainide on heart rate was significant and potentially pathological in cKO mice as this intervention resulted in an overall ~30% decrease in heart rate compared with control mice at baseline (Figure 15E; $p<0.05$). Further, in cKO but not control mice, flecainide caused AV block and ventricular arrhythmia (Figure 15F-H). Specifically, 10% of control mice displayed AV block in response to flecainide, whereas we recorded AV block in ~73% of cKO mice (Figure 15F-G; $p<0.05$). Of the mice showing AV block, the incidence of block was >140 fold greater in cKO mice (control: 0.019 ± 0.019 episodes/min; cKO: 2.75 ± 0.98 episodes/min; $p<0.05$). Moreover >80% of cKO mice showed arrhythmia including bigeminy and non-sustained ventricular arrhythmia, compared to 10% of control mice (Figure 15H, $p<0.05$). Consistent with conscious ECG recordings, anesthetized cKO mice displayed prolonged QRS interval compared with control mice (Figure 16 A-C). This QRS interval difference between genotypes was further accentuated by flecainide administration (Figure 16C; $p<0.05$). Together, these data strongly support the role of

ankyrin-G-protein complex in $Na_v1.5$ regulation *in vivo*, as well as link $Na_v1.5$-based mechanisms with observed cardiac electrical phenotypes in the ankyrin-G cKO mouse.

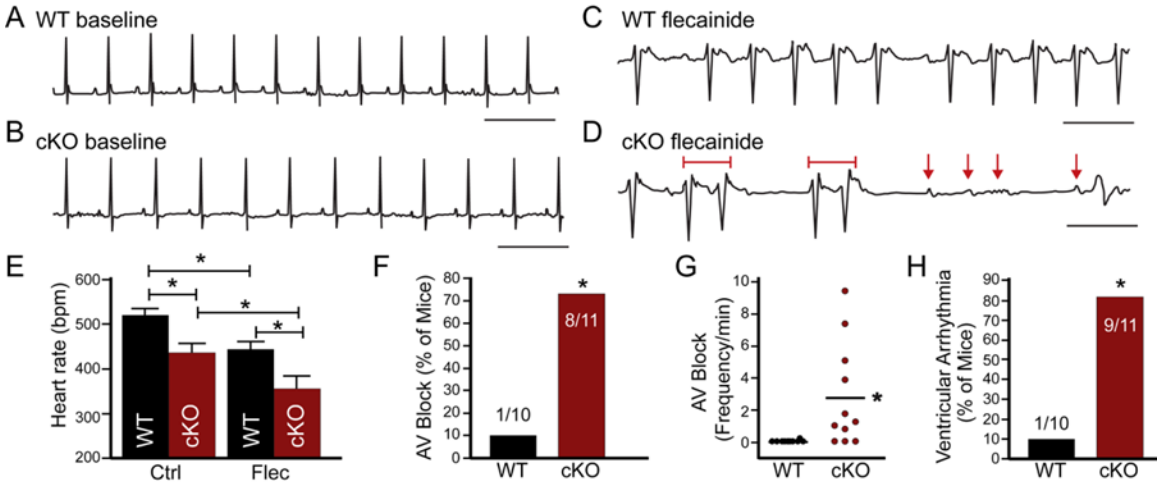

Figure 15. Ankyrin-G cKO mice display conduction defects and arrhythmia in response to Na_v channel antagonist.

(A-B) ECG traces from WT and ankyrin-G cKO mouse 30 seconds prior to flecainide administration. (**C-D**) ECG traces from same mice (in **A-B**) observed 10 minutes post-flecainide administration (20 mg/kg, I.P.; bar=200 ms). Examples of AV block (red arrowheads) and ventricular phenotypes (red brackets) are noted in D. (**E-H**) Ankyrin-G cKO mice show significant decrease in heart rate and increase in frequency of AV block and ventricular arrhythmia following flecainide compared with WT littermates ($p<0.05$).

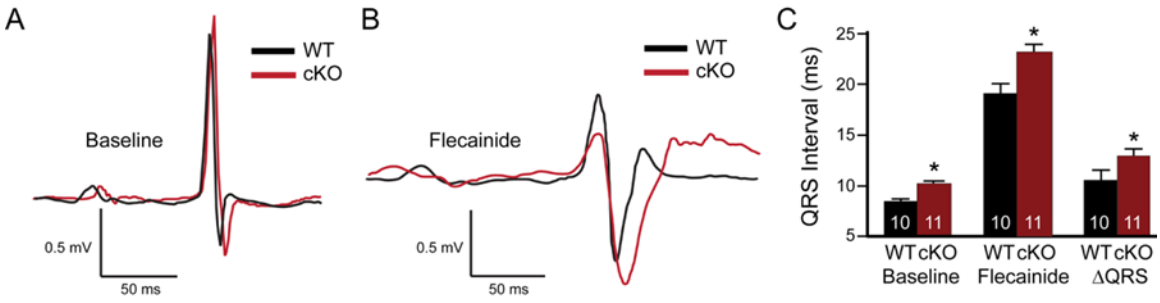

Figure 16. Ankyrin-G cKO mice display significant increase in QRS duration following flecainide challenge.

Representative traces of WT and cKO mice at baseline (A) and post-flecainide infusion (B). (C) Ankyrin-G cKO mice display increased QRS interval at both baseline and after flecainide. ($p<0.05$).

Ankyrin-G cKO mice display defects in plakophilin-2 expression and intercalated disc targeting

Beyond membrane ion channels, *in vitro* work supports roles of ankyrin-G for membrane protein regulation at cell junctions.[94, 237] We therefore tested the *in vivo* requirement of ankyrin-G for expression and localization of key ID proteins as well as Na_v β-subunits that have been previously linked with ankyrin polypeptides.[249] Notably, we observed no difference in expression or localization of disc proteins N-cadherin and β-catenin, or Na_v channel β2 and β4 subunits between control and cKO hearts (Figure 17A-K; Figure 18; Figure 19). In contrast, plakophilin-2 showed a 50% *increase* in expression in cKO hearts (Figure 17A-B). Further, we observed a striking redistribution of plakophilin-2 from the ID of cKO myocytes to the cytosolic regions of isolated cKO myocytes (Figure 17K-L) and in cardiac tissue preparations (Figure 18 A-B). While prior work proposed a link for ankyrin-G in targeting of connexin43 in heart[237], we observed no difference in connexin43 expression by immunoblot, but did observe a minor reduction in membrane localization in cKO myocytes (Figure 17C-D). Finally, whereas ZO-1 expression was not significantly altered between WT and cKO myocytes by immunoblot, we observed reduced membrane ZO-1 immunostaining (Figure 17I-J). Together, our new *in vivo* data clearly support a role of ankyrin-G in ID membrane organization.

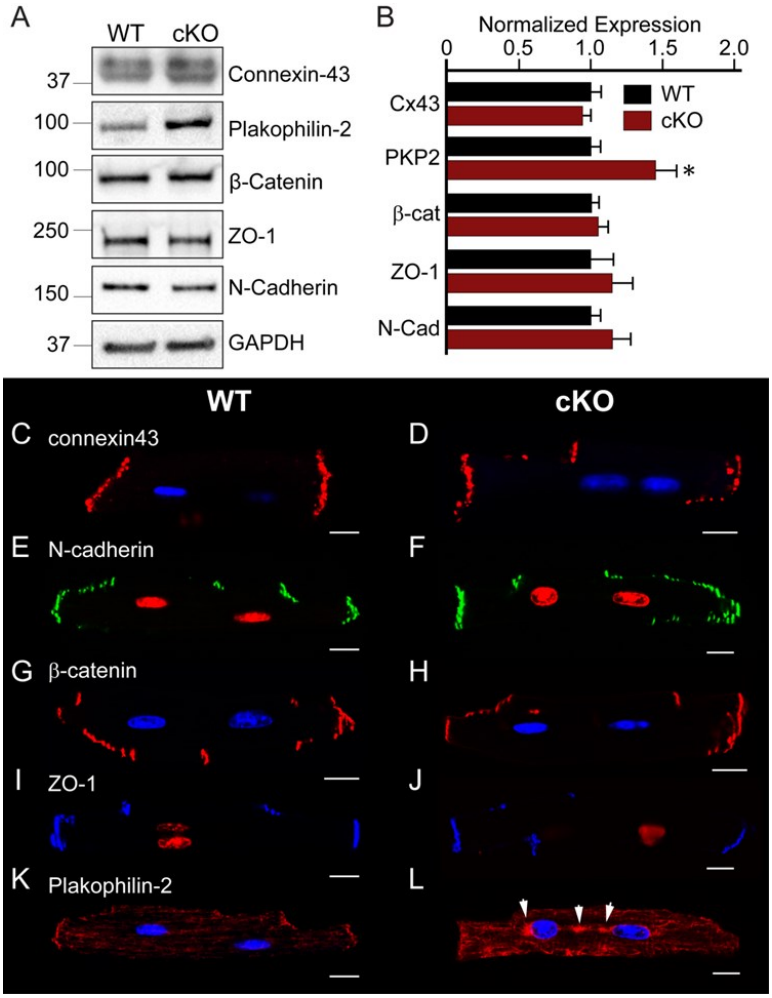

Figure 17. Ankyrin-G is required for plakophilin-2 intercalated disc expression

(**A-B**) Immunoblots of myocyte intercalated disc proteins in WT versus cKO heart. Note

(Continued on Page 116)

(Figure 17 continued from Page 115)

that plakophilin-2 levels are significantly increased in cKO hearts (n=4/genotype; $p<0.05$). (**C-K**) Confocal imaging of WT (left) and cKO (right) myocytes labeled with antibodies for resident intercalated disc proteins. Note that while primarily localized to the disc of WT myocytes, plakophilin-2 is clustered in the peri-nuclear region of cKO myocytes (arrowheads; Bar=10 microns).

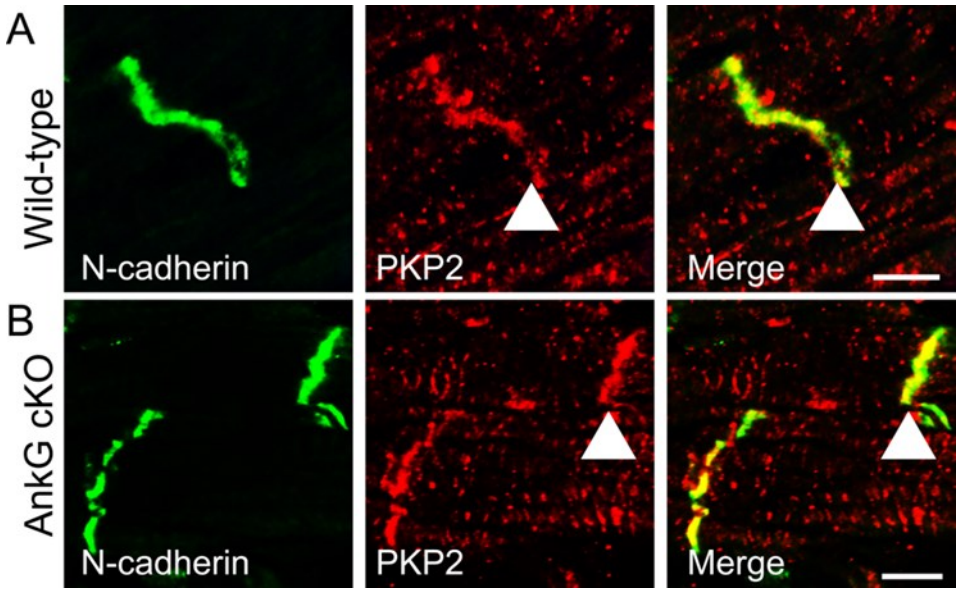

Figure 18. Intercalated disc PKP2 localization maintained in ankyrin-G cKO cardiac tissue.

Heart sections from ankyrin-G cKO mouse display normal plakophilin 2 (PKP2) intercalated disc staining (arrows) compared with WT heart (bar equals ten microns) but increased intracellular staining.

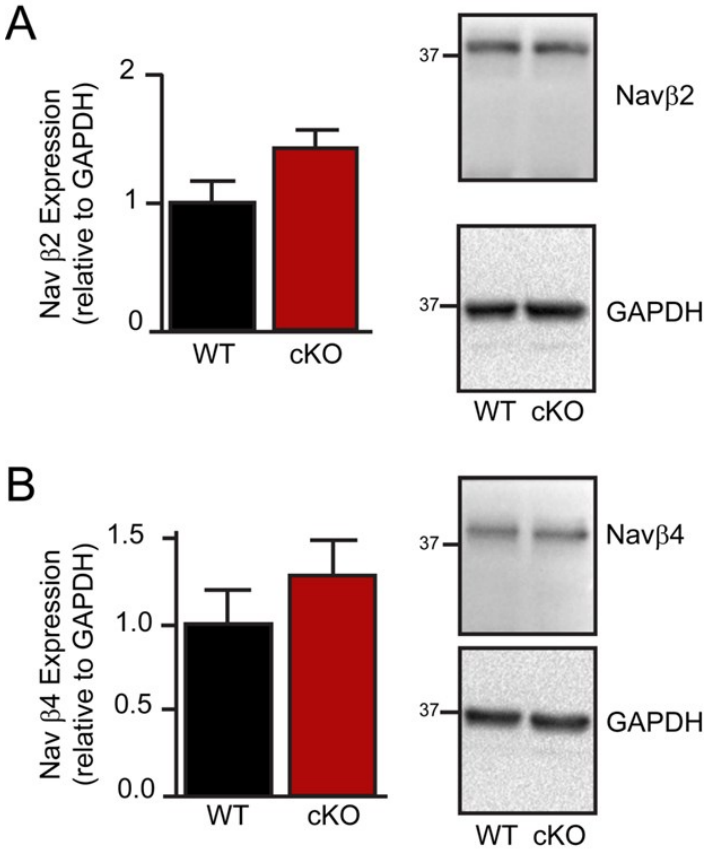

Figure 19. Nav channel beta subunit expression is not altered in cKO heart.

(**A-C**) Immunoblots and normalized expression levels of myocyte proteins in WT versus cKO heart. (n=4/genotype; p=N.S.).

Ankyrin-G cKO mice display catecholamine-induced arrhythmia and death

Ankyrin-G cKO mice display a number of pro-arrhythmic ECG phenotypes associated with reduced I_{Na} (Figures 6-7). However, based on the additional observed molecular defects in ankyrin-G cKO animals (Figure 17), we tested cKO animals for arrhythmia susceptibility in response to elevated adrenergic stimulation. Ankyrin-G cKO mice showed arrhythmia phenotypes following a standard I.P. epinephrine injection protocol to mimic catecholaminergic stress (Figure 20[22]). Specifically, the majority (~62.5%) of cKO mice displayed multiple instances of ventricular arrhythmia and ~38% of cKO mice died of malignant arrhythmias following this protocol (Figure 20 D-E; 3/8 cKO vs 0/6 control; $p<0.05$). Examples of sustained premature ventricular contractions (PVCs) as well as polymorphic ventricular arrhythmia in cKO mice are shown in Figure 20 B-C. While we observed limited examples of sinus pause and rare PVCs in control mice utilizing this protocol, we recorded no incidence of ventricular arrhythmia (0%) or death (0%; Figure 20 A, D, E). In summary, we conclude that loss of the cardiac ankyrin-G-based protein platform results in pro-arrhythmic ECG phenotypes at rest, and arrhythmia and death in response to catecholaminergic stress. Of note, as catecholamine-based arrhythmias in cKO mice were observed in the absence of elevated CaMKIIδ or $I_{Na,L}$, we tested for potential alterations in myocyte calcium handling in cKO myocytes. Consistent with whole animal data (e.g. PVCs), cKO myocytes displayed increased incidence of spontaneous Ca waves compared with WT myocytes (Figure 21; $n>10$/genotype $p<0.05$).

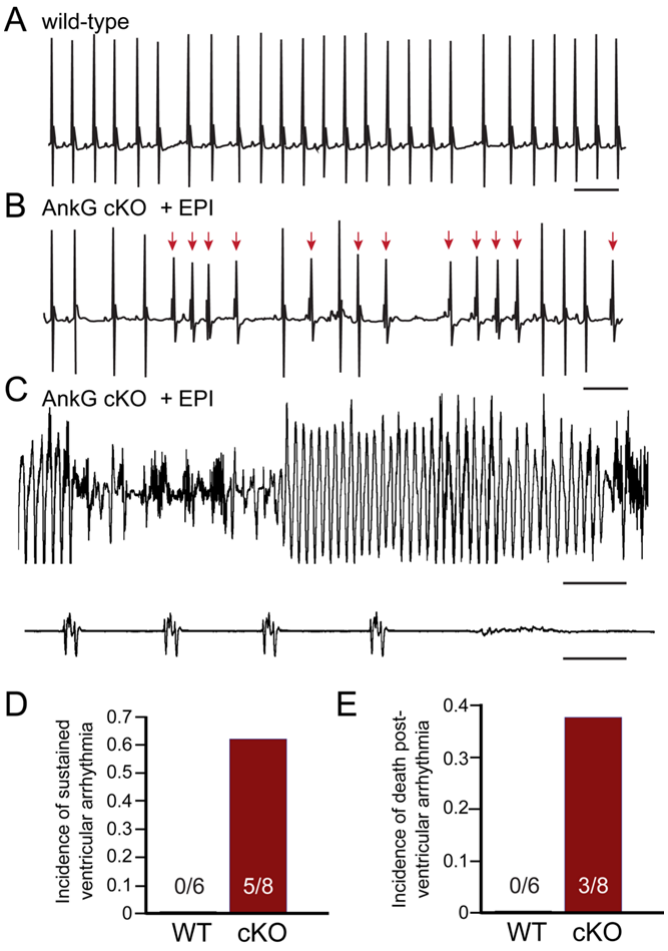

Figure 20. Ankyrin-G cKO mice display EPI-induced arrhythmias and death

(A) ECG of WT mice post-injection of epinephrine (2 mg/kg, I.P.). (**B-C**) Ankyrin-G

(Continued on Page 121)

(Figure 20 continued from Page 120)

cKO mice following identical epinephrine administration display arrhythmia. (**B**) cKO mouse exhibiting ectopic ventricular beats (red arrowheads). (**C**) Ankyrin-G cKO mouse presenting polymorphic ventricular arrhythmia just prior to death (bottom). (**D-E**) Frequency of ventricular arrhythmias and death in WT and cKO mice following epinephrine injection ($p<0.05$). Bars equal 200 msec.

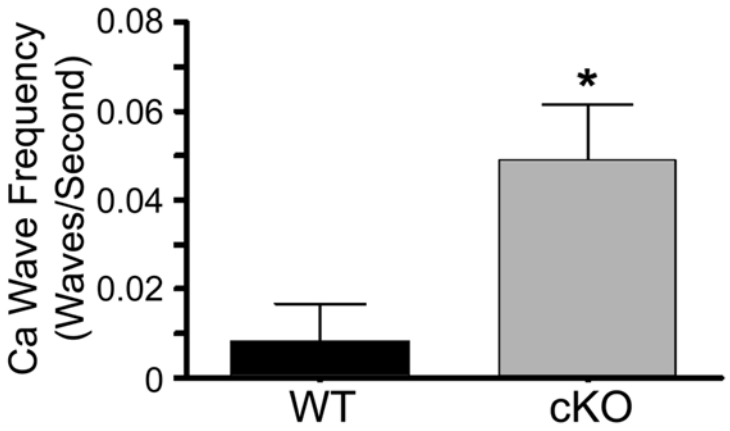

Figure 21. Ankyrin-G cKO myocytes display increased calcium waves compared with myocytes from WT littermates.

Ankyrin-G cKO mice display cardiac structural phenotypes

Ankyrins are linked with assembly and maintenance of structural domains in erythrocytes, epithelia, and neurons.[28, 29, 250] Further, our data, and prior data from Delmar and colleagues [237] link ankyrin-G with plakophilin-2, a protein associated with cardiac structural remodeling in humans and mice.[247, 251, 252] We therefore examined ankyrin-G hearts for changes in cardiac structure or function at baseline and in aging. At 8 weeks, we observed no difference in heart weight/body weight (or tibia length) or systolic or diastolic wall thickness between WT and cKO mice (Figure 22 A-F). While we observed a non-significant trend for increased systolic and diastolic LV diameter in cKO mice (p=N.S.), cKO mice displayed a small, but significant decrease in ejection fraction compared to WT littermates (Figure 22 G-H). Notably, cKO mice displayed obvious cardiac phenotypes with age (~9 months) as indicated by a further depression in ejection fraction, increase in systolic and diastolic chamber diameters, and reduction of both the anterior and posterior wall thickness compared to WT littermates (Figure 23).

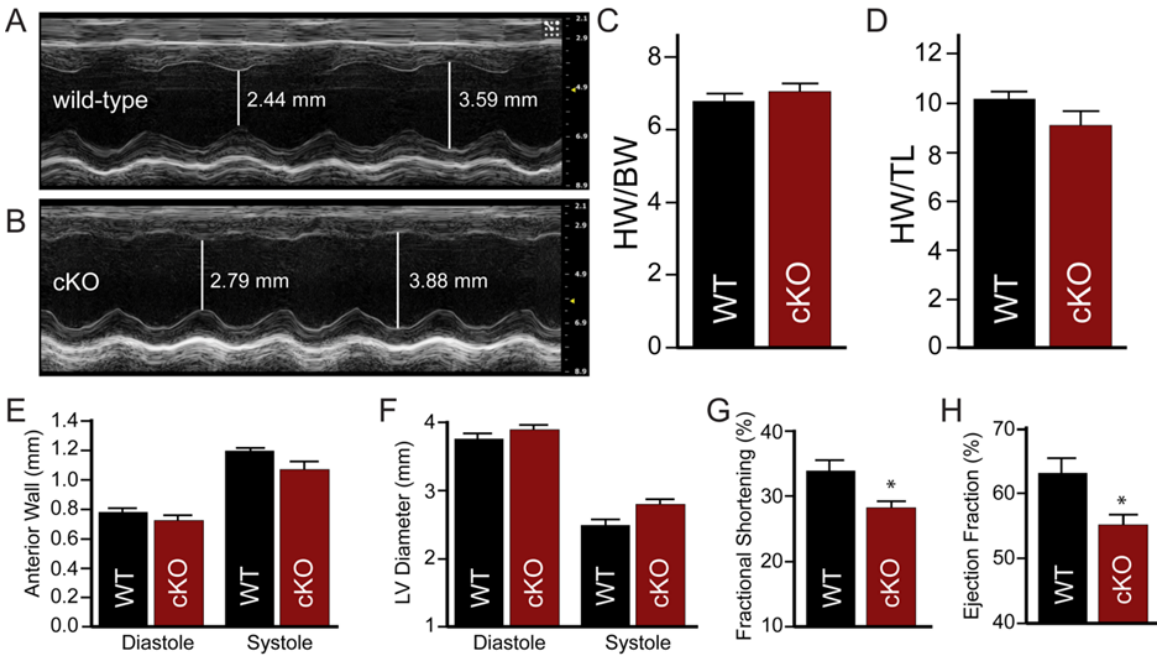

Figure 22. Ankyrin-G cKO mice display minor cardiac structural phenotypes at 8-10 weeks.

Representative short-axis M-mode images of wild-type (**A**) and cKO (**B**) mice at 8 weeks of age. The ratios of HW/BW (**C**) and HW/TL (**D**) are preserved as well as no change in anterior wall thickness (**E**) or LV diameters (**F**) in cKO mice. However, cKO mice display a small but significant decrease in fractional shortening (**G**) and ejection fraction (**H**) compared to WT mice. For each measurement n>5/genotype; *p<0.05.

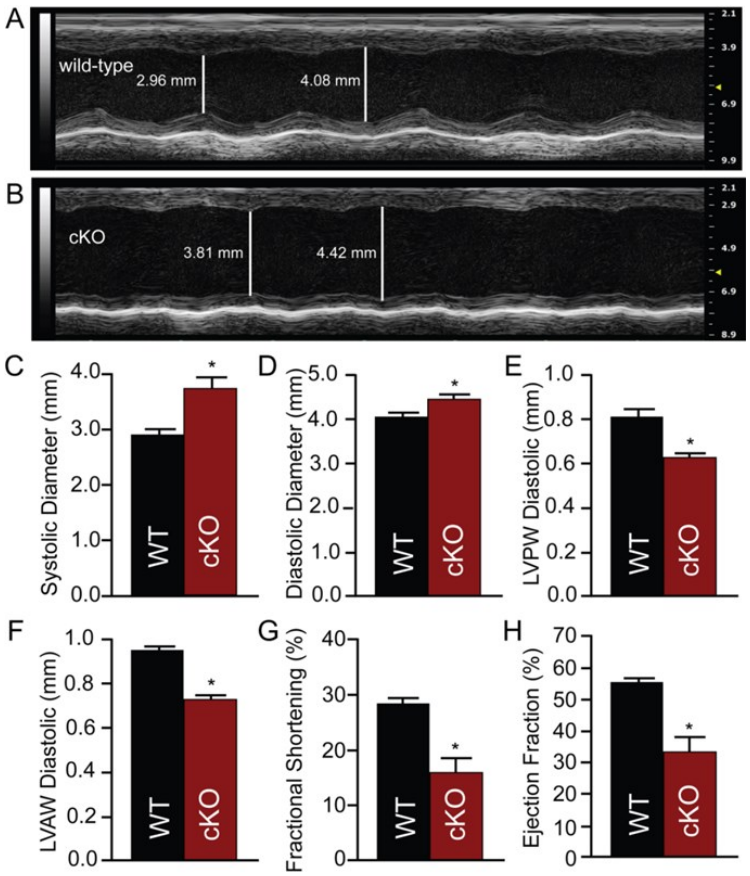

Figure 23. Ankyrin-G cKO mice display structural abnormalities and reduced ventricular function with age.

Representative short-axis M-mode image of 9 month WT (**A**) and cKO (**B**) mice. cKO

(Continued on Page 126)

(Figure 23 continued from Page 125)

mice display an increase in both the systolic (**C**) and diastolic (**D**) left ventricular chamber diameter and a decrease in both the posterior wall (LVPW, **E**) and anterior wall (LVAW, **F**) thickness. Consistent with chamber dilation and thinned walls, cKO mice display a significant reduction in performance as indicated by reduced fractional shortening (**G**) and ejection fraction (**H**). For each measurement $n>5$; $*p<0.05$.

Discussion

Voltage-gated Na_v channels are critical for the rapid upstroke of the cardiac action potential and cardiac conduction. Defects in Na_v channel function are linked with a host of congenital and acquired forms of human disease including sinus node dysfunction, atrial fibrillation, conduction disorders, ventricular arrhythmia, and heart failure.[231-233] Despite these compelling human disease linkages and decades of elegant Na_v channel biophysical studies, the field still lacks significant fundamental knowledge of the regulatory mechanisms governing the function of this critical molecule. Here we use *in vivo* animal models to define the cellular pathway underlying the targeting of $Na_v1.5$ and its regulatory molecule, CaMKIIδ to the intercalated disc membrane. Ankyrin-G, a cytoskeletal adapter protein, associates with $Na_v1.5$ and recruits the channel to the myocyte membrane. Loss of ankyrin-G results in defects in Na_v channel expression, localization, and function. We further show that ankyrin-G, via the recruitment of βIV-spectrin, also targets CaMKIIδ to the intercalated disc. As CaMKIIδ phosphorylates $Na_v1.5$ to modulate cardiac myocyte excitability in health and disease[189, 192], our findings provide data that support the mechanisms underlying the biogenesis of this membrane signaling domain. Finally, our findings confirm *in vivo* protein pathways for ankyrin-G and $Na_v1.5$ in heart. Specifically, as described by Delmar and colleagues in cultured myocytes[237], our *in vivo* data link ankyrin-G with the desmosomal protein plakophilin-2 as well as ZO-1. Further, our data associate ankyrin-G with the disc protein βIV-spectrin.

Ankyrin-G cKO mice were surprisingly viable, but display bradycardia, AV conduction defects, QRS prolongation, and/or arrhythmia associated with flecainide or

epinephrine. Consistent with our proposed mechanism of I_{Na} dysfunction in these animals, $Na_v1.5$ is linked with impulse propagation through the sinoatrial node (SAN[231]), the AV node[253], and the ventricular myocardium.[254] Prior *in vivo* work links $Na_v1.5$ dysfunction with bradycardia, and reduced SAN pacemaker potential.[254] Moreover, consistent with our findings, flecainide has been previously shown to evoke ventricular arrhythmias in multiple mouse models of Na_v channel deficiency.[246, 247] While our findings clearly link ankyrin-G with $Na_v1.5$ targeting, they reveal new ankyrin-G associated pathways that are relevant to cardiac electrical, signaling, and structural roles in both health and disease. Genetic mutation in the ankyrin-binding motif of $Na_v1.5$ has been previously linked with loss of myocyte I_{Na}, abnormal Na_v channel targeting, and human Brugada syndrome.[35] However to date, ankyrin-G (*ANK3*) variants have not yet been linked with human arrhythmia. Based on past findings in other tissues, as well as work in this study, a pure loss-of-function *ANK3* allele may be incompatible with life. Mice simply lacking *Ank3* in the cerebellum are frail and display severe neurological defects. Moreover, human *ANK3* variants have been linked with bipolar disease, schizophrenia, and autism.[105, 255, 256] Ankyrin-G is required for normal retinal protein trafficking, and essential for lateral membrane biogenesis in columnar epithelia.[28, 257] Based on our findings, we predict that more subtle variants may cause sinus node disease, arrhythmia, and even structural heart disease due to defects in intercalated disc infrastructure.

As noted above, our data demonstrate that ankyrin-G recruits βIV-spectrin to the intercalated disc. In other cell types, βIV-spectrin, through their association with βIV-

spectrin and actin form critical submembrane cytoskeletal infrastructure. In fact, defects in spectrins have been linked with a host of pathologies in humans and animals.[243] Moreover, βIV-spectrin associates with, and targets a subpopulation of CaMKIIδ to the intercalated disc to phosphorylate $Na_v1.5$.[189,192] Defects in CaMKIIδ phosphorylation of $Na_v1.5$ have now been linked with multiple forms of heart failure in humans and animal models.[192, 193]

Our *in vivo* data support a role of ankyrin-G in organization of the intercalated disc. Plakophilin-2 is a key disc protein, linking desmosomal cadherins with desmoplakin and the intermediate filament system. Human plakophilin-2 loss-of-function variants are linked with arrhythmogenic right ventricular cardiomyopathy (ARVC) and Brugada syndrome.[207, 258] While cardiac phenotypes in the cKO model are distinct from human ARVC (increased levels of PKP2 in cKO model versus reduced PKP2 levels in ARVC [251]), the unexpected new data on structural defects in ankyrin-G cKO hearts and association with plakophilin-2 alterations are noteworthy. However, the specific relationship between ankyrin-G and plakophilin-2, as well as the potential link between these pathways and the observed structural defects in cKO mice, will require additional investigation. Interestingly, unlike plakophilin-2, we did not observe alterations in intercalated disc N-cadherin or β-catenin in cKO mice. However, we observed minor defects in connexin43 and ZO-1 membrane targeting. Notably, Delmar and colleagues previously showed reduced connexin43 expression in ankyrin-G siRNA transfected neonatal myocytes.[205] While future experiments will be important in defining the relationship between these molecules (i.e. compensatory changes versus direct protein

partners), our findings clearly implicate ankyrin-G as a multifunctional regulatory molecule in the heart. Further, our work demonstrates that phenotypes observed in the ankyrin-G cKO mouse likely extend far beyond simple I_{Na} deficiency.

Our *in vivo* findings demonstrate a critical role for ankyrin-G for intercalated disc $Na_v1.5$ targeting. However, $Na_v1.5$ targeting to non-intercalated disc membranes has been proposed as ankyrin-independent, relying instead on unique cellular machinery including syntrophin/dystrophin, SAP97, caveolin-3, MOG1, and FGF12.[259] Based on the essential role of Na_v channels for myocyte excitability, we propose that the vertebrate has evolved multiple mechanisms for $Na_v1.5$ membrane targeting. Future studies that explore the specific roles of ankyrin-G versus other targeting proteins in ion channel trafficking versus membrane scaffolding will be important to explore the relative contribution of each protein in dictating cardiac excitability and function using *in vivo* models. Further, based on the *in vivo* link between ankyrin-G and plakophilin-2, it will be important to investigate the mechanistic roles of ankyrin-G in regulation of intermediate filaments at the intercalated disc.

Chapter 4: Ankyrin-G expression required for compensatory ventricular response in setting of pressure overload.

Introduction

Maintenance of proper cardiac pump function requires the coordinated conduction of action potentials between cardiomyocytes in concert with sufficient transmission of force from cell to cell. To accomplish this, cardiomyocytes are electrically and mechanically coupled at their terminal ends by a specialized membrane structure known as the intercalated disc, first identified in 1954 by Sjostrand[260]. At the intercalated disc, gap junctions electrically couple adjacent cells, acting as low resistance pathways to propagate action potentials between cardiomyocytes[136]. Mechanical coupling is provided by two cellular structures termed the fascia adherens junction and the cardiac desmosome, integrating the plasma membrane with the actin filaments and intermediate filaments respectively[129, 134] .Importantly, these structures become mislocalized and/or deficient in both congenital and acquired forms of cardiovascular disease, ultimately leading to failure of cardiac pump function[126, 129, 134, 261] . Therefore, elucidating the compensatory molecular pathways responsible for the maintenance of mechanical and electrical coupling of cardiomyocytes is critical to gain insight into the pathogenesis of human heart failure.

Ankyrin polypeptides (ankyrin-R, ankyrin-B, and ankyrin-G) are intracellular scaffolding proteins responsible for targeting membrane proteins in all cells, regulating both cellular excitability and structure. Previously we demonstrated a critical requirement for ankyrin-G in the regulation of cardiac excitability in vivo by controlling membrane targeting of the voltage-gated sodium channel Nav1.5 specifically to the intercalated disc [262]. Interestingly, ankyrin-G has also been implicated in regulating mechanical coupling in cardiomyocytes through its interaction with the desmosomal protein plakophilin-2 (PKP2) [200]. However, the in vivo functional requirement for ankyrin-G in regulating mechanical coupling of cardiomyocytes at baseline and in disease is unknown and untested.

Here we report that mice with cardiac-specific silencing of ankyrin-G demonstrate severe cardiac structural remodeling with age. In response to pressure overload via transaortic constriction, ankyrin-G cKO animals display increased mortality, severe systolic dysfunction and bradycardia leading to spontaneous death. Mechanistically, we link these phenotypes with reduced localization of the desmosomal protein plakophilin-2 at baseline and after transaortic constriction (TAC). In wild type mice, however, ankyrin-G expression is upregulated 2 weeks after TAC concomitant with increased PKP2 expression/localization at the intercalated disc, demonstrating a requirement for ankyrin-G for cardiac compensation in response to stress. In contrast, we also demonstrate that ankyrin-G expression is decreased in samples from failing human hearts. Together, our data demonstrate a necessity for proper ankyrin-G expression for cardiac compensation

under pathological stress and implicate disruption of ankyrin-G in the development and progression of human heart failure.

Results

Ankyrin-G is required for cardiac structure and function during aging

To investigate the role of ankyrin-G in cardiac function in response to normal physiological stress, we evaluated ankyrin-G cKO mice during aging. As reported previously, at two months of age, ankyrin-G cKO mice displayed normal cardiac structure with only minor reductions in ejection fraction compared with WT mice. However, ankyrin-G cKO mice developed severe systolic dysfunction by nine months of age[262]. Further, unlike WT mice, beginning at ten months of age, ankyrin-G cKO mice displayed a sharp increase in mortality. In fact, unlike WT mice, only 30% of ankyrin-G cKO mice survived to the age of 15 months (Figure 24A; 3/10 cKO vs. 10/10 WT; $p<0.05$). Hearts of aged ankyrin-G cKO mice were significantly larger than age-matched WT mice, displaying increases in heart weight / tibia length ratio (Figure 24 B-C). In line with these data, surviving one year old ankyrin-G cKO mice showed pathologic reduction in ejection fraction compared to WT mice (Figure 24 F; WT: $50.20 \pm 1.68\%$; cKO: $31.08 \pm 7.36\%$; $p<0.05$) with no gross changes in ventricular wall thickness or internal diameter (Figure 24 G-I). Instead, ankyrin-G cKO mice displayed increased myocardial vacuolization that was not present in WT mice (Figure 24 J,K). These data support a critical role of ankyrin-G in cardiac structure/function during the normal physiologic aging process.

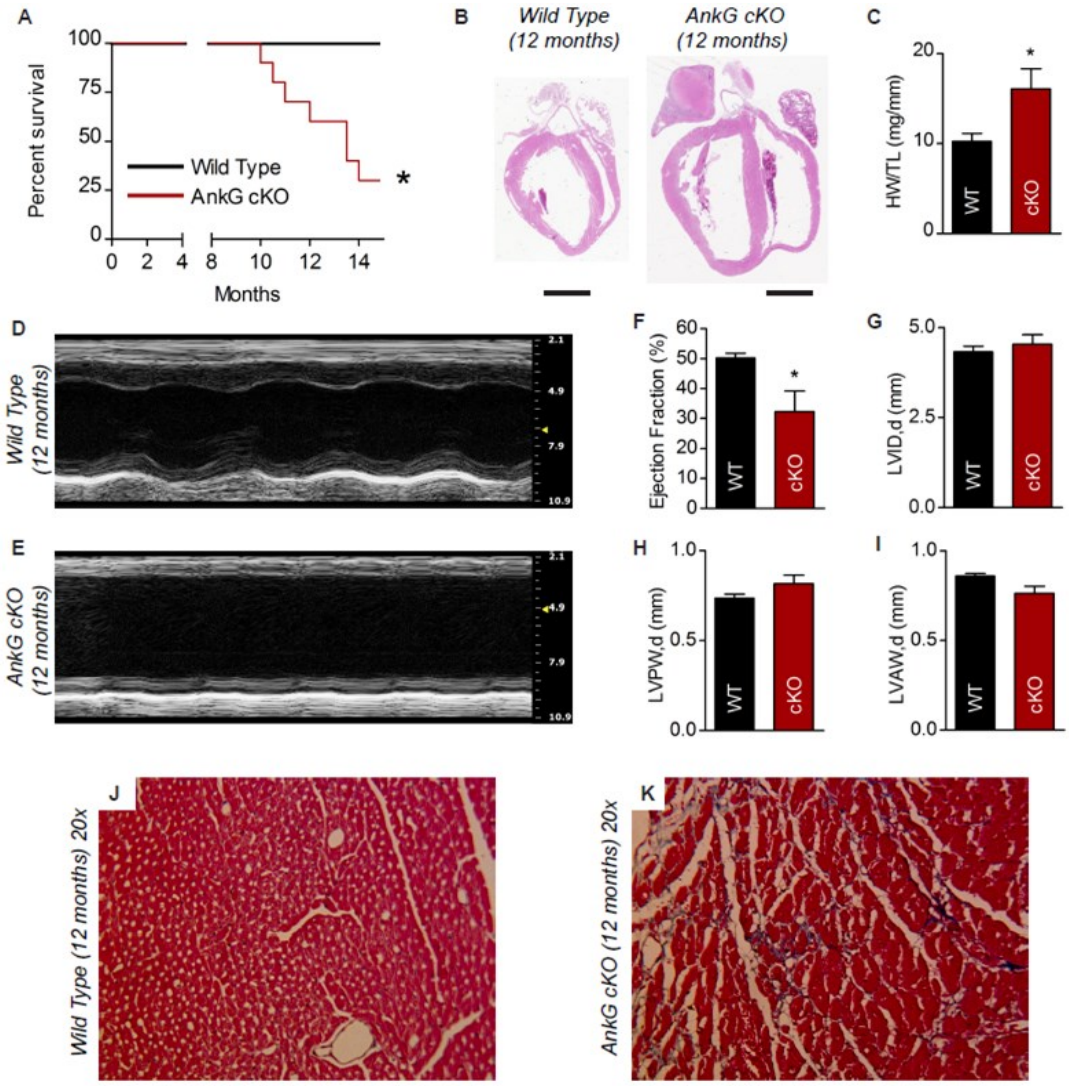

Figure 24. AnkG cKO mice display increased mortality and ventricular dysfunction with age.

(A) Kaplan-Meier survival analysis demonstrates increased mortality in ankG cKO mice

(Continued on Page 135)

(Figure 24 continued from Page 134)

beginning at 10 months of age (15 week survival: WT 10/10; AnkG cKO 3/10; $P<0.05$)). (**B**) Hematoxylin and Eosin staining of wild type and ankG cKO hearts at 12 months of age demonstrate enlarged hearts with (**C**) increased heart weight to tibia ratio (N= 5 WT; 8 ankG cKO ; $P<0.05$). M-mode images of (**D**) wild type and (**E**) ankG cKO hearts demonstrate a significant decrease in (**F**) ejection fraction in ankG cKO mice at 12 months (n= 5 WT, 6 ankG cKO; $P<0.05$). Analysis of M-mode images demonstrates unchanged (**G**) LVID,d, (**H**) LVPW,d, (**I**) LVAW,d in aged ankG cKO at 12 months of age. (**J**) Masson's Trichrome staining of aged wild type heart sections demonstrates preserved myocardial structure. (**K,L**) In contrast, aged ankG cKO heart sections demonstrate severe cardiac structural disruptions including minor fibrosis and severe vacuolization.

Loss of ankyrin-G accelerates cardiac remodeling following pathological stress

To directly test the impact of ankyrin-G loss on cardiac remodeling in the face of pathological stress, we analyzed WT and ankyrin-G cKO mice following transaortic constriction (TAC). This experimental model produces ventricular hypertrophy two weeks following TAC and cardiac decompensation 6 weeks following TAC [263]. Unlike WT controls, ankyrin-G cKO animals displayed increased mortality beginning immediately at two weeks following TAC (Figure 25 A; WT: 1/8 died prior to six weeks post-surgery; cKO: 8/14 died prior to six weeks post-surgery; $p<0.05$). All WT and cKO sham controls survived the six weeks post-surgical time (WT: 5/5; cKO: 6/6). Consistent with the protocol, hearts from both surviving WT and ankyrin-G cKO mice displayed a significant increase in heart weight/tibia length ratio following TAC (Figure 25B). However, unlike WT control mice, ankyrin-G cKO mice displayed increased lung weight/ tibia length ratio, indicative of the development of congestive heart failure in these animals (Figure 25C). Gross histologic examination of cardiac sections (Figure 25D) demonstrated chamber dilation and elongation in ankyrin-G cKO, but not WT animals after only 2 weeks post-TAC. At baseline (prior to TAC), we observed no difference in myocardial fibrosis / necrosis in either WT or cKO animals (Figure 25 E, F). However after only two weeks post-TAC, compared with WT animals, we observed significant myocardial remodeling including increased fibrosis and presence of vacuolization in ankyrin-G cKO mice (Figure 25 G,H).

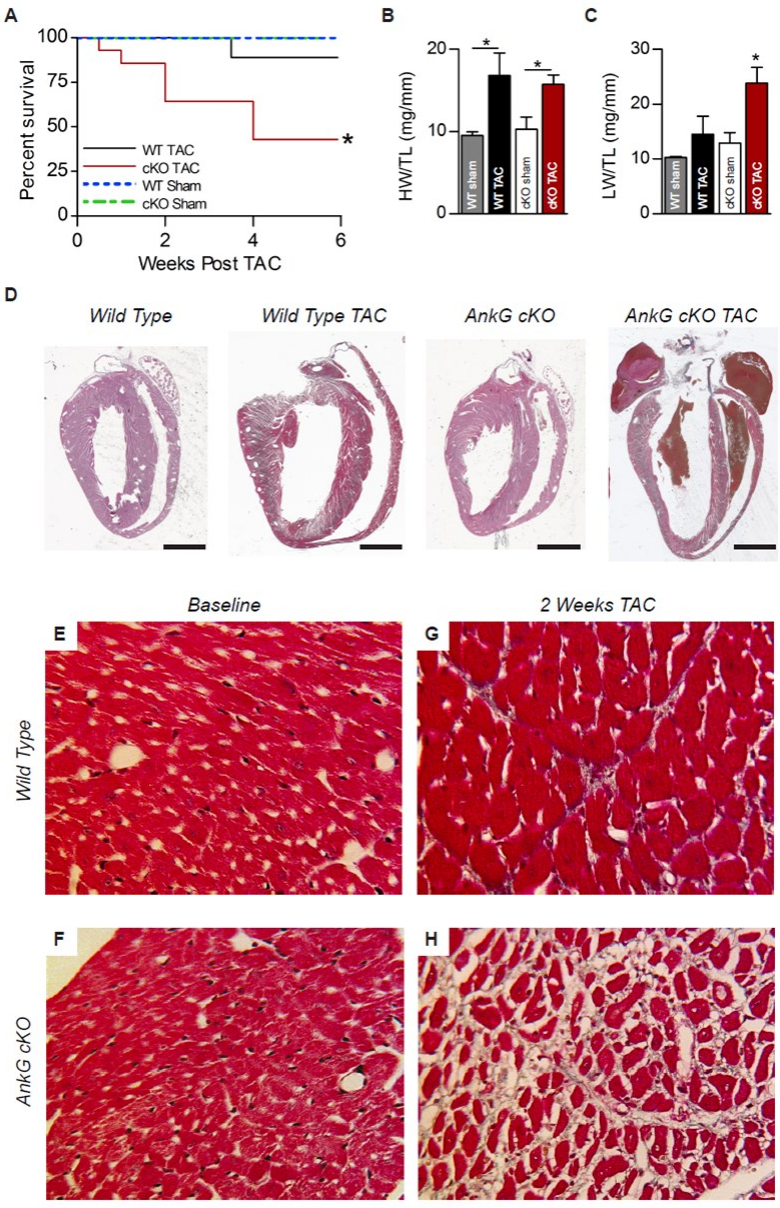

Figure 25. Increased mortality and severe ventricular remodeling in ankG cKO mice following transaortic constriction (TAC).

(Continued on Page 138)

(Figure 25 continued from Page 137)

(**A**) Kaplan-Meier survival analysis demonstrates increased mortality in ankG cKO mice beginning at 2 weeks post TAC (6 week survival: WT TAC: 7/8; AnkG cKO TAC: 6/14; WT sham: 5/5 ankG cKO sham: 6/6). AnkG cKO TAC hearts demonstrate (**B**) statistically similar heart weight to tibia ratio comparted to wild type TAC hearts at 2 and 8 weeks post TAC (N= 4 WT 2 weeks; 5 WT 8 weeks; 10 ankG cKO TAC) (**C**) However ankG cKO TAC hearts demonstrate a statistically significant increase in lung weight to tibia length ratio ($P<0.05$.) (**D**) Representative heart sections stained with Masson's Trichome. Masson's Trichrome staining of (**E**) wild type and (**F**) ankG cKO heart sections at baseline demonstrate preserved myocardial structure. (**G**) Wild type heart sections after TAC also display preserved cardiac tissue structure. In contrast, (**H**) ankG cKO TAC heart sections demonstrate severe vacuolization.

Based on these data, we performed cardiac functional analysis in WT and ankyrin-G cKO mice following TAC. M-mode images of ankyrin-G cKO hearts revealed a small, but significant decrease in ejection fraction at baseline compared to WT controls at baseline (Figure 26E, WT: 55.65 ±1.05% cKO: 52.37 ±1.09%, $p<0.05$). However, following only two weeks post-TAC, ankyrin-G cKO revealed significant and severe decreased ejection fraction (33.55 ± 5.24%, reduced ~35% from baseline $p<0.05$) compared to WT animals (53.85 ±1.79%; reduced ~4% from baseline). We observed no significant difference in ejection fraction compared to baseline for WT and ankyrin-G cKO sham operated animals following TAC.

Related to cardiac chamber size, we observed a small, but significant decrease in diastolic left ventricular internal diameter (LVID,d) in ankyrin-G cKO mice compared to WT controls at baseline (Figure 26F, WT: 4.31 ±0.04 mm; cKO: 4.02 ±0.05 mm; $p<0.05$). After 2 weeks TAC, WT animals demonstrate an insignificant trend for a decrease in LVID,d compared to WT baseline animals (Figure 26F, WT TAC: 4.14 ± 0.04 mm). In contrast, surviving ankyrin-G cKO animals displayed significant ventricular dilation compared to baseline ankyrin-G cKO values (Figure 26F, cKO TAC: 4.45 ±0.13 mm, $p<0.05$) following TAC. WT and ankyrin-G cKO sham operated animals demonstrated no significant difference in LVID,d compared to baseline.

Compared to WT controls, ankyrin-G cKO animals at baseline displayed no difference in diastolic left ventricular anterior wall (LVAW,d) thickness (WT: 0.85 ±0.03 mm; cKO: 0.81±0.02 mm) or left ventricular posterior wall (LVPW,d) thickness(WT: 0.74 ±0.02 mm; cKO: 0.75 ±0.03 mm). In mice, transaortic constriction has been shown

to stimulate ventricular hypertrophy at two weeks post-surgery. In WT mice, this hypertrophic response was demonstrated by significant increases in LVAW,d thickness (Figure 26G WT TAC: 0.99 ± 0.03 mm, $p<0.05$) and LVPW,d thickness (Fig 3H WT TAC: 0.98 ± 0.06 mm, $P<0.05$). Following TAC, however, ankyrin-G cKO mice do not display significant increases in LVAW,d thickness (Figure 26G cKO TAC: 0.88 ±0.04 mm) or LVPW thickness (Figure 26H cKO TAC: 0.83 ± 0.02 mm). Thus, cardiac expression of ankyrin-G is critical for ventricular compensation to pressure overload.

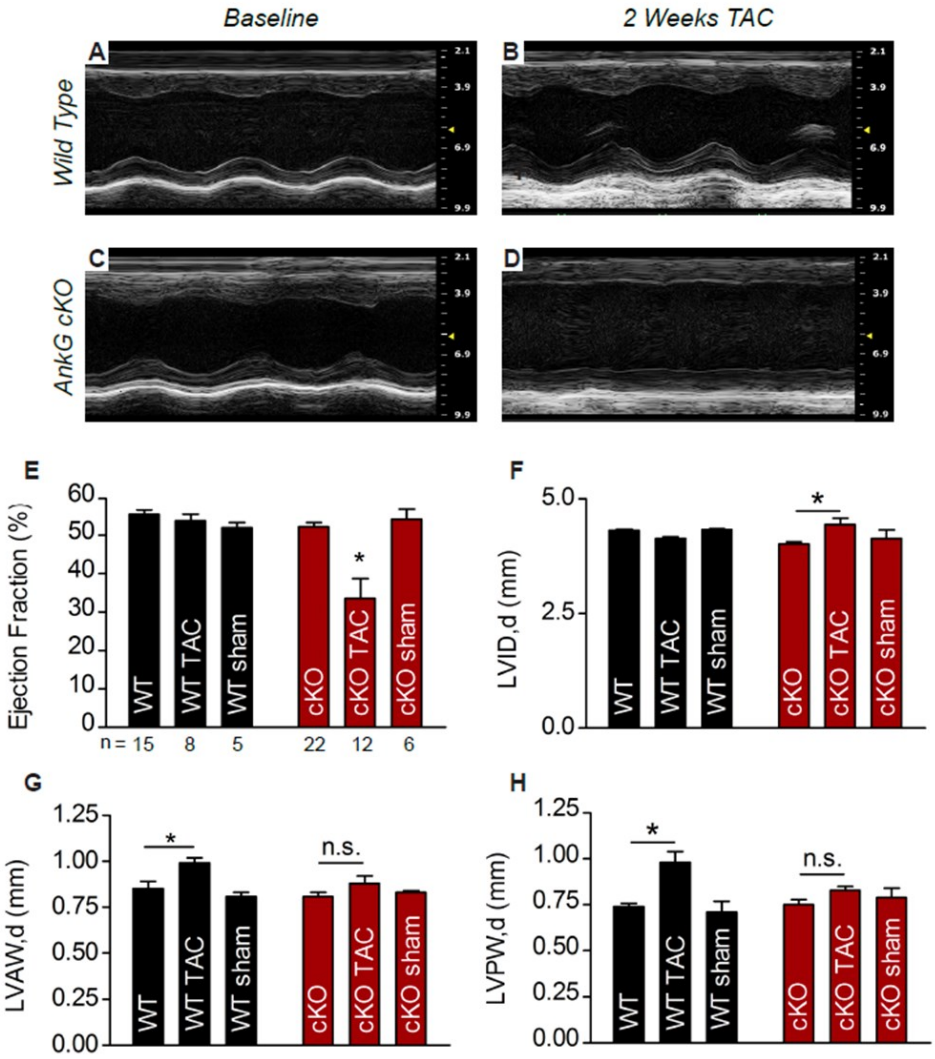

Figure 26. Ankyrin-G cKO mice demonstrate severe systolic dysfunction and ventricular dilation 2 weeks post TAC.

Representative M-mode images of (**A, B**) wild type and (**C, D**) ankG cKO hearts at

(Continued on Page 142)

(Figure 26 continued on Page 141)

baseline and after 2 weeks TAC. Analysis of short-axis M-mode images demonstrates (**E**) decreased ejection fraction and (**F**) increased left ventricular internal dimension during diastole in ankG cKO mice following 2 weeks TAC (N for each group listed below bar graph; $P<0.05$). Measurement of (**G**) left ventricular anterior wall (LVAW,d) and (**H**) left ventricular posterior wall (LVPW,d) thickness during diastole demonstrates increases in wall thicknesses in wild type mice following TAC ($P<0.05$). AnkG cKO mice wall thickness increases, but not significantly (n.s.).

Electrophysiologically, at baseline ankyrin-G cKO animals displayed decreased resting heart rates compared to WT controls (Figure 27E, WT: 600.6 ±7.7 bpm; cKO: 498.2 ±21.1 bpm; $p<0.05$). This trend persisted, and in fact even increased between genotypes two weeks post-TAC. (WT TAC: 678.9 ± 16.9, $p<0.05$). (cKO TAC: 555.4 ± 17.1; p= n.s.) At baseline, cKO animals displayed significantly increased PR and QRS intervals (Figure 27 F, G), similar to previous data presented here, as a result of altered conduction due to reduced I_{Na} [262]. Further, compared to WT TAC animals at two months of age, ankyrin-G cKO TAC mice display significantly increased PR interval length, but statistically insignificant increases in QRS interval length. In contrast to the EPI-induced arrhythmia and death in baseline ankyrin-G cKO animals (Figure 20), tachyarrhythmias, unexpectedly, were not the cause of mortality in ankyrin-G cKO mice post-TAC. Ambulatory recordings of conscious ankyrin-G cKO TAC animals at the time of death revealed higher incidence of brady-arrhythmia preceding death with no arrhythmic events noted in WT TAC animals (Figure 27 H,I; WT: 0/4; cKO: 4/7; $p<0.05$). In summary, these *in vivo* data demonstrate an indispensable role for ankyrin-G in the cardiac compensatory response to pressure overload. Further, these findings illustrate pump failure versus arrhythmia as the cause of mortality in ankyrin-G cKO animals post-TAC.

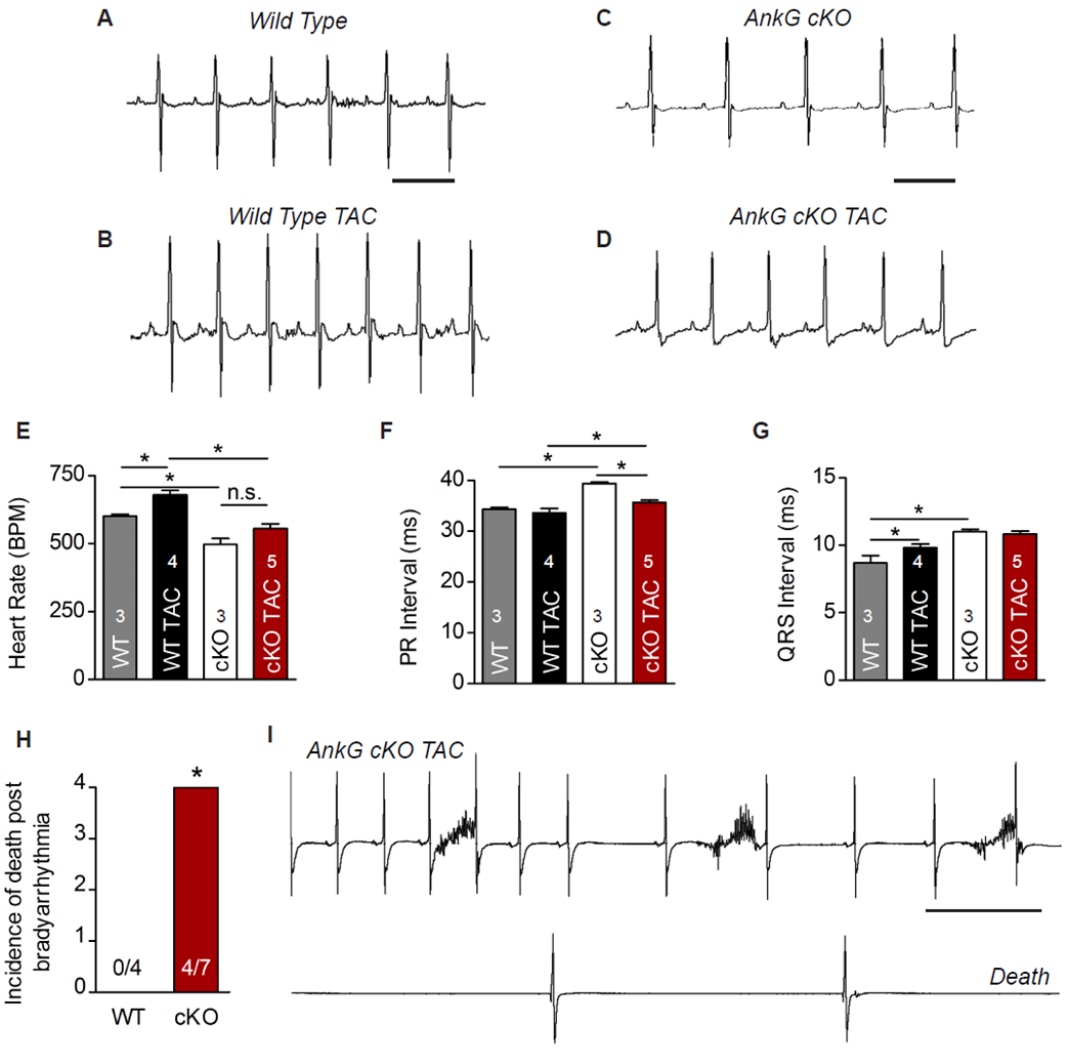

Figure 27. Ankyrin-G cKO TAC mice display abnormal regulation of heart rate.

Representative ECGs from ambulatory wild type mice at (**A**) baseline and (**B**) 2 weeks post TAC reveal an increase in resting heart rate in response to transaortic banding. (**C**)

(Continued on Page 145)

(Figure 27 continued from Page 144)

ECGs from ambulatory ankG cKO mice demonstrate decreased resting heart rate at baseline. (**D**) In response to TAC, ankG cKO mice display decreased resting heart rate relative to wild-type controls. Bar = 100 msec. (**E**) Quantification of average resting heart rates in all experimental groups. AnkG cKO mice display increased (**F**) PR interval and (**G**) QRS interval at baseline and after TAC relative to WT controls. (N for each group listed in bar graph; $P<0.05$) (**H**) AnkG cKO mice show increased rate of spontaneous death. (**I**) Telemetric monitoring demonstrates that ankG cKO animals develop severe bradycardia eventually leading to death. Bar=250 msec.

To investigate ankyrin-G-dependent mechanisms during cardiac remodeling, regulates the cellular response to pressure overload, we next performed immunostaining of WT cardiomyocytes isolated from WT hearts at baseline (Figure 28A) and after 2 weeks TAC (Figure 28B). Ankyrin-G is primarily localized to the intercalated disc of the cardiomyocyte (Figure 28A), consistent with previous reports from our lab and others [126, 189, 262]. However, myocytes isolated from WT hearts following 2 weeks TAC demonstrate a significant upregulation of ankyrin-G at the intercalated disc (Figure 28B). Z-stack confocal microscopy (Figure 28C) confirmed significant increases of ankyrin-G localization at the intercalated disc after 2 weeks TAC concurrent with enlargement of the cardiomyocyte. Consistent with these data, immunoblots demonstrated an ~2.5 fold increase in ankyrin-G expression in WT hearts following 2 weeks TAC compared to WT hearts at baseline (Figure 28D; $p<0.05$). CaMKII expression has also been showed to increase following 2 weeks transaortic constriction. Likewise, we demonstrate ~9 fold upregulation of CaMKII expression after 2 weeks TAC (Figure 28D; $p<0.05$) in agreement with previous data at the same timepoint[263]. Based on our data, we hypothesized that an increase in ankyrin-G expression is necessary to maintain cardiomyocyte structural integrity during pathological stress.

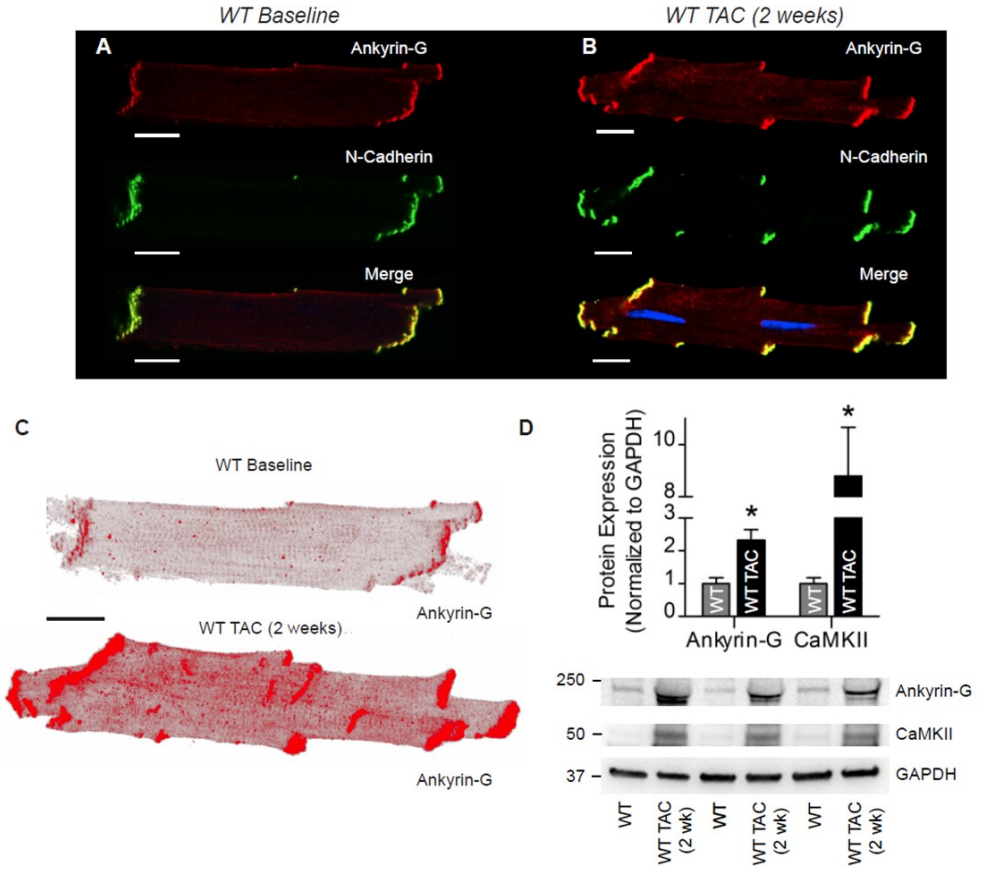

Figure 28. Ankyrin-G expression increases 2 weeks after TAC in WT mice.

Immunofluorescent staining of wild type cardiomyocytes at (**A**) baseline and after (**B**) 2 weeks TAC display increased expression of ankyrin-G (red) at the intercalated disc during hypertrophy. (**C**) Composite z-stack images demonstrate increased intercalated disc expression of ankyrin-G in tandem with an increase in cardiomyocyte size (bar = 20 microns). (**D**) Immunoblot analysis demonstrates an ~ 2.5 fold increase in total ankyrin-G expression as well as ~9 fold increase in CaMKII expression after 2 weeks TAC. N=3/group, $P<0.05$.

Ankyrin-G cKO mice display defects in intermediate filament organization / integration at the intercalated disc.

Interestingly, previous investigations have shown that expression / localization of another desmosomal protein Plakophilin-2 (PKP2), is disrupted in the absence of ankyrin-G [200, 262]. PKP2 functions to integrate intermediate filaments (comprised of desmin) into the desmosomal plaque. Further, previous investigation has demonstrated that DSC-2 membrane targeting is dependent on PKP-2 expression (ref). In WT animals at baseline, PKP2 is normally localized to the intercalated disc (Figure 29A). However, at baseline ankyrin-G cKO animals show mislocalization of PKP2 from the intercalated disc to the cytoplasm (Figure 29B), consistent with previous findings. In WT animals after 2 weeks TAC, PKP2 levels increase at the intercalated disc (Figure 29C) along with ~40% increase in total PKP2 expression (Figure 29E, $p<0.05$). Conversely, ankyrin-G cKO animals display massive disruptions in PKP2 localization at the intercalated disc following 2 weeks TAC (Figure 29D). At baseline, cKO animals demonstrate ~40% increase in PKP2 levels, as demonstrated previously. However, after 2 weeks TAC, PKP2 expression in cKO animals increases ~100% from WT baseline. PKP2 expression in cKO TAC animals was statistically significant compared to all groups tested (#$p<0.05$).

As PKP2 integrates intermediate filaments into the desmosomal plaques found at the intercalated disc, we next examined cryosections of WT and cKO hearts to look at intermediate filament localization. In WT and WT TAC cryosections, desmin is heavily localized at the intercalated disc, but also demonstrates a striated appearance (Figure 29 F, G) e.g. sarcomeric desmin). Conversely, cKO animals at baseline demonstrate reduced

desmin localization at the intercalated disc due to disruptions of plakophilin-2 expression (Figure 29H). Further, cKO hearts subjected to 2 weeks TAC also show disrupted desmin localization (Figure 29I), supporting that ankyrin-G expression, through its interaction with PKP2, regulates the intermediate filament cytoskeleton in the heart. As our new findings are consistent with a model where loss of ankyrin-G-dependent regulation of the intercalated disc intermediate filament network accelerates cardiac remodeling following pathological stress.

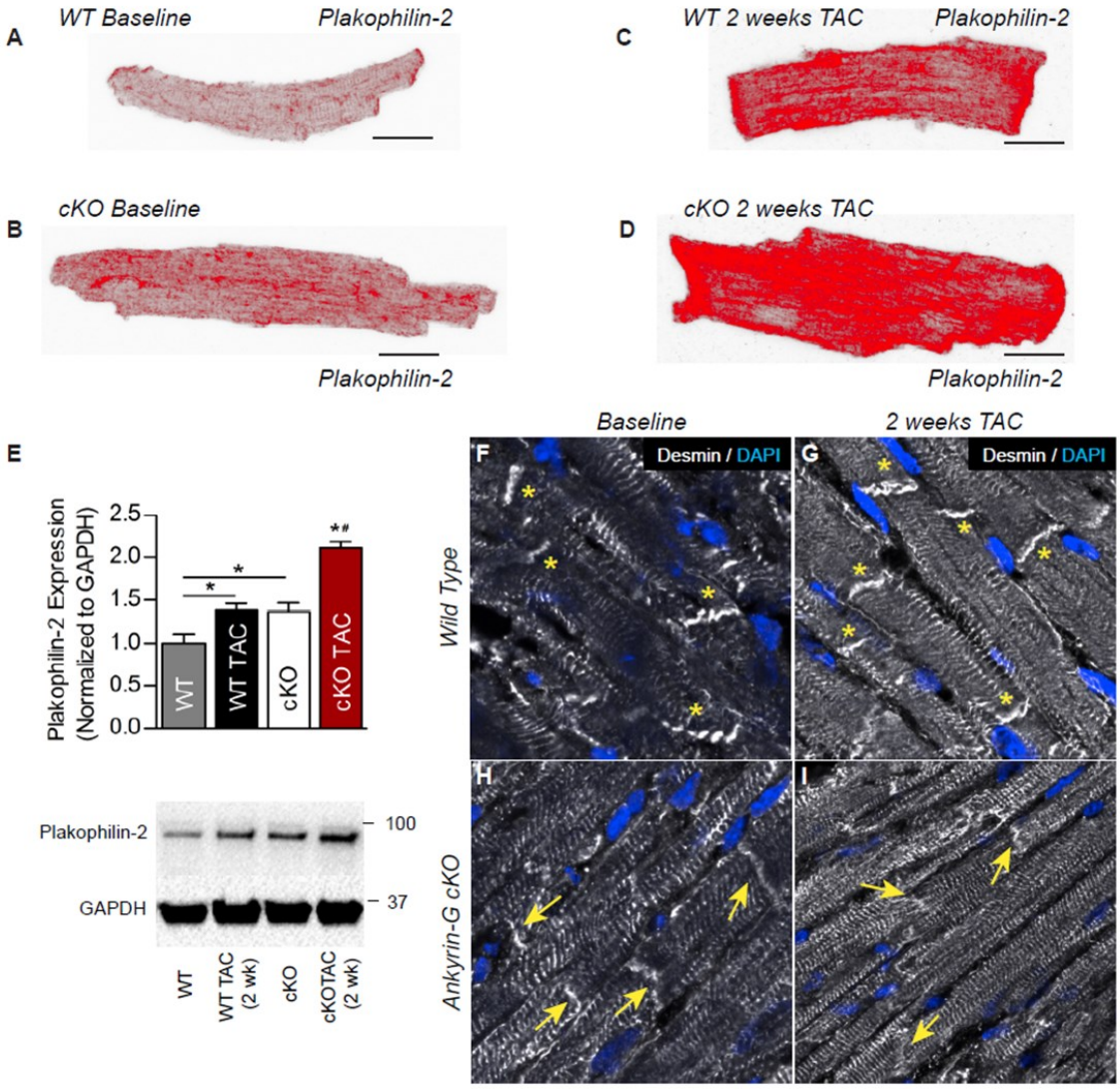

Figure 29. Plakophilin-2 expression is dysregulated in the absence of ankyrin-G

Composite z-stack images of (**A**) wild type and (**B**) cKO cardiomyocytes at baseline demonstrate cellular redistribution of plakophilin-2 in cKO cardiomyocytes. (**C**) After 2

(Continued on Page 151)

(Figure 29 continued from Page 150)

weeks TAC, plakophilin-2 localization at the intercalated disc increases in WT TAC cardiomyocytes. (**D**) Conversely, plakophilin-2 distribution is severely disrupted in cKO TAC cells. (**E**) Immunoblot demonstrates that plakophilin-2 expression is increased cKO hearts relative to WT hearts at baseline and after 2 weeks TAC (N=3/group; $P<0.05$. (**F-I**) Immunofluorescent staining of the intermediate filament protein desmin demonstrates preferential localization to the intercalated disc in WT heart tissue at (**F**) baseline and (**G**) after 2 weeks TAC. (**H**) In cKO hearts at baseline, desmin immunolocalization is decreased at the intercalated disc. (**I**) cKO hearts after 2 weeks TAC further show decreased levels of desmin at the intercalated disc

Ankyrin-G expression is altered in human heart failure

Several reports have demonstrated dysregulated expression of ankyrin-G in multiple non-cardiac pathologies including generalized ischemia [221] and traumatic brain injury [224], Based on our data, we investigated the regulation of ankyrin-G in the setting of human heart failure. Immunostaining of non-failing human heart tissue demonstrated predominant localization of ankyrin-G to the intercalated disc (Figure 30A, white arrows). In both ischemic (Figure 30B) and non-ischemic (Figure 30C) human heart failure, ankyrin-G expression at the intercalated disc was diminished (white asterisks). In line with these data, immunoblot analysis demonstrated a significant reduction (~50%) of ankyrin-G protein expression in ischemic human heart failure tissue (IHF, Figure 30D) and non-ischemic human heart failure tissue (NIHF, Figure 30E) relative to non-failing controls ($p<0.05$). These results demonstrate that expression of ankyrin-G is dysregulated in multiple forms of human heart failure and may be a critical event in the development / progression of heart failure in humans.

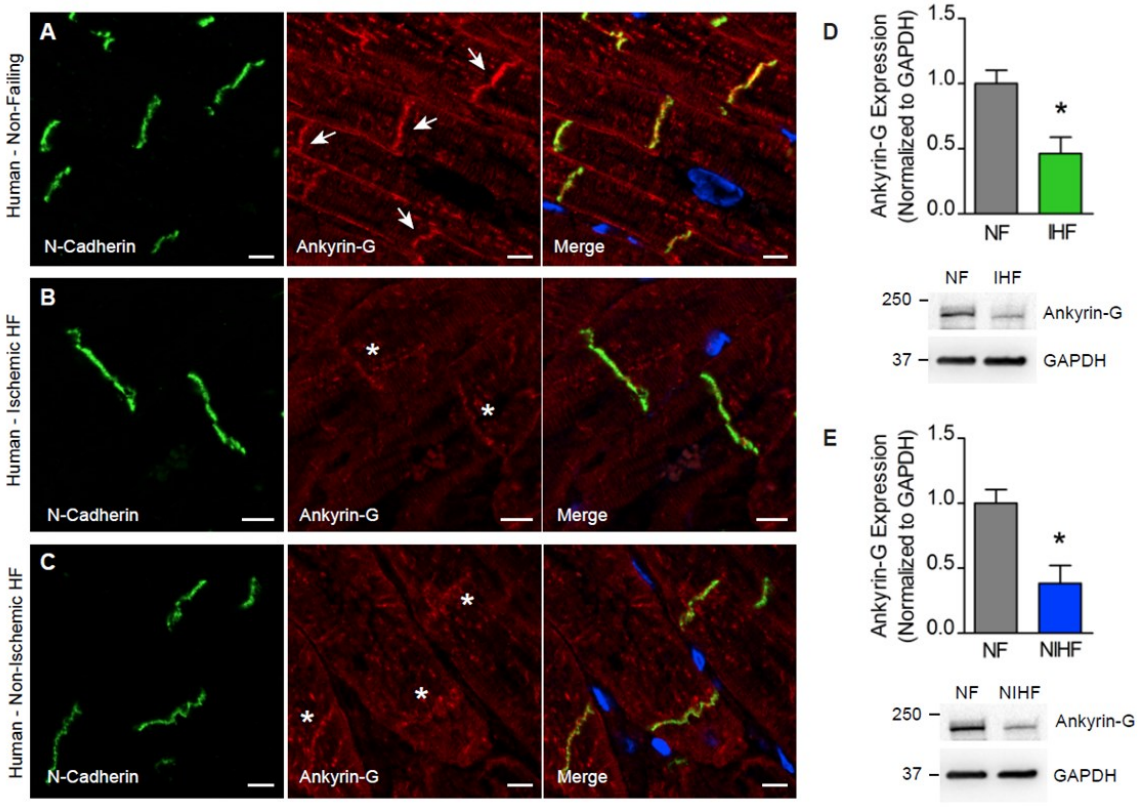

Figure 30. Ankyrin-G expression is dysregulated in human heart failure.

Immunofluorescent staining of (**A**) non-failing human myocardium demonstrates primary localization of ankyrin-G (red) at the intercalated disc (white arrows). In contrast, sections of human hearts diagnosed with (**B**) ischemic and (**C**) non-ischemic heart failure display disruptions of ankyrin-G (red) staining at the intercalated disc (white asterisks). N-cadherin (green) used as marker of intercalated disc (bar = 10 microns). Immunoblot analysis demonstrates a decrease in total ankyrin-G expression in (**D**) ischemic and (**E**) non-ischemic heart failure. (n= 3 NF; 5 IHF; 5 NIHF. $P<0.05$).

Discussion

To our knowledge, this is the first investigation detailing that functional expression of ankyrin-G is required for cardiac compensation in response to pressure overload via transaortic constriction. In both aged systems (Figure 24) and after 2 weeks TAC (Fig 25, 26), cKO animals demonstrate severe heart failure phenotypes including reductions in systolic function as evidenced by reduced ejection fraction and severe cardiac structural remodeling. Ultimately, these aberrances lead to increased mortality in the cKO animal populations (Fig 24, 25). Further, we demonstrate that ankyrin-G expression is upregulated in wild type animals following 2 weeks TAC (Figure 28). Ours is not the first investigation to demonstrate an upregulation of ankyrin-G protein expression in response to cardiac stress. Canine cardiomyocytes isolated from the border zone of a myocardial infarct also demonstrate significant increases in ankyrin-G expression as soon as 48 hours post-occlusion [127]. We propose that this upregulation of ankyrin-G is a compensatory response necessary to increase and/or maintain mechanical coupling of cardiac myocytes during times of cardiac stress.

Mechanistically, we link ankyrin-G deficiency with disrupted cellular localization of the desmosomal protein plakophilin-2 at baseline and after TAC (Figure 29). Following TAC, expression of both ankyrin-G and PKP2 is increased coupled with increased ankyrin-G/PKP2 localization at the intercalated disc. We propose that these events are necessary for cardiac compensation to chronic pressure overload. A functional link between ankyrin-G and PKP2 has been demonstrated previously in vitro by the Delmar lab[200]. An in vitro association between ankyrin-G and PKP-2 has been

demonstrated previously by the Delmar lab. Specifically, siRNA-mediated silencing of ankyrin-G in neonatal rat ventricular cardiac myocytes led to redistribution of plakophilin-2 from sites of cell-cell contact. Consequently, this disruption in PKP-2 localization produced functional decreases in intracellular adhesion strength [200]. Here we demonstrate that cardiac-specific silencing of ankyrin-G leads to decreased localization of PKP2 at the intercalated disc in cKO myocytes at baseline and after TAC. In humans, loss of function mutations in PKP2 have been with severe cardiovascular diseases such as arrhythmogenic right ventricular cardiomyopathy (ARVC) [258], dilated cardiomyopathy[264], and Brugada syndrome [265]. Given the extreme importance of proper PKP2 expression in the human heart, we hypothesize that the severe contractile dysfunction and structural remodeling seen in cKO animals is caused, in part, by deficient PKP2 localization in the absence of ankyrin-G.

Indeed, previous investigations have demonstrated a structural requirement for ankyrin-G in vitro in multiple cell types. In neurons, ankyrin-G is required for the stability of structural components of the axon initial segment including neurofascin-186 (NF-186) and neuronal cell adhesion molecule (NrCAM) [101]. Further, expression of ankyrin-G in CNS neurons and oligodendrocytes is responsible for the rapid structural formation of nodes of Ranvier [121]. Multiple reports have demonstrated that ankyrin-G is necessary for the retention of E-cadherin, a molecular event necessary for the biogenesis of the lateral membrane in human bronchiolar epithelial cells [27, 28]. Given the presence of such severe dysfunction, however, we hypothesized that the phenotypes displayed by the

cKO mice following TAC were likely caused by multiple changes to the cardiac myocyte structural apparatus.

PKP2 is a critical component of the cardiac desmosome. Desmosomes are membrane structures present in multiple human cell types that act to link adjacent cells together into a functional tissue. Specifically in the heart, desmosomal plaques are composed of the transmembrane cadherins desmoglein-2 (DSG2) and desmocollin-2 (DSC2) that act as a "spot weld" between cells. PKP2 and Plakoglobin (JUP) then associate with the cytoplasmic tails of DSC2/DSG2[134]. In order to provide strong, mechanical linking of adjacent cells into a functional tissue, desmosomes couple to the intermediate filament network. In the heart, desmin is the main protein component of intermediate filaments and is mainly localized to sarcomeres and the intercalated disc [266]. The desmosomal protein desmoplakin (DP) binds to desmin in the cardiomyocyte and scaffolds the desmin filaments to PKP2 and Plakoglobin (JUP) in the desmosome[134]. As a result of deficient PKP2 targeting in cKO animals, desmin localization at the intercalated disc is also disrupted at baseline and following 2 weeks TAC, further weakening the cytoarchitecture in cKO cardiomyocytes (Figure 29). Interestingly, human mutations in desmin (DES) have also been linked with congenital dilated cardiomyopathy[267] and right ventricular heart failure [268]. Further, desmin organization is disrupted in acquired human heart failure. Taken together, our data demonstrate a critical regulatory role for ankyrin-G in the regulation of cardiac desmosomal components at baseline and following chronic pressure overload.

One interesting finding given the severe structural abnormalities witnessed in cKO animals after TAC was the absence of fatal tachyarrhythmia (Figure 27). At baseline, we demonstrated that ankyrin-G cKO mice display fatal arrhythmia in the presence of a catecholamine challenge [262]. Surprisingly, after 2 weeks TAC, telemetered cKO animals displayed a progressive bradycardia rapidly leading to death. Interestingly, human *SCN5A* variants have been linked with sick sinus syndrome, suggesting that the bradycardia could be caused by severe I_{Na} deficiency[269]. Although Nav1.5 is not expressed in sinus nodal cells, the transition zone between the SA node proper and atrial myocardium is enriched in Nav1.5. Therefore decreased Nav1.5 expression in these transitional cells may underlie this bradycardic response[176]. However, given the multitude of ankyrin-dependent interacting partners, a remaining question at this time is the functional requirement of ankyrin-G in the SA nodal cells themselves. Future experiments will be necessary to determine if and to what extent ankyrin-G modulates sinoatrial cellular excitability and/or cellular integrity.

Human variants in ankyrin-G (*ANK3*) have been linked with multiple neuropshychiatric disorders including bipolar disorder [270], schizophrenia [104], post-traumatic stress disorder [102], and autism [105]. Surprisingly, none of the reported human ankyrin-G variants has been shown to cause cardiac arrhythmia or cardiomyopathy. While further investigation may uncover such a human variant, our data predict a necessary role for ankyrin-G with respect to cardiac function. Further, neuropsychiatric patients have increased propensity to develop cardiovascular diseases than the general population [271, 272]. Although higher rates of external cardiovascular comorbidities

(smoking, obesity, sedentary life-style) are witnessed in these patients compared to the general population, it is quite intriguing to speculate that a loss-of-function mutation in ankyrin-G may make these patients more susceptible to developing cardiovascular disease. Our data also indicate a decrease in ankyrin-G expression in the setting of acquired human heart failure (Figure 30). Human samples from both ischemic and non-ischemic human heart failure demonstrate ~50% reduction in ankyrin-G expression relative to non-failing control samples. Coupled with our in vivo data and biochemical experiments, we propose that ankyrin-G expression is necessary to properly compensate for stresses placed on the heart and that ankyrin-G dysregulation may be a common event in the development and/or progression of human heart failure.

Chapter 5: Conclusions and Future Directions

In accordance with experimental evidence derived from other cell types, ankyrin-G regulated both cellular excitability and architecture in the cardiomyocyte as hypothesized. Although in vitro evidence had indicated a role for ankyrin-G in regulating these cellular properties, this is the first report detailing the molecular, cellular, and functional consequences of ankyrin-G deficiency in the heart in vivo. Why is this so important? Work from this study has demonstrated that ankyrin-G expression and cellular localization is decreased in the setting of acquired heart failure (Figure 30). Given the severe functional disruptions witnessed in ankyrin-G animals, it is intriguing to speculate that deficiencies in the functional expression of ankyrin-G in humans may underlie multiple pathologies seen in the setting of acquired CVD.

First, ankyrin-G is necessary to target a large proportion of the voltage-gated sodium channel Nav1.5 to the intercalated disc in vivo, as determined by the biochemical and electrophysiological evidence presented earlier. Silencing of ankyrin-G in vivo was sufficient to cause decreased heart rate, significant conduction abnormalities, and severe arrhythmia in response to the Nav channel antagonist flecainide. Nav1.5 is the predominant voltage-gated sodium channel in the cardiomyocyte. However, multiple "neuronal" sodium channels (Nav1.1, Nav1.2, Nav1.3, and Nav1.6) are also present in the cardiomyocyte, preferentially localizing to the transverse-tubule network. As these

channels do contain a consensus ankyrin-G binding sequence, we cannot rule out a direct association between these channels and ankyrin-G. However, multiple studies have shown that the expression level of these channels is relatively low in comparison with Nav1.5, contributing 5-20% of peak sodium current density[172-174]. Recent work from the Mohler laboratory determined the relative contribution of Nav1.5 to peak Na^+ current density using *Scn5a*-floxed neonatal cardiomyocytes treated with Cre recombinase in adenovirus. After treatment, cells receiving Cre recombinase demonstrated >95% reduction in peak sodium current density compared to control cells, indicating a relatively minor role for neuronal Na^+ channel populations for normal cardiomyocyte cellular physiology[173]. However, evidence exists suggesting a role for these neuronal sodium channels in rare cardiovascular diseases (sudden unexplained death in epilepsy[273], CPVT[274]) and ischemic heart failure (Nav1.1 upregulation[275]). Therefore, it will be of interest to investigate the role of ankyrin-G with respect to the cellular targeting of these neuronal sodium channels.

In response to decreased functional expression of Nav1.5 in ankyrin-G cKO cardiomyocytes, resting heart rate was significantly reduced relative to WT controls at baseline. In support of this finding, human *SCN5A* variants have been implicated in sick sinus syndrome and animal models of Nav1.5 deficiency have demonstrated decreased resting heart rate[231, 269]. Although Nav1.5 is not present in the sinus nodal cells, immunofluorescence has demonstrated that the cells peripheral to the sinus node do express Nav1.5, possibly mediating the conduction of the action potential from the sinus node proper to the surrounding atrial tissue[176, 231]. Further, PR and QRS interval were also

prolonged. The PR interval correlates with the time for transmission of the impulse through the AV node, to the AV bundle and through the right and left bundle branches to the Purkinje fibers[15]. Interestingly, human *SCN5A* variants have been linked with AV conduction slowing and/or block[253]. Although the compact node does not express Nav1.5, multiple studies have demonstrated that the inputs to the AV node (e.g. inferior nodal extension, transition zone) and the outputs from the AV node (e.g. AV bundle and bundle branches) express Nav1.5. Therefore, disruptions in Nav1.5 expression could result in conduction slowing / block either before or after the compact node itself, as seen in the ankyrin-G cKO animals[276]. The QRS interval measures the time for activation of the ventricular myocytes[15]. As functional Nav1.5 expression is decreased significantly in ankyrin-G cKO ventricular myocytes (resulting in decreased action potential upstroke velocity[277]), conduction velocity through the ventricles is also decreased, demonstrated by prolonged QRS intervals. Further supporting our findings, mice heterozygous for *Scn5a* develop significant conduction slowing (PR and QRS) and AV nodal block. These conduction disturbances in *Scn5a* $^{+/-}$ animals (similar to ankyrin-G cKO animals) become increasingly severe in the presence of the Nav channel antagonist flecainide[179].

Our results also demonstrate that ankyrin-G is required for the formation of a regulatory complex around Nav1.5. Specifically, we show that ankyrin-G is required for the recruitment of βIV-spectrin to the intercalated disc. Work from the Hund Laboratory previously demonstrated that βIV-spectrin is required to target CaMKIIδ to the intercalated disc to regulate Nav1.5 channel properties[189]. Specifically, activation of CaMKIIδ results in increase in the amount of "persistent" or "late" I_{Na}[191, 192]. After rapid

activation, Na^+ channels rapidly inactivate, diminishing the magnitude of the Na^+ current back to near baseline levels due to channel inactivation[109]. However, a proportion of these Na^+ channels either do not activate properly or reactivate, producing a minor depolarizing current termed "late" Na^+ current[278]. In a setting such as heart failure, this proportion of non-inactivating channels increases, lengthening the action potential and increasing the proarrhythmic potential of the cardiomyocyte[193]. Why, if this current is so detrimental, does it occur in a cardiomyocyte?

In an acute setting of cardiac insufficiency, adrenergic stimulation of the myocardium increases to maintain cardiac output (i.e. increased contractility, increased heart rate, increased rate of relaxation)[107]. This adrenergic input, among other signaling consequences, activates CaMKIIδ to produce multiple end effects[149, 279]. In particular, work from the Hund Laboratory demonstrated that CaMKIIδ phosphorylates Nav1.5 at Serine571[189]. Importantly, this phosphorylation increases late sodium current, causing an increase in the cytoplasmic Na^+ concentration. Recall that one of the main ways to extrude Ca^{+2} from the cytoplasm is through NCX. By decreasing the concentration gradient of Na^+ across the membrane, this will decrease Ca^{+2} efflux. As a result, this increase in cytoplasmic Ca^{+2} will be taken up by SERCA2a into the SR, a finding seen by Sossalla et al. 2008 when stimulating late I_{Na} by *Anemonia sulcata* toxin II[194]. This increase in SR Ca^{+2} would favor increased Ca^{+2} transient height leading to stronger cellular force development during systole as a compensatory function[280]. However, in a state of chronic adrenergic activation such as heart failure, increased late Na^+ current would prolong the action potential duration[193, 281], favoring reactivation of voltage-gated

Na^+ and Ca^{+2} channels, producing an early afterdepolarization (EAD)[189, 282]. Further, increased SR Ca^{+2} load increases RyR2 open probability, favoring spontaneous release of Ca+2 from the SR and increasing the probability of delayed afterdepolarizations (DAD)[196]. As both EADs and DADs are proarrhythmic occurences, inhibition of late I_{Na} has recently been targeted as a potential antiarrhythmic therapy[283].

Experimentally, we can induce late I_{Na} using adrenergic agonists such as isoproterenol (1 μM)[189]. In WT murine cardiomyocytes, this results in an increased influx of late I_{Na}, at a magnitude approximately 1-2% of peak I_{Na}. In ankyrin-G cKO cardiomyocytes, however, late I_{Na} cannot be stimulated by isoproterenol as CaMKIIδ targeting at the intercalated disc is disrupted due to decreased recruitment of βIV-spectrin. This electrophysiological finding was corroborated by the use of a phospho-specific p-Ser571 Nav1.5 antibody. Both whole heart lysates and isolated cardiomyocytes showed reductions in the levels of p-Ser571 Nav1.5. This finding indicates that ankyrin-G expression at the intercalated disc is necessary for CaMKIIδ-dependent regulation of Nav1.5 at baseline. However, viewing the data as a whole, an interesting question arises: If ankyrin-G expression at the intercalated disc is decreased in human heart failure, how could late I_{Na} be increased in this setting? This question is further complicated by recent findings from the Hund Laboratory similarly demonstrating reductions in βIV-spectrin expression under the same disease conditions in humans[284].

At this point, it is necessary to point out that this late I_{Na} parameter was only assessed in non-failing WT and ankyrin-G cKO cardiomyocytes. Therefore, we cannot make any conclusions regarding the dependence of ankyrin-G in stimulating late I_{Na} in a

failing cardiomyocyte at this time. However, a simple hypothesis can be proposed to answer this question at present. Expression of total CaMKIIδ and activated CaMKIIδ is increased in human heart failure[285]. Further, work from the Hund laboratory has also demonstrated no change in total Nav1.5 expression, but increased phosphorylation of Nav1.5 at Ser571 in human heart failure samples[192]. However, coupled with data demonstrating decreased Na^+ current density in failing canine and human ventricular cardiomyocytes, this would suggest that a large proportion of expressed Nav1.5 is not functional in failing cardiomyocytes[218]. This is in agreement with a model whereby ankyrin-G expression is decreased in heart failure, impairing recruitment of Nav1.5 to the plasma membrane at baseline. However, as more CaMKIIδ is expressed in failing cardiomyocytes, the ratio of activated CaMKIIδ to functional Nav1.5 would increase, resulting in an increase in phosphorylated Nav1.5 producing more late I_{Na}. To test this hypothesis, one could over-express CaMKIIδ in an ankyrin-G cKO cell and conduct electrophysiologic recordings to investigate for the presence/absence of late I_{Na} after isoproterenol stimulation. This would confirm whether or not CaMKIIδ requires specific targeting to Nav1.5 to functionally regulate Nav1.5 in a setting of increased CaMKIIδ expression (i.e. heart failure, myocardial infarct).

Although we demonstrate an approximate 60% decrease in total CaMKIIδ expression, localization of this kinase is only disrupted at the intercalated disc whereas transverse-tubule populations of CaMKIIδ (interacting with RyR2 and Cav1.2) are conserved[286, 287]. With respect to CVD, CaMKIIδ activation is increased after myocardial infarction and in non-ischemic heart failure[285, 288]. This hyper-activation of CaMKIIδ is

subsequently linked with spontaneous Ca+2 release from the RyR2, increased cardiomyocyte apoptosis, and activation of pathological ventricular hypertrophy[149, 263]. Given the large decrease in CaMKIIδ expression in ankyrin-G cKO mice, we were surprised to find that ankyrin-G cKO mice had a higher propensity of arrhythmia following sympathetic stimulation at baseline. Although inhibition of CaMKIIδ in animal models has shown to be anti-arrhythmic[289], a simple explanation for this dysfunction in ankyrin-G cKO hearts exists. In a setting of decreased peak and late Na^+ current, the Na^+ concentration gradient across the cell would increase. This would act to increase Ca^{+2} extrusion via NCX. In the setting of unchanged Cav1.2 expression (i.e. same amount of trigger Ca^{+2} entering during the action potential) seen in ankyrin-G cKO cells, one would hypothesize that NCX would extrude more Ca^{+2} than was brought into the cell. This would favor Ca^{+2} under-loading in the SR at baseline.

However, as discussed previously, decreased SR Ca^{+2} content would cause decreases in Ca^{+2} transient height (i.e. less Ca^{+2} released to activate the myofilaments per excitation) resulting in decreased contractile force[280]. Although a significant reduction in ejection fraction is noticed in ankyrin-G cKO hearts at baseline, these differences are quite minor relative to WT controls. As a result, we would hypothesize that the Ca^{+2} transients in ankyrin-G cKO cells are also unchanged at baseline. In a setting of decreased SR Ca^{+2} content with unchanged Ca^{+2} transient height, RyR2 would have to become sensitized to release more Ca^{+2} per excitation in ankyrin-G cKO cells. One of the major ways that RyR2 becomes sensitized is through phosphorylation at Ser2814 by CaMKIIδ[287]. Phosphorylation of RyR2 at Ser2814 increases the open probability of

RyR2, causing this Ca^{+2} release unit to release relatively more Ca^{+2} per excitation. However, this CaMKIIδ-dependent RyR2 hypersensitivity has been shown to cause spontaneous Ca^{+2} release and leak from the SR, resulting in the production of pro-arrhythmic DADs[290]. As CaMKIIδ targeting to RyR2 appears unaffected, increased RyR2 phosphorylation at Ser2814 in ankyrin-G cKO cardiomyocytes could be a plausible mechanism that would produce unchanged Ca^{+2} transient height with an increased propensity for arrhythmia witnessed in ankyrin-G cKO mice after sympathetic stimulation. However, this hypothesis remains to be tested.

We were further surprised that ankyrin-G mice spontaneously develop pathological remodeling at an accelerated rate with age. This was further surprising given the drastic reduction in the expression of CaMKIIδ in ankyrin-G cKO mice. Although these phenotypes were incredibly severe in aged ankyrin-G cKO mice, a recent report demonstrated that expression of Cre recombinase alone was sufficient to produce minor systolic deficiency and structural remodeling in aged animals[291]. As we had evidence that ankyrin-G expression was decreased in human heart failure, we wanted to test whether ankyrin-G deficiency in cardiomyocytes was a cause or an effect of heart failure. To sidestep any confounding variables with an aging system, we instead elected to experimentally produce heart failure via transverse aortic constriction (TAC) in young (8 weeks old) mice. As TAC produces ventricular hypertrophy by two weeks and heart failure by six to eight weeks WT mice post operation[263], this model avoids any cardiotoxic effects mediated by overexpression of the Cre transgene in ankyrin-G cKO animals. Very interestingly, ankyrin-G cKO mice began to suffer mortality as early as

two weeks post TAC. Surprisingly in WT animals, ankyrin-G expression was increased after 2 weeks TAC. Coupled with increased mortality of ankyrin-G cKO animals at this timepoint, we hypothesized that upregulation of ankyrin-G may be a necessary event for early ventricular compensation to TAC.

Interestingly, ankyrin-G cKO cells demonstrated altered cellular localization of the desmosomal protein plakophilin-2 (PKP2). Evidence from the Delmar group had previously reported that ankyrin-G and PKP2 associate in the cardiomyocyte and that siRNA-mediated silencing of ankyrin-G resulted in cellular mislocalization of PKP2[200]. This was functionally correlated with decreased cell-cell adhesion strength in the absence of ankyrin-G. Our in vivo data further implicate a regulatory role for ankyrin-G with respect to the cardiac desmosome. Interestingly, we were also able to demonstrate that ankyrin-G cKO cells present with decreased expression of the intermediate filament protein desmin at the intercalated disc, implying that ankyrin-G, through its direct or indirect association with PKP2, regulates intercalated disc intermediate filament integration / organization. Further, as human variants in desmosomal proteins have been linked with arrhythmogenic right ventricular cardiomyopathy[292], desmosomal disruption may be a causal mechanism for the accelerated heart failure phenotypes and pathological remodeling witnessed in ankyrin-G cKO animals after aging and following TAC. Although PKP2 expression was not tested in aged animals, WT TAC animals demonstrate significantly increased PKP2 expression following transaortic constriction similar to ankyrin-G expression. Although expression of PKP2 and ankyrin-G at the intercalated disc is disrupted in an experimental model of heart failure[126], further

investigation will be required to determine if functional PKP2 expression is disrupted in acquired human cardiovascular disease states.

Although ankyrin-G and PKP2 have been shown to associate via coimmunoprecipitation experiments, a direct association between these two molecules has not yet been demonstrated. Future experiments will be necessary to determine if the association between ankyrin-G and PKP2 is direct or indirect through an intermediary protein. Mechanistically, we link the phenotypes seen in the ankyrin-G cKO TAC mice with disrupted cellular PKP2 targeting. Importantly, PKP2 has been shown to be a critical regulator of both Hippo/Wnt[293] and EGFR signaling[294]. As both of these pathways have been linked with severe cardiac pathologies[295, 296], PKP2-dependent signaling may represent a critical signaling mechanism for cardiac compensation. However, we cannot rule out direct regulation of intracellular signaling cascades by ankyrin-G. Previous work has demonstrated that ankyrin-G is a critical regulator of Wnt signaling in developing neurons through its interaction with β-catenin. In neurons, the absence of ankyrin-G in β-catenin translocates to the nucleus, turning on a proliferative gene program[297]. However, ankyrin-G cKO animals exhibit no nuclear accumulation of β-catenin at baseline making this mechanism implausible as an explanation for the phenomena witnessed after TAC in the ankyrin-G cKO cohort.

Prior investigation has also demonstrated a role for ankyrin-G in the regulation of gap junctional protein connexin-43. Connexin-43 is the primary connexin isoform comprising gap junctions in ventricular cardiomyocytes, facilitating proper transmission of action potentials through cardiac tissue[137]. Further, in the setting of acquired and

congenital heart disease, connexin-43 has been shown to redistribute to the lateral aspects of the cardiomyocyte[140]. This uncoupling of cardiomyocytes, if extreme enough, leads to conduction slowing and the production of arrhythmia[298]. Upon siRNA-mediated silencing of ankyrin-G in neonatal rat ventricular myocyte monolayers, connexin-43 localization was disrupted[200]. Further, silencing of ankyrin-G in adult cardiomyocytes led to the development of larger connexin-43 plaques at the intercalated disc[213]. This investigation, conducted by the Delmar laboratory, hypothesized that in the absence of ankyrin-G, expression of the gap junction interacting protein ZO-1 at the intercalated disc would increase. ZO-1 associates with uncoupled connexin-43 hexamers[261]. Further, ZO-1 scaffolds to αII-spectrin, the predominant α-spectrin isoform in the cardiomyocyte[212]. Therefore, if there were less ankyrin-G to interact with βIV-spectrin of the spectrin dimer, more αII-spectrin would be available to bind ZO-1 and increase the amount of connexin-43 hexamers at the intercalated disc leading to larger connexin-43 positive plaques.

Interestingly, we observe only minor changes in the expression / localization of connexin-43 in ankyrin-G cKO cardiomyocytes at baseline. Several explanations could account for this observation. First, although we do not see changes in levels of ZO-1 protein expression, immunofluorescent experiments reveal minor reductions in ZO-1 localization at the intercalated disc. This would result in decreased binding sites for connexin-43 hexamers, causing minor reductions in connexin-43 localization. Further, as we show decreased recruitment of βIV-spectrin to the intercalated disc, we would hypothesize that functional expression of αII-spectrin may also be disrupted. However,

this hypothesis remains to be tested. Further, anterograde traffic of connexin-43 depends on the expression of the N-cadherin / β-catenin complex at sites of cell-cell interaction[202]. As we see no changes in the expression/localization of either N-cadherin or β-catenin, we would hypothesize that anterograde traffic of connexin-43 is unaffected.

However, significant evidence exists suggesting a functional interaction between the connexin-43 macromolecular complex and the ankyrin-G-dependent complex at the intercalated disc. Connexin-43 heterozygous mice display significant reductions in tissue conduction velocity explained by ~50% reduction in Na^+ current density in isolated cardiomyocytes[215]. Further, connexin-43 isoforms with a C-terminal truncation localize and couple normally at the intercalated disc in vivo, but show significant reductions in peak Na^+ current density explained by disrupted expression and localization of Nav1.5 at the intercalated disc[216]. Work from the Delmar laboratory has further suggested that these C-terminal amino acids act to promote microtubule +end capture due to a proposed interaction with the microtubule +end binding protein EB-1[203]. This, therefore, would result in decreased microtubule-dependent forward traffic of Nav1.5 to the intercalated disc. However, this hypothesis is unlikely given that EB-1 is required for forward traffic of connexin-43 itself[202].

Instead, I would propose a model whereby anterograde traffic of connexin-43 to the intercalated disc is a rate-limiting step in the maintenance of membrane constituents. As connexin-43 has a relatively short half-life (~2-4 hours)[299], anterograde traffic of connexin-43 must occur at a higher rate than Nav1.5 that has a much longer half-life (32-36 hours)[300]. As these two proteins inevitably use the same endosomal machinery for

forward traffic, even minor disruptions in the forward traffic of connexin-43 may cause major decreases in forward traffic of Nav1.5, accounting for the decreases in Na^+ current density. Further, as traffic of connexin-43 is also dependent on proper expression of desmosomal components[301], this hypothesis would account for decreases in Na^+ current and Nav1.5 expression seen in cells expressing loss-of-function mutations in desmosomal proteins[206, 208, 209]. Interestingly, $Scn5a^{+/-}$ mice do display decreases in connexin-43 localization at the intercalated disc, but only with increased age (12-17 months)[254]. These data strongly suggest a model whereby the majority of endosomal traffic to the intercalated disc is for the maintenance of connexin-43 plaques. As a result, any disruption in the proper proportions of forward traffic will affect connexin-43 localization first. This explains how seemingly incomparable disruptions to the intercalated disc all produce the same functional consequence of impaired connexin-43 and Nav1.5 localization. Further, this would explain our observation of only slightly reduced connexin-43 targeting to the intercalated disc in ankyrin-G cKO mice. However, these hypotheses remains to be tested.

Given the severe disruptions in expression of Nav1.5 and PKP2 in ankyrin-G cKO cardiomyocytes at baseline, one could theoretically explain the development of tachyarrhythmia after adrenergic stimulation. However, we were surprised to find that ankyrin-G cKO mice suffered from severe bradycardia prior to mortality after TAC. Although initially perplexing, a simple mechanism again may provide explanation. If we accept the hypothesis proposed earlier, SR Ca^{+2} content may be decreased at baseline in ankyrin-G cKO myocytes due to decreased Na^+ current density. In response to TAC, WT

mice can upregulate ankyrin-G to increase Na^+ current density to prevent Ca^{+2} unloading from the cardiomyocyte. I hypothesize that ankyrin-G cKO cardiomyocytes do not have this ability to increase functional Nav1.5 expression, leading to severe reductions in SR Ca^{+2} content. As RyR2 open probability is directly related to SR Ca^{+2} content[170], this SR unloading would decrease the frequency of proarrhythmic spontaneous Ca^{+2} release from the SR, preventing tachyarrhythmia in this setting. Further SR Ca^{+2} unloading would decrease cardiomyocyte contractile force, possibly explaining the observed systolic dysfunction in ankyrin-G cKO mice after TAC. In support of this hypothesis, mice expressing mutant Nav1.5 channels (ΔKPQ) modeling long QT type 3 have increased SR Ca^{+2} content relative to WT mice. Further, treatment of the ΔKPQ myocytes with ranolazine (i.e. late current blocker) was sufficient to reduce SR Ca^{+2} concentration[302]. To address these hypotheses, whole-cell Na^+ current density and Ca^{+2} handling dynamics will need to be investigated in ankyrin-G cKO cardiomyocytes following TAC surgery of the animal.

Regardless of the mechanism whereby these dysfunctions arise in ankyrin-G cKO animals, a very interesting finding is a decrease in ankyrin-G expression and localization in human heart failure. Although the mechanisms producing this deficiency may be multiple, prior investigations have demonstrated that ankyrins can be degraded by Ca^{+2} activated proteases known as calpains in disease conditions[221, 223, 224]. We hypothesize that calpain-dependent degradation of ankyrin-G is the probable mechanism producing reductions in ankyrin-G expression. To test this in vitro, we can expose cardiac lysate to increasing concentrations of Ca^{+2} to activate these calpains and monitor for reductions in

ankyrin-G expression. We can then determine if calpains are in fact degrading the endogenous ankyrin-G by using specific calpain inhibitors (MDL-28170)[224]. These experiments would provide a critical mechanistic link between the phenotypes witnessed experimentally and the pathogenesis of human heart failure.

In conclusion, this dissertation demonstrates a critical requirement for ankyrin-G expression in the cardiomyocyte at baseline and in disease conditions. In the absence of ankyrin-G, cKO mice display significant reductions in Nav1.5 membrane targeting leading to severely reduced functional I_{Na}, leading to significant conduction abnormalities, bradycardia, and ventricular arrhythmia and AV nodal block following infusion of the Na_V channel antagonist flecainide. In addition to regulating cardiac excitability, we also demonstrate a critical role for ankyrin-G in the regulation of the cardiomyocyte cytoarchitecture. Specifically, ankyrin-G cKO mice show disrupted cellular distribution of the desmosomal protein PKP2 at baseline. In a setting of pressure overload-induced heart failure (TAC), we demonstrate severe disruptions to the cellular localization of PKP2. Further, as desmosomes mediate the integration of the intermediate filament protein desmin, we demonstrate the reduced expression of desmin at the ID in the setting of mislocalized PKP2. Mechanistically, we correlate these molecular changes with significant reductions in systolic function and increased propensity for bradyarrhythmia in ankyrin-G cKO TAC mice. As ankyrin-G is significantly increased two weeks post TAC, we hypothesize that ankyrin-G expression is required for the early, compensatory phase of ventricular remodeling. Our hypothesis is further strengthened by the observation that functional ankyrin-G expression is severely reduced in multiple

forms of human heart failure. We conclude that ankyrin-G is a critical regulator of both excitability and cytoarchitecture of the intercalated disc. We further hypothesize that remodeling of this ankyrin-G-dependent molecular environment is a critical step in the development of human arrhythmia and structural heart diseases.

List of Cited References

1. Mozaffarian D, Benjamin EJ, Go AS, Arnett DK, Blaha MJ, Cushman M, de Ferranti S, Despres J, Fullerton HJ, Howard VJ, Huffman MD, Judd SE, Kissela BM, Lackland DT, Lichtman JH, Lisabeth LD, Liu S, Mackey RH, Matchar DB, McGuire DK, Mohler ER, 3rd, Moy CS, Muntner P, Mussolino ME, Nasir K, Neumar RW, Nichol G, Palaniappan L, Pandey DK, Reeves MJ, Rodriguez CJ, Sorlie PD, Stein J, Towfighi A, Turan TN, Virani SS, Willey JZ, Woo D, Yeh RW, Turner MB. Heart disease and stroke statistics-2015 update: A report from the american heart association. *Circulation*. 2014
2. Mozaffarian D, Benjamin EJ, Go AS, Arnett DK, Blaha MJ, Cushman M, Das SR, de Ferranti S, Despres JP, Fullerton HJ, Howard VJ, Huffman MD, Isasi CR, Jimenez MC, Judd SE, Kissela BM, Lichtman JH, Lisabeth LD, Liu S, Mackey RH, Magid DJ, McGuire DK, Mohler ER, 3rd, Moy CS, Muntner P, Mussolino ME, Nasir K, Neumar RW, Nichol G, Palaniappan L, Pandey DK, Reeves MJ, Rodriguez CJ, Rosamond W, Sorlie PD, Stein J, Towfighi A, Turan TN, Virani SS, Woo D, Yeh RW, Turner MB. Heart disease and stroke statistics-2016 update: A report from the american heart association. *Circulation*. 2015
3. Hayashi M, Shimizu W, Albert CM. The spectrum of epidemiology underlying sudden cardiac death. *Circulation research*. 2015;116:1887-1906
4. Yousuf O, Chrispin J, Tomaselli GF, Berger RD. Clinical management and prevention of sudden cardiac death. *Circulation research*. 2015;116:2020-2040
5. Kong MH, Fonarow GC, Peterson ED, Curtis AB, Hernandez AF, Sanders GD, Thomas KL, Hayes DL, Al-Khatib SM. Systematic review of the incidence of sudden cardiac death in the united states. *Journal of the American College of Cardiology*. 2011;57:794-801
6. Deyell MW, Krahn AD, Goldberger JJ. Sudden cardiac death risk stratification. *Circulation research*. 2015;116:1907-1918
7. The cardiac insufficiency bisoprolol study ii (cibis-ii): A randomised trial. *Lancet*. 1999;353:9-13
8. Effect of metoprolol cr/xl in chronic heart failure: Metoprolol cr/xl randomised intervention trial in congestive heart failure (merit-hf). *Lancet*. 1999;353:2001-2007
9. The cardiac arrhythmia suppression trial. *The New England journal of medicine*. 1989;321:1754-1756
10. Effect of the antiarrhythmic agent moricizine on survival after myocardial infarction. The cardiac arrhythmia suppression trial ii investigators. *The New England journal of medicine*. 1992;327:227-233

11. Bers DM. Cardiac excitation-contraction coupling. *Nature*. 2002;415:198-205
12. Amin AS, Tan HL, Wilde AA. Cardiac ion channels in health and disease. *Heart rhythm : the official journal of the Heart Rhythm Society*. 2010;7:117-126
13. Unudurthi SD, Wolf RM, Hund TJ. Role of sinoatrial node architecture in maintaining a balanced source-sink relationship and synchronous cardiac pacemaking. *Frontiers in physiology*. 2014;5:446
14. Park DS, Fishman GI. The cardiac conduction system. *Circulation*. 2011;123:904-915
15. Zipes DP, Libby, P., Bonow, R.O., Braunwald, E. *Braunwald's heart disease: A textbook of cardiovascular medicine*. Philadelphia: Elsevier Saunders; 2005.
16. Mitchell JR, Wang JJ. Expanding application of the wiggers diagram to teach cardiovascular physiology. *Advances in physiology education*. 2014;38:170-175
17. Ferrari R, Bertini M, Blomstrom-Lundqvist C, Dobrev D, Kirchhof P, Pappone C, Ravens U, Tamargo J, Tavazzi L, Vicedomini GG. An update on atrial fibrillation in 2014: From pathophysiology to treatment. *International journal of cardiology*. 2016;203:22-29
18. Schwartz PJ, Crotti L, Insolia R. Long-qt syndrome: From genetics to management. *Circulation. Arrhythmia and electrophysiology*. 2012;5:868-877
19. Antzelevitch C, Brugada P, Borggrefe M, Brugada J, Brugada R, Corrado D, Gussak I, LeMarec H, Nademanee K, Perez Riera AR, Shimizu W, Schulze-Bahr E, Tan H, Wilde A. Brugada syndrome: Report of the second consensus conference: Endorsed by the heart rhythm society and the european heart rhythm association. *Circulation*. 2005;111:659-670
20. Tucker NR, Clauss S, Ellinor PT. Common variation in atrial fibrillation: Navigating the path from genetic association to mechanism. *Cardiovascular research*. 2016
21. Bezzina CR, Lahrouchi N, Priori SG. Genetics of sudden cardiac death. *Circulation research*. 2015;116:1919-1936
22. Mohler PJ, Schott JJ, Gramolini AO, Dilly KW, Guatimosim S, duBell WH, Song LS, Haurogne K, Kyndt F, Ali ME, Rogers TB, Lederer WJ, Escande D, Le Marec H, Bennett V. Ankyrin-b mutation causes type 4 long-qt cardiac arrhythmia and sudden cardiac death. *Nature*. 2003;421:634-639
23. Bennett V, Stenbuck PJ. Identification and partial purification of ankyrin, the high affinity membrane attachment site for human erythrocyte spectrin. *The Journal of biological chemistry*. 1979;254:2533-2541
24. Bennett V, Stenbuck PJ. The membrane attachment protein for spectrin is associated with band 3 in human erythrocyte membranes. *Nature*. 1979;280:468-473
25. Srinivasan Y, Elmer L, Davis J, Bennett V, Angelides K. Ankyrin and spectrin associate with voltage-dependent sodium channels in brain. *Nature*. 1988;333:177-180
26. Zhou D, Lambert S, Malen PL, Carpenter S, Boland LM, Bennett V. Ankyring is required for clustering of voltage-gated na channels at axon initial segments and

for normal action potential firing. *The Journal of cell biology*. 1998;143:1295-1304
27. Kizhatil K, Bennett V. Lateral membrane biogenesis in human bronchial epithelial cells requires 190-kda ankyrin-g. *The Journal of biological chemistry*. 2004;279:16706-16714
28. Kizhatil K, Yoon W, Mohler PJ, Davis LH, Hoffman JA, Bennett V. Ankyrin-g and beta2-spectrin collaborate in biogenesis of lateral membrane of human bronchial epithelial cells. *The Journal of biological chemistry*. 2007;282:2029-2037
29. Agre P, Orringer EP, Chui DH, Bennett V. A molecular defect in two families with hemolytic poikilocytic anemia: Reduction of high affinity membrane binding sites for ankyrin. *The Journal of clinical investigation*. 1981;68:1566-1576
30. Tesli M, Koefoed P, Athanasiu L, Mattingsdal M, Gustafsson O, Agartz I, Rimol LM, Brown A, Wirgenes KV, Smorr LL, Kahler AK, Werge T, Mors O, Mellerup E, Jonsson EG, Melle I, Morken G, Djurovic S, Andreassen OA. Association analysis of ank3 gene variants in nordic bipolar disorder and schizophrenia case-control samples. *American journal of medical genetics. Part B, Neuropsychiatric genetics : the official publication of the International Society of Psychiatric Genetics*. 2011;156B:969-974
31. Cunha SR, Hund TJ, Hashemi S, Voigt N, Li N, Wright P, Koval O, Li J, Gudmundsson H, Gumina RJ, Karck M, Schott JJ, Probst V, Le Marec H, Anderson ME, Dobrev D, Wehrens XH, Mohler PJ. Defects in ankyrin-based membrane protein targeting pathways underlie atrial fibrillation. *Circulation*. 2011;124:1212-1222
32. Le Scouarnec S, Bhasin N, Vieyres C, Hund TJ, Cunha SR, Koval O, Marionneau C, Chen B, Wu Y, Demolombe S, Song LS, Le Marec H, Probst V, Schott JJ, Anderson ME, Mohler PJ. Dysfunction in ankyrin-b-dependent ion channel and transporter targeting causes human sinus node disease. *Proc Natl Acad Sci U S A*. 2008;105:15617-15622
33. Mohler PJ, Le Scouarnec S, Denjoy I, Lowe JS, Guicheney P, Caron L, Driskell IM, Schott JJ, Norris K, Leenhardt A, Kim RB, Escande D, Roden DM. Defining the cellular phenotype of "ankyrin-b syndrome" variants: Human ank2 variants associated with clinical phenotypes display a spectrum of activities in cardiomyocytes. *Circulation*. 2007;115:432-441
34. Mohler PJ, Healy JA, Xue H, Puca AA, Kline CF, Allingham RR, Kranias EG, Rockman HA, Bennett V. Ankyrin-b syndrome: Enhanced cardiac function balanced by risk of cardiac death and premature senescence. *PloS one*. 2007;2:e1051
35. Mohler PJ, Rivolta I, Napolitano C, LeMaillet G, Lambert S, Priori SG, Bennett V. Nav1.5 e1053k mutation causing brugada syndrome blocks binding to ankyrin-g and expression of nav1.5 on the surface of cardiomyocytes. *Proceedings of the National Academy of Sciences of the United States of America*. 2004;101:17533-17538

36. Bayes de Luna A, Brugada J, Baranchuk A, Borggrefe M, Breithardt G, Goldwasser D, Lambiase P, Riera AP, Garcia-Niebla J, Pastore C, Oreto G, McKenna W, Zareba W, Brugada R, Brugada P. Current electrocardiographic criteria for diagnosis of brugada pattern: A consensus report. *Journal of electrocardiology*. 2012;45:433-442
37. Gussak I, Antzelevitch C, Bjerregaard P, Towbin JA, Chaitman BR. The brugada syndrome: Clinical, electrophysiologic and genetic aspects. *Journal of the American College of Cardiology*. 1999;33:5-15
38. Garrido JJ, Giraud P, Carlier E, Fernandes F, Moussif A, Fache MP, Debanne D, Dargent B. A targeting motif involved in sodium channel clustering at the axonal initial segment. *Science*. 2003;300:2091-2094
39. Lemaillet G, Walker B, Lambert S. Identification of a conserved ankyrin-binding motif in the family of sodium channel alpha subunits. *The Journal of biological chemistry*. 2003;278:27333-27339
40. Lowe JS, Palygin O, Bhasin N, Hund TJ, Boyden PA, Shibata E, Anderson ME, Mohler PJ. Voltage-gated nav channel targeting in the heart requires an ankyrin-g dependent cellular pathway. *The Journal of cell biology*. 2008;180:173-186
41. Turner W. The cell theory, past and present. *Journal of anatomy and physiology*. 1890;24:253-287
42. Al-Awqati Q. One hundred years of membrane permeability: Does overton still rule? *Nature cell biology*. 1999;1:E201-202
43. Gorter E, Grendel F. On bimolecular layers of lipoids on the chromocytes of the blood. *The Journal of experimental medicine*. 1925;41:439-443
44. Danielli JF. Structure of the cell surface. *Circulation*. 1962;26:1163-1166
45. Singer SJ, Nicolson GL. The fluid mosaic model of the structure of cell membranes. *Science*. 1972;175:720-731
46. Marchesi VT, Palade GE. Inactivation of adenosine triphosphatase and disruption of red cell membrances by trypsin: Protective effect of adenosine triphosphate. *Proceedings of the National Academy of Sciences of the United States of America*. 1967;58:991-995
47. Marchesi VT, Steers E, Jr. Selective solubilization of a protein component of the red cell membrane. *Science*. 1968;159:203-204
48. Pinder JC, Bray D, Gratzer WB. Actin polymerisation induced by spectrin. *Nature*. 1975;258:765-766
49. Nicolson GL, Marchesi VT, Singer SJ. The localization of spectrin on the inner surface of human red blood cell membranes by ferritin-conjugated antibodies. *The Journal of cell biology*. 1971;51:265-272
50. Bennett V, Branton D. Selective association of spectrin with the cytoplasmic surface of human erythrocyte plasma membranes. Quantitative determination with purified (32p)spectrin. *The Journal of biological chemistry*. 1977;252:2753-2763
51. Bennett V. Purification of an active proteolytic fragment of the membrane attachment site for human erythrocyte spectrin. *The Journal of biological chemistry*. 1978;253:2292-2299

52. Bennett V, Stenbuck PJ. Association between ankyrin and the cytoplasmic domain of band 3 isolated from the human erythrocyte membrane. *The Journal of biological chemistry*. 1980;255:6424-6432
53. Agre P, Orringer EP, Bennett V. Deficient red-cell spectrin in severe, recessively inherited spherocytosis. *N Engl J Med*. 1982;306:1155-1161
54. Ribeiro ML, Alloisio N, Almeida H, Gomes C, Texier P, Lemos C, Mimoso G, Morle L, Bey-Cabet F, Rudigoz RC, Delaunay J, Tamagnini G. Severe hereditary spherocytosis and distal renal tubular acidosis associated with the total absence of band 3. *Blood*. 2000;96:1602-1604
55. Davis JQ, Bennett V. Brain ankyrin. A membrane-associated protein with binding sites for spectrin, tubulin, and the cytoplasmic domain of the erythrocyte anion channel. *The Journal of biological chemistry*. 1984;259:13550-13559
56. Davis LH, Otto E, Bennett V. Specific 33-residue repeat(s) of erythrocyte ankyrin associate with the anion exchanger. *The Journal of biological chemistry*. 1991;266:11163-11169
57. Sedgwick SG, Smerdon SJ. The ankyrin repeat: A diversity of interactions on a common structural framework. *Trends in biochemical sciences*. 1999;24:311-316
58. Michaely P, Tomchick DR, Machius M, Anderson RG. Crystal structure of a 12 ank repeat stack from human ankyrinr. *The EMBO journal*. 2002;21:6387-6396
59. Michaely P, Bennett V. The ank repeat: A ubiquitous motif involved in macromolecular recognition. *Trends in cell biology*. 1992;2:127-129
60. Wang R, Wei Z, Jin H, Wu H, Yu C, Wen W, Chan LN, Wen Z, Zhang M. Autoinhibition of unc5b revealed by the cytoplasmic domain structure of the receptor. *Molecular cell*. 2009;33:692-703
61. Wang C, Yu C, Ye F, Wei Z, Zhang M. Structure of the zu5-zu5-upa-dd tandem of ankyrin-b reveals interaction surfaces necessary for ankyrin function. *Proceedings of the National Academy of Sciences of the United States of America*. 2012;109:4822-4827
62. Mohler PJ, Yoon W, Bennett V. Ankyrin-b targets beta2-spectrin to an intracellular compartment in neonatal cardiomyocytes. *The Journal of biological chemistry*. 2004;279:40185-40193
63. Gudmundsson H, Hund TJ, Wright PJ, Kline CF, Snyder JS, Qian L, Koval OM, Cunha SR, George M, Rainey MA, Kashef FE, Dun W, Boyden PA, Anderson ME, Band H, Mohler PJ. Eh domain proteins regulate cardiac membrane protein targeting. *Circulation research*. 2010;107:84-95
64. Hall TG, Bennett V. Regulatory domains of erythrocyte ankyrin. *The Journal of biological chemistry*. 1987;262:10537-10545
65. Mohler PJ, Gramolini AO, Bennett V. The ankyrin-b c-terminal domain determines activity of ankyrin-b/g chimeras in rescue of abnormal inositol 1,4,5-trisphosphate and ryanodine receptor distribution in ankyrin-b (-/-) neonatal cardiomyocytes. *J Biol Chem*. 2002;277:10599-10607
66. Ji TH, Kiehm DJ, Middaugh CR. Presence of spectrin tetramer on the erythrocyte membrane. *The Journal of biological chemistry*. 1980;255:2990-2993

67. Tse WT, Lecomte MC, Costa FF, Garbarz M, Feo C, Boivin P, Dhermy D, Forget BG. Point mutation in the beta-spectrin gene associated with alpha i/74 hereditary elliptocytosis. Implications for the mechanism of spectrin dimer self-association. *The Journal of clinical investigation*. 1990;86:909-916
68. Morrow JS, Haigh WB, Jr., Marchesi VT. Spectrin oligomers: A structural feature of the erythrocyte cytoskeleton. *Journal of supramolecular structure and cellular biochemistry*. 1981;17:275-287
69. Shotton DM, Burke BE, Branton D. The molecular structure of human erythrocyte spectrin. Biophysical and electron microscopic studies. *Journal of molecular biology*. 1979;131:303-329
70. Speicher DW, Marchesi VT. Erythrocyte spectrin is comprised of many homologous triple helical segments. *Nature*. 1984;311:177-180
71. Davis JQ, Bennett V. Brain ankyrin. Purification of a 72,000 mr spectrin-binding domain. *The Journal of biological chemistry*. 1984;259:1874-1881
72. Kennedy SP, Warren SL, Forget BG, Morrow JS. Ankyrin binds to the 15th repetitive unit of erythroid and nonerythroid beta-spectrin. *The Journal of cell biology*. 1991;115:267-277
73. Karinch AM, Zimmer WE, Goodman SR. The identification and sequence of the actin-binding domain of human red blood cell beta-spectrin. *The Journal of biological chemistry*. 1990;265:11833-11840
74. Bennett V. Immunoreactive forms of human erythrocyte ankyrin are present in diverse cells and tissues. *Nature*. 1979;281:597-599
75. White RA, Birkenmeier CS, Lux SE, Barker JE. Ankyrin and the hemolytic anemia mutation, nb, map to mouse chromosome 8: Presence of the nb allele is associated with a truncated erythrocyte ankyrin. *Proceedings of the National Academy of Sciences of the United States of America*. 1990;87:3117-3121
76. Tse WT, Menninger JC, Yang-Feng TL, Francke U, Sahr KE, Lux SE, Ward DC, Forget BG. Isolation and chromosomal localization of a novel nonerythroid ankyrin gene. *Genomics*. 1991;10:858-866
77. Kapfhamer D, Miller DE, Lambert S, Bennett V, Glover TW, Burmeister M. Chromosomal localization of the ankyring gene (ank3/ank3) to human 10q21 and mouse 10. *Genomics*. 1995;27:189-191
78. Peters LL, John KM, Lu FM, Eicher EM, Higgins A, Yialamas M, Turtzo LC, Otsuka AJ, Lux SE. Ank3 (epithelial ankyrin), a widely distributed new member of the ankyrin gene family and the major ankyrin in kidney, is expressed in alternatively spliced forms, including forms that lack the repeat domain. *The Journal of cell biology*. 1995;130:313-330
79. Jenkins PM, Vasavda C, Hostettler J, Davis JQ, Abdi K, Bennett V. E-cadherin polarity is determined by a multifunction motif mediating lateral membrane retention through ankyrin-g and apical-lateral transcytosis through clathrin. *The Journal of biological chemistry*. 2013;288:14018-14031
80. Sauer B, Henderson N. Site-specific DNA recombination in mammalian cells by the cre recombinase of bacteriophage p1. *Proceedings of the National Academy of Sciences of the United States of America*. 1988;85:5166-5170

81. Agah R, Frenkel PA, French BA, Michael LH, Overbeek PA, Schneider MD. Gene recombination in postmitotic cells. Targeted expression of cre recombinase provokes cardiac-restricted, site-specific rearrangement in adult ventricular muscle in vivo. *The Journal of clinical investigation*. 1997;100:169-179
82. Ng WA, Grupp IL, Subramaniam A, Robbins J. Cardiac myosin heavy chain mrna expression and myocardial function in the mouse heart. *Circulation research*. 1991;68:1742-1750
83. Wright EM, Loo DD, Hirayama BA. Biology of human sodium glucose transporters. *Physiological reviews*. 2011;91:733-794
84. Rose AM, Valdes R, Jr. Understanding the sodium pump and its relevance to disease. *Clinical chemistry*. 1994;40:1674-1685
85. Morrow JS, Cianci CD, Ardito T, Mann AS, Kashgarian M. Ankyrin links fodrin to the alpha subunit of na,k-atpase in madin-darby canine kidney cells and in intact renal tubule cells. *The Journal of cell biology*. 1989;108:455-465
86. Drenckhahn D, Schluter K, Allen DP, Bennett V. Colocalization of band 3 with ankyrin and spectrin at the basal membrane of intercalated cells in the rat kidney. *Science*. 1985;230:1287-1289
87. Nelson WJ, Veshnock PJ. Dynamics of membrane-skeleton (fodrin) organization during development of polarity in madin-darby canine kidney epithelial cells. *The Journal of cell biology*. 1986;103:1751-1765
88. Nelson WJ, Veshnock PJ. Ankyrin binding to (na+ + k+)atpase and implications for the organization of membrane domains in polarized cells. *Nature*. 1987;328:533-536
89. Davis JQ, Bennett V. The anion exchanger and na+k(+)-atpase interact with distinct sites on ankyrin in in vitro assays. *The Journal of biological chemistry*. 1990;265:17252-17256
90. Thevananther S, Kolli AH, Devarajan P. Identification of a novel ankyrin isoform (ankg190) in kidney and lung that associates with the plasma membrane and binds alpha-na, k-atpase. *The Journal of biological chemistry*. 1998;273:23952-23958
91. Van Itallie CM, Anderson JM. Architecture of tight junctions and principles of molecular composition. *Seminars in cell & developmental biology*. 2014;36:157-165
92. Angst BD, Marcozzi C, Magee AI. The cadherin superfamily: Diversity in form and function. *Journal of cell science*. 2001;114:629-641
93. Nelson WJ, Shore EM, Wang AZ, Hammerton RW. Identification of a membrane-cytoskeletal complex containing the cell adhesion molecule uvomorulin (e-cadherin), ankyrin, and fodrin in madin-darby canine kidney epithelial cells. *The Journal of cell biology*. 1990;110:349-357
94. Kizhatil K, Davis JQ, Davis L, Hoffman J, Hogan BL, Bennett V. Ankyrin-g is a molecular partner of e-cadherin in epithelial cells and early embryos. *J Biol Chem*. 2007;282:26552-26561
95. Jenkins PM, He M, Bennett V. Dynamic spectrin/ankyrin-g microdomains promote lateral membrane assembly by opposing endocytosis. *Science advances*. 2015;1:e1500301

96. Cadwell CM, Jenkins PM, Bennett V, Kowalczyk AP. Ankyrin-g inhibits endocytosis of cadherin dimers. *The Journal of biological chemistry*. 2016;291:691-704
97. Tseng WC, Jenkins PM, Tanaka M, Mooney R, Bennett V. Giant ankyrin-g stabilizes somatodendritic gabaergic synapses through opposing endocytosis of gabaa receptors. *Proceedings of the National Academy of Sciences of the United States of America*. 2014
98. Purves D. *Neuroscience*. Sinauer Associates, Inc; 2007.
99. Lustig M, Zanazzi G, Sakurai T, Blanco C, Levinson SR, Lambert S, Grumet M, Salzer JL. Nr-cam and neurofascin interactions regulate ankyrin g and sodium channel clustering at the node of ranvier. *Current biology : CB*. 2001;11:1864-1869
100. Jenkins SM, Bennett V. Developing nodes of ranvier are defined by ankyrin-g clustering and are independent of paranodal axoglial adhesion. *Proceedings of the National Academy of Sciences of the United States of America*. 2002;99:2303-2308
101. Jenkins SM, Bennett V. Ankyrin-g coordinates assembly of the spectrin-based membrane skeleton, voltage-gated sodium channels, and l1 cams at purkinje neuron initial segments. *The Journal of cell biology*. 2001;155:739-746
102. Logue MW, Solovieff N, Leussis MP, Wolf EJ, Melista E, Baldwin C, Koenen KC, Petryshen TL, Miller MW. The ankyrin-3 gene is associated with posttraumatic stress disorder and externalizing comorbidity. *Psychoneuroendocrinology*. 2013;38:2249-2257
103. Iqbal Z, Vandeweyer G, van der Voet M, Waryah AM, Zahoor MY, Besseling JA, Roca LT, Vulto-van Silfhout AT, Nijhof B, Kramer JM, Van der Aa N, Ansar M, Peeters H, Helsmoortel C, Gilissen C, Vissers LE, Veltman JA, de Brouwer AP, Frank Kooy R, Riazuddin S, Schenck A, van Bokhoven H, Rooms L. Homozygous and heterozygous disruptions of ank3: At the crossroads of neurodevelopmental and psychiatric disorders. *Human molecular genetics*. 2013;22:1960-1970
104. Yuan A, Yi Z, Wang Q, Sun J, Li Z, Du Y, Zhang C, Yu T, Fan J, Li H, Yu S. Ank3 as a risk gene for schizophrenia: New data in han chinese and meta analysis. *American journal of medical genetics. Part B, Neuropsychiatric genetics : the official publication of the International Society of Psychiatric Genetics*. 2012;159B:997-1005
105. Bi C, Wu J, Jiang T, Liu Q, Cai W, Yu P, Cai T, Zhao M, Jiang YH, Sun ZS. Mutations of ank3 identified by exome sequencing are associated with autism susceptibility. *Hum Mutat*. 2012;33:1635-1638
106. Hille B. Ion channels of excitable membranes. 2001
107. Bers DM. *Excitation-contraction coupling and cardiac contractile force*. Springer Netherlands; 2001.
108. Nichols CG, Lopatin AN. Inward rectifier potassium channels. *Annual review of physiology*. 1997;59:171-191

109. Catterall WA. From ionic currents to molecular mechanisms: The structure and function of voltage-gated sodium channels. *Neuron*. 2000;26:13-25
110. Drenckhahn D, Bennett V. Polarized distribution of mr 210,000 and 190,000 analogs of erythrocyte ankyrin along the plasma membrane of transporting epithelia, neurons and photoreceptors. *European journal of cell biology*. 1987;43:479-486
111. Srinivasan Y, Lewallen M, Angelides KJ. Mapping the binding site on ankyrin for the voltage-dependent sodium channel from brain. *The Journal of biological chemistry*. 1992;267:7483-7489
112. Kordeli E, Lambert S, Bennett V. Ankyring. A new ankyrin gene with neural-specific isoforms localized at the axonal initial segment and node of ranvier. *The Journal of biological chemistry*. 1995;270:2352-2359
113. Zhang X, Bennett V. Restriction of 480/270-kd ankyrin g to axon proximal segments requires multiple ankyrin g-specific domains. *The Journal of cell biology*. 1998;142:1571-1581
114. Pan Z, Kao T, Horvath Z, Lemos J, Sul JY, Cranstoun SD, Bennett V, Scherer SS, Cooper EC. A common ankyrin-g-based mechanism retains kcnq and nav channels at electrically active domains of the axon. *The Journal of neuroscience : the official journal of the Society for Neuroscience*. 2006;26:2599-2613
115. Berghs S, Aggujaro D, Dirkx R, Jr., Maksimova E, Stabach P, Hermel JM, Zhang JP, Philbrick W, Slepnev V, Ort T, Solimena M. Betaiv spectrin, a new spectrin localized at axon initial segments and nodes of ranvier in the central and peripheral nervous system. *The Journal of cell biology*. 2000;151:985-1002
116. Davis JQ, Lambert S, Bennett V. Molecular composition of the node of ranvier: Identification of ankyrin-binding cell adhesion molecules neurofascin (mucin+/third fniii domain-) and nrcam at nodal axon segments. *The Journal of cell biology*. 1996;135:1355-1367
117. Zhang X, Davis JQ, Carpenter S, Bennett V. Structural requirements for association of neurofascin with ankyrin. *The Journal of biological chemistry*. 1998;273:30785-30794
118. Colombo F, Meldolesi J. L1-cam and n-cam: From adhesion proteins to pharmacological targets. *Trends in pharmacological sciences*. 2015;36:769-781
119. Joe EH, Angelides K. Clustering of voltage-dependent sodium channels on axons depends on schwann cell contact. *Nature*. 1992;356:333-335
120. Dzhashiashvili Y, Zhang Y, Galinska J, Lam I, Grumet M, Salzer JL. Nodes of ranvier and axon initial segments are ankyrin g-dependent domains that assemble by distinct mechanisms. *The Journal of cell biology*. 2007;177:857-870
121. Chang KJ, Zollinger DR, Susuki K, Sherman DL, Makara MA, Brophy PJ, Cooper EC, Bennett V, Mohler PJ, Rasband MN. Glial ankyrins facilitate paranodal axoglial junction assembly. *Nature neuroscience*. 2014;17:1673-1681
122. Komada M, Soriano P. [beta]iv-spectrin regulates sodium channel clustering through ankyrin-g at axon initial segments and nodes of ranvier. *The Journal of cell biology*. 2002;156:337-348

123. Yang Y, Ogawa Y, Hedstrom KL, Rasband MN. Betaiv spectrin is recruited to axon initial segments and nodes of ranvier by ankyring. *The Journal of cell biology*. 2007;176:509-519
124. Lacas-Gervais S, Guo J, Strenzke N, Scarfone E, Kolpe M, Jahkel M, De Camilli P, Moser T, Rasband MN, Solimena M. Betaivsigma1 spectrin stabilizes the nodes of ranvier and axon initial segments. *The Journal of cell biology*. 2004;166:983-990
125. Jenkins PM, Kim N, Jones SL, Tseng WC, Svitkina TM, Yin HH, Bennett V. Giant ankyrin-g: A critical innovation in vertebrate evolution of fast and integrated neuronal signaling. *Proceedings of the National Academy of Sciences of the United States of America*. 2015;112:957-964
126. Chkourko HS, Guerrero-Serna G, Lin X, Darwish N, Pohlmann JR, Cook KE, Martens JR, Rothenberg E, Musa H, Delmar M. Remodeling of mechanical junctions and of microtubule-associated proteins accompany cardiac connexin43 lateralization. *Heart rhythm : the official journal of the Heart Rhythm Society*. 2012;9:1133-1140 e1136
127. Dun W, Lowe JS, Wright P, Hund TJ, Mohler PJ, Boyden PA. Ankyrin-g participates in ina remodeling in myocytes from the border zones of infarcted canine heart. *PloS one*. 2013;8:e78087
128. Balse E, Steele DF, Abriel H, Coulombe A, Fedida D, Hatem SN. Dynamic of ion channel expression at the plasma membrane of cardiomyocytes. *Physiological reviews*. 2012;92:1317-1358
129. Li J, Patel VV, Radice GL. Dysregulation of cell adhesion proteins and cardiac arrhythmogenesis. *Clinical medicine & research*. 2006;4:42-52
130. Ozawa M, Baribault H, Kemler R. The cytoplasmic domain of the cell adhesion molecule uvomorulin associates with three independent proteins structurally related in different species. *The EMBO journal*. 1989;8:1711-1717
131. Radice GL, Rayburn H, Matsunami H, Knudsen KA, Takeichi M, Hynes RO. Developmental defects in mouse embryos lacking n-cadherin. *Developmental biology*. 1997;181:64-78
132. Kostetskii I, Li J, Xiong Y, Zhou R, Ferrari VA, Patel VV, Molkentin JD, Radice GL. Induced deletion of the n-cadherin gene in the heart leads to dissolution of the intercalated disc structure. *Circulation research*. 2005;96:346-354
133. Kline CF, Mohler PJ. Evolving form to fit function: Cardiomyocyte intercalated disc and transverse-tubule membranes. *Current topics in membranes*. 2013;72:121-158
134. Saffitz JE. The pathobiology of arrhythmogenic cardiomyopathy. *Annual review of pathology*. 2011;6:299-321
135. Marcus FI, Edson S, Towbin JA. Genetics of arrhythmogenic right ventricular cardiomyopathy: A practical guide for physicians. *Journal of the American College of Cardiology*. 2013;61:1945-1948
136. Severs NJ. The cardiac gap junction and intercalated disc. *International journal of cardiology*. 1990;26:137-173

137. Davis LM, Kanter HL, Beyer EC, Saffitz JE. Distinct gap junction protein phenotypes in cardiac tissues with disparate conduction properties. *Journal of the American College of Cardiology*. 1994;24:1124-1132
138. Kleber AG, Rudy Y. Basic mechanisms of cardiac impulse propagation and associated arrhythmias. *Physiological reviews*. 2004;84:431-488
139. Guerrero PA, Schuessler RB, Davis LM, Beyer EC, Johnson CM, Yamada KA, Saffitz JE. Slow ventricular conduction in mice heterozygous for a connexin43 null mutation. *The Journal of clinical investigation*. 1997;99:1991-1998
140. Severs NJ, Bruce AF, Dupont E, Rothery S. Remodelling of gap junctions and connexin expression in diseased myocardium. *Cardiovascular research*. 2008;80:9-19
141. Cohen SA. Immunocytochemical localization of rh1 sodium channel in adult rat heart atria and ventricle. Presence in terminal intercalated disks. *Circulation*. 1996;94:3083-3086
142. Kleber AG, Saffitz JE. Role of the intercalated disc in cardiac propagation and arrhythmogenesis. *Frontiers in physiology*. 2014;5:404
143. Kucera JP, Rohr S, Rudy Y. Localization of sodium channels in intercalated disks modulates cardiac conduction. *Circulation research*. 2002;91:1176-1182
144. Nakamura TY, Artman M, Rudy B, Coetzee WA. Inhibition of rat ventricular ik1 with antisense oligonucleotides targeted to kir2.1 mrna. *The American journal of physiology*. 1998;274:H892-900
145. Nerbonne JM, Kass RS. Molecular physiology of cardiac repolarization. *Physiological reviews*. 2005;85:1205-1253
146. Bers DM, Perez-Reyes E. Ca channels in cardiac myocytes: Structure and function in ca influx and intracellular ca release. *Cardiovascular research*. 1999;42:339-360
147. Shattock MJ, Ottolia M, Bers DM, Blaustein MP, Boguslavskyi A, Bossuyt J, Bridge JH, Chen-Izu Y, Clancy CE, Edwards A, Goldhaber J, Kaplan J, Lingrel JB, Pavlovic D, Philipson K, Sipido KR, Xie ZJ. Na+/ca2+ exchange and na+/k+-atpase in the heart. *The Journal of physiology*. 2015;593:1361-1382
148. Franzini-Armstrong C, Protasi F, Ramesh V. Shape, size, and distribution of ca(2+) release units and couplons in skeletal and cardiac muscles. *Biophysical journal*. 1999;77:1528-1539
149. Curran J, Hinton MJ, Rios E, Bers DM, Shannon TR. Beta-adrenergic enhancement of sarcoplasmic reticulum calcium leak in cardiac myocytes is mediated by calcium/calmodulin-dependent protein kinase. *Circulation research*. 2007;100:391-398
150. Louch WE, Stokke MK, Sjaastad I, Christensen G, Sejersted OM. No rest for the weary: Diastolic calcium homeostasis in the normal and failing myocardium. *Physiology*. 2012;27:308-323
151. Ibrahim M, Gorelik J, Yacoub MH, Terracciano CM. The structure and function of cardiac t-tubules in health and disease. *Proceedings. Biological sciences / The Royal Society*. 2011;278:2714-2723

152. Huxley HE. Fifty years of muscle and the sliding filament hypothesis. *European journal of biochemistry / FEBS*. 2004;271:1403-1415
153. Gordon AM, Regnier M, Homsher E. Skeletal and cardiac muscle contractile activation: Tropomyosin "rocks and rolls". *News in physiological sciences : an international journal of physiology produced jointly by the International Union of Physiological Sciences and the American Physiological Society*. 2001;16:49-55
154. Kobayashi T, Solaro RJ. Calcium, thin filaments, and the integrative biology of cardiac contractility. *Annual review of physiology*. 2005;67:39-67
155. Reeves JP, Hale CC. The stoichiometry of the cardiac sodium-calcium exchange system. *The Journal of biological chemistry*. 1984;259:7733-7739
156. Armoundas AA, Hobai IA, Tomaselli GF, Winslow RL, O'Rourke B. Role of sodium-calcium exchanger in modulating the action potential of ventricular myocytes from normal and failing hearts. *Circulation research*. 2003;93:46-53
157. Pieske B, Maier LS, Bers DM, Hasenfuss G. Ca2+ handling and sarcoplasmic reticulum ca2+ content in isolated failing and nonfailing human myocardium. *Circulation research*. 1999;85:38-46
158. Vangheluwe P, Louch WE, Ver Heyen M, Sipido K, Raeymaekers L, Wuytack F. Ca2+ transport atpase isoforms serca2a and serca2b are targeted to the same sites in the murine heart. *Cell calcium*. 2003;34:457-464
159. Kadambi VJ, Ponniah S, Harrer JM, Hoit BD, Dorn GW, 2nd, Walsh RA, Kranias EG. Cardiac-specific overexpression of phospholamban alters calcium kinetics and resultant cardiomyocyte mechanics in transgenic mice. *The Journal of clinical investigation*. 1996;97:533-539
160. Koss KL, Kranias EG. Phospholamban: A prominent regulator of myocardial contractility. *Circulation research*. 1996;79:1059-1063
161. Wegener AD, Simmerman HK, Lindemann JP, Jones LR. Phospholamban phosphorylation in intact ventricles. Phosphorylation of serine 16 and threonine 17 in response to beta-adrenergic stimulation. *The Journal of biological chemistry*. 1989;264:11468-11474
162. Mohler PJ, Splawski I, Napolitano C, Bottelli G, Sharpe L, Timothy K, Priori SG, Keating MT, Bennett V. A cardiac arrhythmia syndrome caused by loss of ankyrin-b function. *Proceedings of the National Academy of Sciences of the United States of America*. 2004;101:9137-9142
163. Li ZP, Burke EP, Frank JS, Bennett V, Philipson KD. The cardiac na+-ca2+ exchanger binds to the cytoskeletal protein ankyrin. *The Journal of biological chemistry*. 1993;268:11489-11491
164. Chen F, Mottino G, Shin VY, Frank JS. Subcellular distribution of ankyrin in developing rabbit heart--relationship to the na+-ca2+ exchanger. *Journal of molecular and cellular cardiology*. 1997;29:2621-2629
165. Chauhan VS, Tuvia S, Buhusi M, Bennett V, Grant AO. Abnormal cardiac na(+) channel properties and qt heart rate adaptation in neonatal ankyrin(b) knockout mice. *Circulation research*. 2000;86:441-447

166. Tuvia S, Buhusi M, Davis L, Reedy M, Bennett V. Ankyrin-b is required for intracellular sorting of structurally diverse ca2+ homeostasis proteins. *The Journal of cell biology*. 1999;147:995-1008
167. Mohler PJ, Davis JQ, Davis LH, Hoffman JA, Michaely P, Bennett V. Inositol 1,4,5-trisphosphate receptor localization and stability in neonatal cardiomyocytes requires interaction with ankyrin-b. *The Journal of biological chemistry*. 2004;279:12980-12987
168. Cunha SR, Bhasin N, Mohler PJ. Targeting and stability of na/ca exchanger 1 in cardiomyocytes requires direct interaction with the membrane adaptor ankyrin-b. *The Journal of biological chemistry*. 2007;282:4875-4883
169. Reuter H, Henderson SA, Han T, Ross RS, Goldhaber JI, Philipson KD. The na+-ca2+ exchanger is essential for the action of cardiac glycosides. *Circulation research*. 2002;90:305-308
170. Gyorke I, Gyorke S. Regulation of the cardiac ryanodine receptor channel by luminal ca2+ involves luminal ca2+ sensing sites. *Biophysical journal*. 1998;75:2801-2810
171. Camors E, Mohler PJ, Bers DM, Despa S. Ankyrin-b reduction enhances ca spark-mediated sr ca release promoting cardiac myocyte arrhythmic activity. *Journal of molecular and cellular cardiology*. 2012;52:1240-1248
172. Maier SK, Westenbroek RE, McCormick KA, Curtis R, Scheuer T, Catterall WA. Distinct subcellular localization of different sodium channel alpha and beta subunits in single ventricular myocytes from mouse heart. *Circulation*. 2004;109:1421-1427
173. Musa H, Kline CF, Sturm AC, Murphy N, Adelman S, Wang C, Yan H, Johnson BL, Csepe TA, Kilic A, Higgins RS, Janssen PM, Fedorov VV, Weiss R, Salazar C, Hund TJ, Pitt GS, Mohler PJ. Scn5a variant that blocks fibroblast growth factor homologous factor regulation causes human arrhythmia. *Proceedings of the National Academy of Sciences of the United States of America*. 2015;112:12528-12533
174. Rook MB, Evers MM, Vos MA, Bierhuizen MF. Biology of cardiac sodium channel nav1.5 expression. *Cardiovascular research*. 2012;93:12-23
175. Amin AS, Asghari-Roodsari A, Tan HL. Cardiac sodium channelopathies. *Pflugers Archiv : European journal of physiology*. 2010;460:223-237
176. Butters TD, Aslanidi OV, Inada S, Boyett MR, Hancox JC, Lei M, Zhang H. Mechanistic links between na+ channel (scn5a) mutations and impaired cardiac pacemaking in sick sinus syndrome. *Circulation research*. 2010;107:126-137
177. McNair WP, Sinagra G, Taylor MR, Di Lenarda A, Ferguson DA, Salcedo EE, Slavov D, Zhu X, Caldwell JH, Mestroni L, Familial Cardiomyopathy Registry Research G. Scn5a mutations associate with arrhythmic dilated cardiomyopathy and commonly localize to the voltage-sensing mechanism. *Journal of the American College of Cardiology*. 2011;57:2160-2168
178. Papadatos GA, Wallerstein PM, Head CE, Ratcliff R, Brady PA, Benndorf K, Saumarez RC, Trezise AE, Huang CL, Vandenberg JI, Colledge WH, Grace AA. Slowed conduction and ventricular tachycardia after targeted disruption of the

cardiac sodium channel gene scn5a. *Proceedings of the National Academy of Sciences of the United States of America*. 2002;99:6210-6215
179. Stokoe KS, Balasubramaniam R, Goddard CA, Colledge WH, Grace AA, Huang CL. Effects of flecainide and quinidine on arrhythmogenic properties of scn5a+/- murine hearts modelling the brugada syndrome. *The Journal of physiology*. 2007;581:255-275
180. Gee SH, Madhavan R, Levinson SR, Caldwell JH, Sealock R, Froehner SC. Interaction of muscle and brain sodium channels with multiple members of the syntrophin family of dystrophin-associated proteins. *The Journal of neuroscience : the official journal of the Society for Neuroscience*. 1998;18:128-137
181. Gavillet B, Rougier JS, Domenighetti AA, Behar R, Boixel C, Ruchat P, Lehr HA, Pedrazzini T, Abriel H. Cardiac sodium channel nav1.5 is regulated by a multiprotein complex composed of syntrophins and dystrophin. *Circulation research*. 2006;99:407-414
182. Petitprez S, Zmoos AF, Ogrodnik J, Balse E, Raad N, El-Haou S, Albesa M, Bittihn P, Luther S, Lehnart SE, Hatem SN, Coulombe A, Abriel H. Sap97 and dystrophin macromolecular complexes determine two pools of cardiac sodium channels nav1.5 in cardiomyocytes. *Circulation research*. 2011;108:294-304
183. Shy D, Gillet L, Ogrodnik J, Albesa M, Verkerk AO, Wolswinkel R, Rougier JS, Barc J, Essers MC, Syam N, Marsman RF, van Mil AM, Rotman S, Redon R, Bezzina CR, Remme CA, Abriel H. Pdz-domain-binding motif regulates cardiomyocyte compartment-specific nav1.5 channel expression and function. *Circulation*. 2014
184. Gillet L, Rougier JS, Shy D, Sonntag S, Mougenot N, Essers M, Shmerling D, Balse E, Hatem SN, Abriel H. Cardiac-specific ablation of synapse-associated protein sap97 in mice decreases potassium currents but not sodium current. *Heart rhythm : the official journal of the Heart Rhythm Society*. 2015;12:181-192
185. Milstein ML, Musa H, Balbuena DP, Anumonwo JM, Auerbach DS, Furspan PB, Hou L, Hu B, Schumacher SM, Vaidyanathan R, Martens JR, Jalife J. Dynamic reciprocity of sodium and potassium channel expression in a macromolecular complex controls cardiac excitability and arrhythmia. *Proceedings of the National Academy of Sciences of the United States of America*. 2012;109:E2134-2143
186. Ziane R, Huang H, Moghadaszadeh B, Beggs AH, Levesque G, Chahine M. Cell membrane expression of cardiac sodium channel na(v)1.5 is modulated by alpha-actinin-2 interaction. *Biochemistry*. 2010;49:166-178
187. Wu L, Yong SL, Fan C, Ni Y, Yoo S, Zhang T, Zhang X, Obejero-Paz CA, Rho HJ, Ke T, Szafranski P, Jones SW, Chen Q, Wang QK. Identification of a new co-factor, mog1, required for the full function of cardiac sodium channel nav 1.5. *The Journal of biological chemistry*. 2008;283:6968-6978
188. Smith SA, Sturm AC, Curran J, Kline CF, Little SC, Bonilla IM, Long VP, Makara M, Polina I, Hughes LD, Webb TR, Wei Z, Wright P, Voigt N, Bhakta D, Spoonamore KG, Zhang C, Weiss R, Binkley PF, Janssen PM, Kilic A, Higgins RS, Sun M, Ma J, Dobrev D, Zhang M, Carnes CA, Vatta M, Rasband MN, Hund

TJ, Mohler PJ. Dysfunction in the betaii spectrin-dependent cytoskeleton underlies human arrhythmia. *Circulation*. 2015;131:695-708
189. Hund TJ, Koval OM, Li J, Wright PJ, Qian L, Snyder JS, Gudmundsson H, Kline CF, Davidson NP, Cardona N, Rasband MN, Anderson ME, Mohler PJ. A beta(iv)-spectrin/camkii signaling complex is essential for membrane excitability in mice. *J Clin Invest*. 2010;120:3508-3519
190. Swaminathan PD, Purohit A, Hund TJ, Anderson ME. Calmodulin-dependent protein kinase ii: Linking heart failure and arrhythmias. *Circulation research*. 2012;110:1661-1677
191. Ashpole NM, Herren AW, Ginsburg KS, Brogan JD, Johnson DE, Cummins TR, Bers DM, Hudmon A. Ca2+/calmodulin-dependent protein kinase ii (camkii) regulates cardiac sodium channel nav1.5 gating by multiple phosphorylation sites. *The Journal of biological chemistry*. 2012;287:19856-19869
192. Koval OM, Snyder JS, Wolf RM, Pavlovicz RE, Glynn P, Curran J, Leymaster ND, Dun W, Wright PJ, Cardona N, Qian L, Mitchell CC, Boyden PA, Binkley PF, Li C, Anderson ME, Mohler PJ, Hund TJ. Ca2+/calmodulin-dependent protein kinase ii-based regulation of voltage-gated na+ channel in cardiac disease. *Circulation*. 2012;126:2084-2094
193. Toischer K, Hartmann N, Wagner S, Fischer TH, Herting J, Danner BC, Sag CM, Hund TJ, Mohler PJ, Belardinelli L, Hasenfuss G, Maier LS, Sossalla S. Role of late sodium current as a potential arrhythmogenic mechanism in the progression of pressure-induced heart disease. *Journal of molecular and cellular cardiology*. 2013;61:111-122
194. Sossalla S, Wagner S, Rasenack EC, Ruff H, Weber SL, Schondube FA, Tirilomis T, Tenderich G, Hasenfuss G, Belardinelli L, Maier LS. Ranolazine improves diastolic dysfunction in isolated myocardium from failing human hearts--role of late sodium current and intracellular ion accumulation. *Journal of molecular and cellular cardiology*. 2008;45:32-43
195. Wasserstrom JA, Sharma R, O'Toole MJ, Zheng J, Kelly JE, Shryock J, Belardinelli L, Aistrup GL. Ranolazine antagonizes the effects of increased late sodium current on intracellular calcium cycling in rat isolated intact heart. *The Journal of pharmacology and experimental therapeutics*. 2009;331:382-391
196. Sag CM, Mallwitz A, Wagner S, Hartmann N, Schotola H, Fischer TH, Ungeheuer N, Herting J, Shah AM, Maier LS, Sossalla S, Unsold B. Enhanced late ina induces proarrhythmogenic sr ca leak in a camkii-dependent manner. *Journal of molecular and cellular cardiology*. 2014;76:94-105
197. Bairey Merz CN, Handberg EM, Shufelt CL, Mehta PK, Minissian MB, Wei J, Thomson LE, Berman DS, Shaw LJ, Petersen JW, Brown GH, Anderson RD, Shuster JJ, Cook-Wiens G, Rogatko A, Pepine CJ. A randomized, placebo-controlled trial of late na current inhibition (ranolazine) in coronary microvascular dysfunction (cmd): Impact on angina and myocardial perfusion reserve. *European heart journal*. 2015
198. Reiffel JA, Camm AJ, Belardinelli L, Zeng D, Karwatowska-Prokopczuk E, Olmsted A, Zareba W, Rosero S, Kowey P, Investigators H. The harmony trial:

Combined ranolazine and dronedarone in the management of paroxysmal atrial fibrillation: Mechanistic and therapeutic synergism. *Circulation. Arrhythmia and electrophysiology*. 2015;8:1048-1056
199. Glynn P, Musa H, Wu X, Unudurthi SD, Little S, Qian L, Wright PJ, Radwanski PB, Gyorke S, Mohler PJ, Hund TJ. Voltage-gated sodium channel phosphorylation at ser571 regulates late current, arrhythmia, and cardiac function in vivo. *Circulation*. 2015;132:567-577
200. Sato PY, Coombs W, Lin X, Nekrasova O, Green KJ, Isom LL, Taffet SM, Delmar M. Interactions between ankyrin-g, plakophilin-2, and connexin43 at the cardiac intercalated disc. *Circulation research*. 2011;109:193-201
201. Li J, Patel VV, Kostetskii I, Xiong Y, Chu AF, Jacobson JT, Yu C, Morley GE, Molkentin JD, Radice GL. Cardiac-specific loss of n-cadherin leads to alteration in connexins with conduction slowing and arrhythmogenesis. *Circulation research*. 2005;97:474-481
202. Shaw RM, Fay AJ, Puthenveedu MA, von Zastrow M, Jan YN, Jan LY. Microtubule plus-end-tracking proteins target gap junctions directly from the cell interior to adherens junctions. *Cell*. 2007;128:547-560
203. Agullo-Pascual E, Lin X, Leo-Macias A, Zhang M, Liang FX, Li Z, Pfenniger A, Lubkemeier I, Keegan S, Fenyo D, Willecke K, Rothenberg E, Delmar M. Super-resolution imaging reveals that loss of the c-terminus of connexin43 limits microtubule plus-end capture and nav1.5 localization at the intercalated disc. *Cardiovascular research*. 2014;104:371-381
204. Oxford EM, Musa H, Maass K, Coombs W, Taffet SM, Delmar M. Connexin43 remodeling caused by inhibition of plakophilin-2 expression in cardiac cells. *Circulation research*. 2007;101:703-711
205. Sato PY, Musa H, Coombs W, Guerrero-Serna G, Patino GA, Taffet SM, Isom LL, Delmar M. Loss of plakophilin-2 expression leads to decreased sodium current and slower conduction velocity in cultured cardiac myocytes. *Circulation research*. 2009;105:523-526
206. Cerrone M, Noorman M, Lin X, Chkourko H, Liang FX, van der Nagel R, Hund T, Birchmeier W, Mohler P, van Veen TA, van Rijen HV, Delmar M. Sodium current deficit and arrhythmogenesis in a murine model of plakophilin-2 haploinsufficiency. *Cardiovascular research*. 2012;95:460-468
207. Cerrone M, Lin X, Zhang M, Agullo-Pascual E, Pfenniger A, Chkourko-Gusky H, Novelli V, Kim C, Tirasawadichai T, Judge DP, Rothenberg E, Chen HS, Napolitano C, Priori S, Delmar M. Missense mutations in plakophilin-2 cause sodium current deficit and associate with a brugada syndrome phenotype. *Circulation*. 2013
208. Rizzo S, Lodder EM, Verkerk AO, Wolswinkel R, Beekman L, Pilichou K, Basso C, Remme CA, Thiene G, Bezzina CR. Intercalated disc abnormalities, reduced na(+) current density, and conduction slowing in desmoglein-2 mutant mice prior to cardiomyopathic changes. *Cardiovascular research*. 2012;95:409-418
209. Zhang Q, Deng C, Rao F, Modi RM, Zhu J, Liu X, Mai L, Tan H, Yu X, Lin Q, Xiao D, Kuang S, Wu S. Silencing of desmoplakin decreases connexin43/nav1.5

expression and sodium current in hl1 cardiomyocytes. *Molecular medicine reports*. 2013;8:780-786

210. Noorman M, Hakim S, Kessler E, Groeneweg JA, Cox MG, Asimaki A, van Rijen HV, van Stuijvenberg L, Chkourko H, van der Heyden MA, Vos MA, de Jonge N, van der Smagt JJ, Dooijes D, Vink A, de Weger RA, Varro A, de Bakker JM, Saffitz JE, Hund TJ, Mohler PJ, Delmar M, Hauer RN, van Veen TA. Remodeling of the cardiac sodium channel, connexin43, and plakoglobin at the intercalated disk in patients with arrhythmogenic cardiomyopathy. *Heart rhythm : the official journal of the Heart Rhythm Society*. 2013;10:412-419
211. Rhett JM, Gourdie RG. The perinexus: A new feature of cx43 gap junction organization. *Heart rhythm : the official journal of the Heart Rhythm Society*. 2012;9:619-623
212. Toyofuku T, Yabuki M, Otsu K, Kuzuya T, Hori M, Tada M. Direct association of the gap junction protein connexin-43 with zo-1 in cardiac myocytes. *The Journal of biological chemistry*. 1998;273:12725-12731
213. Agullo-Pascual E, Reid DA, Keegan S, Sidhu M, Fenyo D, Rothenberg E, Delmar M. Super-resolution fluorescence microscopy of the cardiac connexome reveals plakophilin-2 inside the connexin43 plaque. *Cardiovascular research*. 2013;100:231-240
214. Gutstein DE, Liu FY, Meyers MB, Choo A, Fishman GI. The organization of adherens junctions and desmosomes at the cardiac intercalated disc is independent of gap junctions. *Journal of cell science*. 2003;116:875-885
215. Jansen JA, Noorman M, Musa H, Stein M, de Jong S, van der Nagel R, Hund TJ, Mohler PJ, Vos MA, van Veen TA, de Bakker JM, Delmar M, van Rijen HV. Reduced heterogeneous expression of cx43 results in decreased nav1.5 expression and reduced sodium current that accounts for arrhythmia vulnerability in conditional cx43 knockout mice. *Heart rhythm : the official journal of the Heart Rhythm Society*. 2012;9:600-607
216. Lubkemeier I, Requardt RP, Lin X, Sasse P, Andrie R, Schrickel JW, Chkourko H, Bukauskas FF, Kim JS, Frank M, Malan D, Zhang J, Wirth A, Dobrowolski R, Mohler PJ, Offermanns S, Fleischmann BK, Delmar M, Willecke K. Deletion of the last five c-terminal amino acid residues of connexin43 leads to lethal ventricular arrhythmias in mice without affecting coupling via gap junction channels. *Basic research in cardiology*. 2013;108:348
217. Cerrone M, Delmar M. Desmosomes and the sodium channel complex: Implications for arrhythmogenic cardiomyopathy and brugada syndrome. *Trends in cardiovascular medicine*. 2014;24:184-190
218. Valdivia CR, Chu WW, Pu J, Foell JD, Haworth RA, Wolff MR, Kamp TJ, Makielski JC. Increased late sodium current in myocytes from a canine heart failure model and from failing human heart. *Journal of molecular and cellular cardiology*. 2005;38:475-483
219. Fontes MS, Raaijmakers AJ, van Doorn T, Kok B, Nieuwenhuis S, van der Nagel R, Vos MA, de Boer TP, van Rijen HV, Bierhuizen MF. Changes in cx43 and

nav1.5 expression precede the occurrence of substantial fibrosis in calcineurin-induced murine cardiac hypertrophy. *PloS one*. 2014;9:e87226
220. Stables CL, Musa H, Mitra A, Bhushal S, Deo M, Guerrero-Serna G, Mironov S, Zarzoso M, Vikstrom KL, Cawthorn W, Pandit SV. Reduced na(+) current density underlies impaired propagation in the diabetic rabbit ventricle. *Journal of molecular and cellular cardiology*. 2014;69:24-31
221. Doctor RB, Bennett V, Mandel LJ. Degradation of spectrin and ankyrin in the ischemic rat kidney. *The American journal of physiology*. 1993;264:C1003-1013
222. Yoshida K, Harada K. Proteolysis of erythrocyte-type and brain-type ankyrins in rat heart after postischemic reperfusion. *Journal of biochemistry*. 1997;122:279-285
223. Kashef F, Li J, Wright P, Snyder J, Suliman F, Kilic A, Higgins RS, Anderson ME, Binkley PF, Hund TJ, Mohler PJ. Ankyrin-b protein in heart failure: Identification of a new component of metazoan cardioprotection. *The Journal of biological chemistry*. 2012;287:30268-30281
224. Schafer DP, Jha S, Liu F, Akella T, McCullough LD, Rasband MN. Disruption of the axon initial segment cytoskeleton is a new mechanism for neuronal injury. *The Journal of neuroscience : the official journal of the Society for Neuroscience*. 2009;29:13242-13254
225. Parkinson NJ, Olsson CL, Hallows JL, McKee-Johnson J, Keogh BP, Noben-Trauth K, Kujawa SG, Tempel BL. Mutant beta-spectrin 4 causes auditory and motor neuropathies in quivering mice. *Nature genetics*. 2001;29:61-65
226. Martin CA, Zhang Y, Grace AA, Huang CL. In vivo studies of scn5a+/- mice modeling brugada syndrome demonstrate both conduction and repolarization abnormalities. *Journal of electrocardiology*. 2010;43:433-439
227. Watanabe H, Chopra N, Laver D, Hwang HS, Davies SS, Roach DE, Duff HJ, Roden DM, Wilde AAM, Knollmann BC. Flecainide prevents catecholaminergic polymorphic ventricular tachycardia in mice and humans. *Nature Medicine*. 2009;15:380-383
228. Hund TJ, Snyder JS, Wu X, Glynn P, Koval OM, Onal B, Leymaster ND, Unudurthi SD, Curran J, Camardo C, Wright PJ, Binkley PF, Anderson ME, Mohler PJ. Betaiv-spectrin regulates trek-1 membrane targeting in heart. *Cardiovasc Res*. 2014
229. Curran J, Makara MA, Little SC, Musa H, Liu B, Wu X, Polina I, Alecusan JS, Wright P, Li J, Billman GE, Boyden PA, Gyorke S, Band H, Hund TJ, Mohler PJ. Ehd3-dependent endosome pathway regulates cardiac membrane excitability and physiology. *Circ Res*. 2014;115:68-78
230. Abriel H. Roles and regulation of the cardiac sodium channel na v 1.5: Recent insights from experimental studies. *Cardiovascular research*. 2007;76:381-389
231. Lei M, Goddard C, Liu J, Leoni AL, Royer A, Fung SS, Xiao G, Ma A, Zhang H, Charpentier F, Vandenberg JI, Colledge WH, Grace AA, Huang CL. Sinus node dysfunction following targeted disruption of the murine cardiac sodium channel gene scn5a. *The Journal of physiology*. 2005;567:387-400

232. Abriel H. Roles and regulation of the cardiac sodium channel na v 1.5: Recent insights from experimental studies. *Cardiovascular research*. 2007;76:381-389
233. Wilde AA, Brugada R. Phenotypical manifestations of mutations in the genes encoding subunits of the cardiac sodium channel. *Circulation research*. 2011;108:884-897
234. Frommeyer G, Milberg P, Maier LS, Eckardt L. Late sodium channel inhibition: The most promising antiarrhythmic principle in the near future? *Curr Med Chem*. 2013
235. Kline CF, Kurata HT, Hund TJ, Cunha SR, Koval OM, Wright PJ, Christensen M, Anderson ME, Nichols CG, Mohler PJ. Dual role of k atp channel c-terminal motif in membrane targeting and metabolic regulation. *Proc Natl Acad Sci U S A*. 2009;106:16669-16674
236. Kline CF, Wright PJ, Koval OM, Zmuda EJ, Johnson BL, Anderson ME, Hai T, Hund TJ, Mohler PJ. Betaiv-spectrin and camkii facilitate kir6.2 regulation in pancreatic beta cells. *Proceedings of the National Academy of Sciences of the United States of America*. 2013;110:17576-17581
237. Sato PY, Coombs W, Lin X, Nekrasova O, Green KJ, Isom LL, Taffet SM, Delmar M. Interactions between ankyrin-g, plakophilin-2, and connexin43 at the cardiac intercalated disc. *Circulation research*. 2011;109:193-201
238. Wagner S, Dybkova N, Rasenack EC, Jacobshagen C, Fabritz L, Kirchhof P, Maier SK, Zhang T, Hasenfuss G, Brown JH, Bers DM, Maier LS. Ca2+/calmodulin-dependent protein kinase ii regulates cardiac na+ channels. *J Clin Invest*. 2006;116:3127-3138
239. Luo M, Anderson ME. Mechanisms of altered ca(2)(+) handling in heart failure. *Circ Res*. 2013;113:690-708
240. Zhou D, Lambert S, Malen PL, Carpenter S, Boland LM, Bennett V. Ankyring is required for clustering of voltage-gated na channels at axon initial segments and for normal action potential firing. *J Cell Biol*. 1998;143:1295-1304.
241. Lin X, Liu N, Lu J, Zhang J, Anumonwo JM, Isom LL, Fishman GI, Delmar M. Subcellular heterogeneity of sodium current properties in adult cardiac ventricular myocytes. *Heart rhythm : the official journal of the Heart Rhythm Society*. 2011;8:1923-1930
242. Leoni AL, Gavillet B, Rougier JS, Marionneau C, Probst V, Le Scouarnec S, Schott JJ, Demolombe S, Bruneval P, Huang CL, Colledge WH, Grace AA, Le Marec H, Wilde AA, Mohler PJ, Escande D, Abriel H, Charpentier F. Variable na(v)1.5 protein expression from the wild-type allele correlates with the penetrance of cardiac conduction disease in the scn5a(+/-) mouse model. *PLoS ONE*. 2010;5:e9298
243. Bennett V, Lorenzo DN. Spectrin- and ankyrin-based membrane domains and the evolution of vertebrates. *Current topics in membranes*. 2013;72:1-37
244. Yang Y, Lacas-Gervais S, Morest DK, Solimena M, Rasband MN. Betaiv spectrins are essential for membrane stability and the molecular organization of nodes of ranvier. *J Neurosci*. 2004;24:7230-7240

245. Brugada R, Brugada J, Antzelevitch C, Kirsch GE, Potenza D, Towbin JA, Brugada P. Sodium channel blockers identify risk for sudden death in patients with st-segment elevation and right bundle branch block but structurally normal hearts. *Circulation*. 2000;101:510-515
246. Stokoe KS, Balasubramaniam R, Goddard CA, Colledge WH, Grace AA, Huang CL. Effects of flecainide and quinidine on arrhythmogenic properties of scn5a+/- murine hearts modelling the brugada syndrome. *The Journal of physiology*. 2007;581:255-275
247. Cerrone M, Noorman M, Lin X, Chkourko H, Liang FX, van der Nagel R, Hund T, Birchmeier W, Mohler P, van Veen TA, van Rijen HV, Delmar M. Sodium current deficit and arrhythmogenesis in a murine model of plakophilin-2 haploinsufficiency. *Cardiovascular research*. 2012;95:460-468
248. Leoni AL, Gavillet B, Rougier JS, Marionneau C, Probst V, Le Scouarnec S, Schott JJ, Demolombe S, Bruneval P, Huang CL, Colledge WH, Grace AA, Le Marec H, Wilde AA, Mohler PJ, Escande D, Abriel H, Charpentier F. Variable na(v)1.5 protein expression from the wild-type allele correlates with the penetrance of cardiac conduction disease in the scn5a mouse model. *PLoS ONE*. 2010;5:e9298
249. Malhotra JD, Kazen-Gillespie K, Hortsch M, Isom LL. Sodium channel beta subunits mediate homophilic cell adhesion and recruit ankyrin to points of cell-cell contact. *J Biol Chem*. 2000;275:11383-11388.
250. Hedstrom KL, Ogawa Y, Rasband MN. Ankyring is required for maintenance of the axon initial segment and neuronal polarity. *J Cell Biol*. 2008;183:635-640
251. Asimaki A, Tandri H, Huang H, Halushka MK, Gautam S, Basso C, Thiene G, Tsatsopoulou A, Protonotarios N, McKenna WJ, Calkins H, Saffitz JE. A new diagnostic test for arrhythmogenic right ventricular cardiomyopathy. *The New England journal of medicine*. 2009;360:1075-1084
252. Unsoeld B, Gunkel S, Vouffo J, Pfeiffer C, Kranz A, Lossnitzer D, Wollnik B, Fabritz L, Fortmueller L, Paul M, Schulze-Bahr E, Kirchhoff P, Hasenfuss G, Knoell R. Recapitulation of a right ventricular phenotype in a transgenic mouse model overexpressing the plakophilin-2 r413x mutation that causes severe arvc in a large family. *Circulation*. 2009;120:S618
253. Wang DW, Viswanathan PC, Balser JR, George AL, Jr., Benson DW. Clinical, genetic, and biophysical characterization of scn5a mutations associated with atrioventricular conduction block. *Circulation*. 2002;105:341-346
254. van Veen TA, Stein M, Royer A, Le Quang K, Charpentier F, Colledge WH, Huang CL, Wilders R, Grace AA, Escande D, de Bakker JM, van Rijen HV. Impaired impulse propagation in scn5a-knockout mice: Combined contribution of excitability, connexin expression, and tissue architecture in relation to aging. *Circulation*. 2005;112:1927-1935
255. Genome-wide association study identifies five new schizophrenia loci. *Nat Genet*. 2011;43:969-976
256. Ferreira MA, O'Donovan MC, Meng YA, Jones IR, Ruderfer DM, Jones L, Fan J, Kirov G, Perlis RH, Green EK, Smoller JW, Grozeva D, Stone J, Nikolov I,

Chambert K, Hamshere ML, Nimgaonkar VL, Moskvina V, Thase ME, Caesar S, Sachs GS, Franklin J, Gordon-Smith K, Ardlie KG, Gabriel SB, Fraser C, Blumenstiel B, Defelice M, Breen G, Gill M, Morris DW, Elkin A, Muir WJ, McGhee KA, Williamson R, MacIntyre DJ, MacLean AW, St CD, Robinson M, Van Beck M, Pereira AC, Kandaswamy R, McQuillin A, Collier DA, Bass NJ, Young AH, Lawrence J, Ferrier IN, Anjorin A, Farmer A, Curtis D, Scolnick EM, McGuffin P, Daly MJ, Corvin AP, Holmans PA, Blackwood DH, Gurling HM, Owen MJ, Purcell SM, Sklar P, Craddock N. Collaborative genome-wide association analysis supports a role for ank3 and cacna1c in bipolar disorder. *Nat Genet*. 2008;40:1056-1058

257. Kizhatil K, Baker SA, Arshavsky VY, Bennett V. Ankyrin-g promotes cyclic nucleotide-gated channel transport to rod photoreceptor sensory cilia. *Science*. 2009;323:1614-1617
258. Gerull B, Heuser A, Wichter T, Paul M, Basson CT, McDermott DA, Lerman BB, Markowitz SM, Ellinor PT, MacRae CA, Peters S, Grossmann KS, Drenckhahn J, Michely B, Sasse-Klaassen S, Birchmeier W, Dietz R, Breithardt G, Schulze-Bahr E, Thierfelder L. Mutations in the desmosomal protein plakophilin-2 are common in arrhythmogenic right ventricular cardiomyopathy. *Nature genetics*. 2004;36:1162-1164
259. Hund TJ, Mohler PJ. Nav channel complex heterogeneity: New targets for the treatment of arrhythmia? *Circulation*. 2014;130:132-134
260. Sjostrand FS, Andersson E. Electron microscopy of the intercalated discs of cardiac muscle tissue. *Experientia*. 1954;10:369-370
261. Barker RJ, Price RL, Gourdie RG. Increased association of zo-1 with connexin43 during remodeling of cardiac gap junctions. *Circulation research*. 2002;90:317-324
262. Makara MA, Curran J, Little SC, Musa H, Polina I, Smith SA, Wright PJ, Unudurthi SD, Snyder J, Bennett V, Hund TJ, Mohler PJ. Ankyrin-g coordinates intercalated disc signaling platform to regulate cardiac excitability in vivo. *Circulation research*. 2014;115:929-938
263. Ling H, Zhang T, Pereira L, Means CK, Cheng H, Gu Y, Dalton ND, Peterson KL, Chen J, Bers D, Brown JH. Requirement for ca2+/calmodulin-dependent kinase ii in the transition from pressure overload-induced cardiac hypertrophy to heart failure in mice. *The Journal of clinical investigation*. 2009;119:1230-1240
264. Haas J, Frese KS, Peil B, Kloos W, Keller A, Nietsch R, Feng Z, Muller S, Kayvanpour E, Vogel B, Sedaghat-Hamedani F, Lim WK, Zhao X, Fradkin D, Kohler D, Fischer S, Franke J, Marquart S, Barb I, Li DT, Amr A, Ehlermann P, Mereles D, Weis T, Hassel S, Kremer A, King V, Wirsz E, Isnard R, Komajda M, Serio A, Grasso M, Syrris P, Wicks E, Plagnol V, Lopes L, Gadgaard T, Eiskjaer H, Jorgensen M, Garcia-Giustiniani D, Ortiz-Genga M, Crespo-Leiro MG, Deprez RH, Christiaans I, van Rijsingen IA, Wilde AA, Waldenstrom A, Bolognesi M, Bellazzi R, Morner S, Bermejo JL, Monserrat L, Villard E, Mogensen J, Pinto YM, Charron P, Elliott P, Arbustini E, Katus HA, Meder B. Atlas of the clinical

genetics of human dilated cardiomyopathy. *European heart journal*. 2015;36:1123-1135a
265. Cerrone M, Lin X, Zhang M, Agullo-Pascual E, Pfenniger A, Chkourko Gusky H, Novelli V, Kim C, Tirasawadichai T, Judge DP, Rothenberg E, Chen HS, Napolitano C, Priori SG, Delmar M. Missense mutations in plakophilin-2 cause sodium current deficit and associate with a brugada syndrome phenotype. *Circulation*. 2014;129:1092-1103
266. Schaper J, Froede R, Hein S, Buck A, Hashizume H, Speiser B, Friedl A, Bleese N. Impairment of the myocardial ultrastructure and changes of the cytoskeleton in dilated cardiomyopathy. *Circulation*. 1991;83:504-514
267. Li D, Tapscoft T, Gonzalez O, Burch PE, Quinones MA, Zoghbi WA, Hill R, Bachinski LL, Mann DL, Roberts R. Desmin mutation responsible for idiopathic dilated cardiomyopathy. *Circulation*. 1999;100:461-464
268. Otten E, Asimaki A, Maass A, van Langen IM, van der Wal A, de Jonge N, van den Berg MP, Saffitz JE, Wilde AA, Jongbloed JD, van Tintelen JP. Desmin mutations as a cause of right ventricular heart failure affect the intercalated disks. *Heart rhythm : the official journal of the Heart Rhythm Society*. 2010;7:1058-1064
269. Benson DW, Wang DW, Dyment M, Knilans TK, Fish FA, Strieper MJ, Rhodes TH, George AL, Jr. Congenital sick sinus syndrome caused by recessive mutations in the cardiac sodium channel gene (scn5a). *The Journal of clinical investigation*. 2003;112:1019-1028
270. Ferreira MA, O'Donovan MC, Meng YA, Jones IR, Ruderfer DM, Jones L, Fan J, Kirov G, Perlis RH, Green EK, Smoller JW, Grozeva D, Stone J, Nikolov I, Chambert K, Hamshere ML, Nimgaonkar VL, Moskvina V, Thase ME, Caesar S, Sachs GS, Franklin J, Gordon-Smith K, Ardlie KG, Gabriel SB, Fraser C, Blumenstiel B, Defelice M, Breen G, Gill M, Morris DW, Elkin A, Muir WJ, McGhee KA, Williamson R, MacIntyre DJ, MacLean AW, St CD, Robinson M, Van Beck M, Pereira AC, Kandaswamy R, McQuillin A, Collier DA, Bass NJ, Young AH, Lawrence J, Ferrier IN, Anjorin A, Farmer A, Curtis D, Scolnick EM, McGuffin P, Daly MJ, Corvin AP, Holmans PA, Blackwood DH, Gurling HM, Owen MJ, Purcell SM, Sklar P, Craddock N, Wellcome Trust Case Control C. Collaborative genome-wide association analysis supports a role for ank3 and cacna1c in bipolar disorder. *Nature genetics*. 2008;40:1056-1058
271. Weiner M, Warren L, Fiedorowicz JG. Cardiovascular morbidity and mortality in bipolar disorder. *Annals of clinical psychiatry : official journal of the American Academy of Clinical Psychiatrists*. 2011;23:40-47
272. Ringen PA, Engh JA, Birkenaes AB, Dieset I, Andreassen OA. Increased mortality in schizophrenia due to cardiovascular disease - a non-systematic review of epidemiology, possible causes, and interventions. *Frontiers in psychiatry*. 2014;5:137
273. Kalume F, Westenbroek RE, Cheah CS, Yu FH, Oakley JC, Scheuer T, Catterall WA. Sudden unexpected death in a mouse model of dravet syndrome. *The Journal of clinical investigation*. 2013;123:1798-1808

274. Radwanski PB, Brunello L, Veeraraghavan R, Ho HT, Lou Q, Makara MA, Belevych AE, Anghelescu M, Priori SG, Volpe P, Hund TJ, Janssen PM, Mohler PJ, Bridge JH, Poelzing S, Gyorke S. Neuronal na+ channel blockade suppresses arrhythmogenic diastolic ca2+ release. *Cardiovascular research*. 2015;106:143-152
275. Mishra S, Reznikov V, Maltsev VA, Undrovinas NA, Sabbah HN, Undrovinas A. Contribution of sodium channel neuronal isoform nav1.1 to late sodium current in ventricular myocytes from failing hearts. *The Journal of physiology*. 2015;593:1409-1427
276. Yoo S, Dobrzynski H, Fedorov VV, Xu SZ, Yamanushi TT, Jones SA, Yamamoto M, Nikolski VP, Efimov IR, Boyett MR. Localization of na+ channel isoforms at the atrioventricular junction and atrioventricular node in the rat. *Circulation*. 2006;114:1360-1371
277. Cohen CJ, Bean BP, Tsien RW. Maximal upstroke velocity as an index of available sodium conductance. Comparison of maximal upstroke velocity and voltage clamp measurements of sodium current in rabbit purkinje fibers. *Circulation research*. 1984;54:636-651
278. Undrovinas AI, Maltsev VA, Kyle JW, Silverman N, Sabbah HN. Gating of the late na+ channel in normal and failing human myocardium. *Journal of molecular and cellular cardiology*. 2002;34:1477-1489
279. Anderson ME, Brown JH, Bers DM. Camkii in myocardial hypertrophy and heart failure. *Journal of molecular and cellular cardiology*. 2011;51:468-473
280. Bassani JW, Yuan W, Bers DM. Fractional sr ca release is regulated by trigger ca and sr ca content in cardiac myocytes. *The American journal of physiology*. 1995;268:C1313-1319
281. Kiyosue T, Arita M. Late sodium current and its contribution to action potential configuration in guinea pig ventricular myocytes. *Circulation research*. 1989;64:389-397
282. Morita N, Lee JH, Xie Y, Sovari A, Qu Z, Weiss JN, Karagueuzian HS. Suppression of re-entrant and multifocal ventricular fibrillation by the late sodium current blocker ranolazine. *Journal of the American College of Cardiology*. 2011;57:366-375
283. Antzelevitch C, Burashnikov A, Sicouri S, Belardinelli L. Electrophysiologic basis for the antiarrhythmic actions of ranolazine. *Heart rhythm : the official journal of the Heart Rhythm Society*. 2011;8:1281-1290
284. Hund TJ, Snyder JS, Wu X, Glynn P, Koval OM, Onal B, Leymaster ND, Unudurthi SD, Curran J, Camardo C, Wright PJ, Binkley PF, Anderson ME, Mohler PJ. Beta(iv)-spectrin regulates trek-1 membrane targeting in the heart. *Cardiovascular research*. 2014;102:166-175
285. Ai X, Curran JW, Shannon TR, Bers DM, Pogwizd SM. Ca2+/calmodulin-dependent protein kinase modulates cardiac ryanodine receptor phosphorylation and sarcoplasmic reticulum ca2+ leak in heart failure. *Circulation research*. 2005;97:1314-1322

286. Koval OM, Guan X, Wu Y, Joiner ML, Gao Z, Chen B, Grumbach IM, Luczak ED, Colbran RJ, Song LS, Hund TJ, Mohler PJ, Anderson ME. Cav1.2 beta-subunit coordinates camkii-triggered cardiomyocyte death and afterdepolarizations. *Proceedings of the National Academy of Sciences of the United States of America*. 2010;107:4996-5000
287. Wehrens XH, Lehnart SE, Reiken SR, Marks AR. Ca2+/calmodulin-dependent protein kinase ii phosphorylation regulates the cardiac ryanodine receptor. *Circulation research*. 2004;94:e61-70
288. Hund TJ, Decker KF, Kanter E, Mohler PJ, Boyden PA, Schuessler RB, Yamada KA, Rudy Y. Role of activated camkii in abnormal calcium homeostasis and i(na) remodeling after myocardial infarction: Insights from mathematical modeling. *Journal of molecular and cellular cardiology*. 2008;45:420-428
289. Bers DM. Camkii inhibition in heart failure makes jump to human. *Circulation research*. 2010;107:1044-1046
290. van Oort RJ, McCauley MD, Dixit SS, Pereira L, Yang Y, Respress JL, Wang Q, De Almeida AC, Skapura DG, Anderson ME, Bers DM, Wehrens XH. Ryanodine receptor phosphorylation by calcium/calmodulin-dependent protein kinase ii promotes life-threatening ventricular arrhythmias in mice with heart failure. *Circulation*. 2010;122:2669-2679
291. Pugach EK, Richmond PA, Azofeifa JG, Dowell RD, Leinwand LA. Prolonged cre expression driven by the alpha-myosin heavy chain promoter can be cardiotoxic. *Journal of molecular and cellular cardiology*. 2015;86:54-61
292. Fressart V, Duthoit G, Donal E, Probst V, Deharo JC, Chevalier P, Klug D, Dubourg O, Delacretaz E, Cosnay P, Scanu P, Extramiana F, Keller D, Hidden-Lucet F, Simon F, Bessirard V, Roux-Buisson N, Hebert JL, Azarine A, Casset-Senon D, Rouzet F, Lecarpentier Y, Fontaine G, Coirault C, Frank R, Hainque B, Charron P. Desmosomal gene analysis in arrhythmogenic right ventricular dysplasia/cardiomyopathy: Spectrum of mutations and clinical impact in practice. *Europace : European pacing, arrhythmias, and cardiac electrophysiology : journal of the working groups on cardiac pacing, arrhythmias, and cardiac cellular electrophysiology of the European Society of Cardiology*. 2010;12:861-868
293. Chen SN, Gurha P, Lombardi R, Ruggiero A, Willerson JT, Marian AJ. The hippo pathway is activated and is a causal mechanism for adipogenesis in arrhythmogenic cardiomyopathy. *Circulation research*. 2014;114:454-468
294. Arimoto K, Burkart C, Yan M, Ran D, Weng S, Zhang DE. Plakophilin-2 promotes tumor development by enhancing ligand-dependent and -independent epidermal growth factor receptor dimerization and activation. *Molecular and cellular biology*. 2014;34:3843-3854
295. Crone SA, Zhao YY, Fan L, Gu Y, Minamisawa S, Liu Y, Peterson KL, Chen J, Kahn R, Condorelli G, Ross J, Jr., Chien KR, Lee KF. Erbb2 is essential in the prevention of dilated cardiomyopathy. *Nature medicine*. 2002;8:459-465
296. Garcia-Gras E, Lombardi R, Giocondo MJ, Willerson JT, Schneider MD, Khoury DS, Marian AJ. Suppression of canonical wnt/beta-catenin signaling by nuclear

plakoglobin recapitulates phenotype of arrhythmogenic right ventricular cardiomyopathy. *The Journal of clinical investigation*. 2006;116:2012-2021
297. Durak O, de Anda FC, Singh KK, Leussis MP, Petryshen TL, Sklar P, Tsai LH. Ankyrin-g regulates neurogenesis and wnt signaling by altering the subcellular localization of beta-catenin. *Molecular psychiatry*. 2014
298. Danik SB, Liu F, Zhang J, Suk HJ, Morley GE, Fishman GI, Gutstein DE. Modulation of cardiac gap junction expression and arrhythmic susceptibility. *Circulation research*. 2004;95:1035-1041
299. Rhett JM, Jourdan J, Gourdie RG. Connexin 43 connexon to gap junction transition is regulated by zonula occludens-1. *Molecular biology of the cell*. 2011;22:1516-1528
300. Maltsev VA, Kyle JW, Mishra S, Undrovinas A. Molecular identity of the late sodium current in adult dog cardiomyocytes identified by nav1.5 antisense inhibition. *American journal of physiology. Heart and circulatory physiology*. 2008;295:H667-676
301. Patel DM, Dubash AD, Kreitzer G, Green KJ. Disease mutations in desmoplakin inhibit cx43 membrane targeting mediated by desmoplakin-eb1 interactions. *The Journal of cell biology*. 2014;206:779-797
302. Lindegger N, Hagen BM, Marks AR, Lederer WJ, Kass RS. Diastolic transient inward current in long qt syndrome type 3 is caused by ca2+ overload and inhibited by ranolazine. *Journal of molecular and cellular cardiology*. 2009;47:326-334